DOKTORSAVHANDLINGAR
VID
CHALMERS TEKNISKA HÖGSKOLA
Nr 115

SOME BASIC PROBLEMS IN PERCUSSIVE ROCK DESTRUCTION

BY
BENGT LUNDBERG

GÖTEBORG 1971

SOME BASIC PROBLEMS IN PERCUSSIVE ROCK DESTRUCTION

by

BENGT LUNDBERG

AKADEMISK AVHANDLING

SOM MED TILLSTÅND AV DEKANUS VID SEKTIONEN FÖR MASKINTEKNIK VID CHALMERS TEKNISKA HÖGSKOLA FRAMLÄGGES TILL OFFENTLIG GRANSKNING FÖR TEKNOLOGIE DOKTORSGRADS VINNANDE FREDAGEN DEN 14 JANUARI 1972 KL. 10 Å PALMSTEDTSSALEN INOM KANSLIBYGGNADEN, SVEN HULTINS GATA, GÖTEBORG.

GÖTEBORG
GÖTEBORGS OFFSETTRYCKERI AB
1971

DOKTORSAVHANDLINGAR
VID
CHALMERS TEKNISKA HÖGSKOLA

SOME BASIC PROBLEMS IN PERCUSSIVE ROCK DESTRUCTION

BY

BENGT LUNDBERG

GÖTEBORG 1971

Printed in Sweden, Gotab, Surte 71.7826

CONTENTS

ABSTRACT

The mechanism of rock failure and the transfer of impact energy in percussive rock destruction are considered.

The indentor force at chip failure, and a lower limit for the crater volume to work ratio are obtained theoretically for a conical indentor and a brittle rock material. Comparison with experimental results indicates that the prescription of a conical failure surface and a Coulomb-Mohr failure criterion that is satisfied all over the failure surface leads to an overestimation of the force required to fracture the rock.

Methods of percussive rock destruction corresponding to churn drilling, down-the-hole drilling and hammer drilling are compared. Theoretically, efficiencies (work performed on rock/impact energy) higher than 90 per cent are attainable for any of the methods. These efficiencies are fairly insensitive to variations in bit mass, force-penetration constants, hammer cross sectional area and hammer length.

The hammer drilling method is examined in greater detail. It is found that no energy is transferred from the second incident stress wave to the rock when the hammer length is greater than a certain value. The influence of incident stress wave shape and also of non-linear force-penetration path at loading is demonstrated.

The efficiency of stress wave energy transfer through joints between drill rods is determined. It is shown that only slightly lower efficiencies are normally obtained by treating the joints as being rigid instead of elastic. For a single rigid joint and a rectangular incident wave it is found that the efficiency is nearly as high as the highest one attainable for any incident wave of equal length.

Stress waves determined theoretically from the models employed agree well with those measured.

ZUSAMMENFASSUNG

Der Bruchmechanismus in Gestein und die Umwandlung von Stossenergie beim schlagenden Gesteinsbohren werden behandelt.

Die Kraft an der Schneide beim Splitterbruch und eine untere Grenze für das Verhältnis zwischen Kratervolumen und an der Schneide geleisteter Arbeit werden für eine konische Schneide und sprödes Gesteinsmaterial bestimmt. Ein Vergleich mit experimentellen Resultaten zeigt, dass die Annahme einer konischen Form der Bruchfläche und das Erfüllen eines Coulomb-Mohr-Bruchkriteriums auf der ganzen Bruchfläche zu einer Ueberschätzung der erforderlichen Bruchlast führt.

Methoden der schlagenden Gesteinszerstörung, welche dem Stossbohren, dem Senkbohren und dem Hammerbohren entsprechen, werden verglichen. Theoretisch können mit jeder dieser Methoden Wirkungsgrade (am Gestein geleistete Arbeit/Stossenergie) von mehr als 90 Prozent erzielt werden. Diese Wirkungsgrade sind relativ unempfindlich gegen Aenderungen der Masse der Bohrkrone, der Kraft-Eindringtiefe-Konstanten, der Querschnittsfläche und der Länge des Hammers.

Die Methode des Hammerbohrens wird detaillierter untersucht. Es zeigt sich, dass von der zweiten einfallenden Spannungswelle keine Energie auf das Gestein übertragen wird, wenn die Hammerlänge grösser ist als ein bestimmter Wert. Der Einfluss der Form der einfallenden Spannungswelle und derjenige eines nichtlinearen Verlaufs der Kraft-Eindringtiefe-Funktion bei Belastung wird aufgezeigt.

Der Wirkungsgrad des Spannungswellen-Energietransportes durch Verbindungen zwischen Verlängerungsbohrstangen wird bestimmt. Es wird gezeigt, dass man normalerweise nur wenig kleinere Wirkungsgrade erhält, wenn man die Verbindungen so behandelt, wie wenn sie starr statt elastisch wären. Man findet, dass für eine einzelne starre Verbindung der Wirkungsgrad für eine einfallende Welle mit Rechtecksform fast eben-

so hoch ist wie der Höchste für irgendeine einfallende Welle derselben Wellenlänge erzielbare.

Spannungswellen, die mithilfe der verwendeten Modelle theoretisch bestimmt werden, stimmen gut mit den Gemessenen überein.

RESUME

On considère le mécanisme de rupture de la roche et le transfert de l'énergie d'impact lors de la destruction de roche par percussion.

On obtient théoriquement la force nécessaire à une pointe pour détacher un éclat de roche et une limite inférieure du rapport du volume de cratère au travail, ceci pour une pointe conique et une roche cassante. La comparaison avec des résultats expérimentaux montre que si l'on admet l'hypothèse que la rupture se fait suivant une surface conique et que le critère de rupture de Coulomb-Mohr s'applique à toute cette surface, on est amené à une surestimation de la force nécessaire à la rupture de la roche.

On compare les méthodes de destruction de roche par percussion qui correspondent au forage par battage, au forage par marteau perforateur (noyé) en fond de trou, et au forage au marteau perforateur. Théoriquement, des rendements (travail transmis à la roche/énergie d'impact) de plus de 90 pour cent peuvent être obtenus pour chaque méthode. Ces rendements varient assez faiblement avec la masse du burin, les constantes de forces de pénétration, la section et la longueur du marteau.

La méthode au marteau perforateur est examinée plus en détail. On montre qu'il n'y a pas transmission d'énergie à la roche par la seconde onde de contrainte incidente, lorsque la longueur du marteau dépasse une certaine valeur. On montre l'influence de la forme de l'onde incidente ainsi que de l'évolution non linéaire de la force de pénétration lors de la charge.

On détermine l'efficacité du transfert d'énergie (onde de contrainte) au travers des jonctions réunissant les barres de forage. On démontre que si l'on suppose les jonctions rigides, l'on obtient des efficacités qui ne sont que faiblement inférieures à celles calculées en supposant les jonctions élastiques. Pour une jonction unique rigide et une onde incidente rectangulaire on trouve que l'efficacité est presque aussi bonne que la meilleure efficacité obtenable par n'importe quelle onde incidente de même longueur.

Les ondes de contrainte déterminées théoriquement à partir des modèles employés coïncident bien avec celles mesurées.

LIST OF SYMBOLS

General Symbols

A, A_1, A_2	Cross sectional areas
a	Constant defined in Appendices C and D
a_1, a_2	Arbitrary constants
B_1, B_2	Constants defined in Appendix C
b	Constant defined in Appendices C and D
b_1, b_2	Arbitrary constants
C	Cohesive strength
c, c_1, c_2	Sonic velocities = $(E/\rho)^{1/2}$, etc.
D_1	Arbitrary constant
E, E_1, E_2	Young's moduli
F	Force acting between bit and rock
F_0	Force constant; 2) = 0, 3) = AEV/2c, 4) = AEV/2c or $A\sigma_0$
F_1, F_2, ...	Discrete values of F
F_M	= $F(x_M)$ (in general maximum value of F; in case of hammer drilling ~ during 1st stress wave reflection)
F_{M2}	Maximum value of F during 2nd stress wave reflection
F_m	Measured value of F
F_{m1}, F_{m2}, ...	Discrete values of F_m
f	= F/F_0
f_M	= F_M/F_0
f_{M2}	= F_{M2}/F_0

G	Function; Eq. (3.149)
g	Function; Eqs. (3.114) and (3.125)
$g_1, g_2, \ldots$	Functions; Eq. (5.69)
H	Transfer function; Eqs. (3.108) and (5.25)
h	Non-dimensional parameter; Eq. (4.83)
I	Integral; Eq. (3.88)
J	Integral; Eq. (3.89)
j	0, 1, 2, ...
K	Force-penetration constant (loading)
K	$= (1/2)e^{-\lvert\tau\rvert}$
$k, k_1, k_2, \ldots$	Force-penetration constants (loading)
k_{co}	Force-penetration constant (cone, chip formation)
k_e	Force-penetration constant (unloading)
k_{we}	Force-penetration constant (wedge, chip formation)
L	Length
M	Mass
m	$= t_p/t_J$ (sometimes $= L_H/L_J$)
N	Normal force per unit central angle acting on surface of failure
N	Number of joints
n	= 0, 1, 2, ...
P	Force acting between hammer and bit
P_1, P_2	Constants defined in Appendix C
p	$= (r-1)/(r+1)$

Q	Force per unit central angle acting between indentor and rock
q	$= (R-1)/(R+1)$
R	Dynamic stiffness ratio $= A_H E_H c_R / A_R E_R c_H$
R_1, R_2	Constants defined in Appendix C
r	$= A_J / A_R$
S	Shear force per unit central angle acting on surface of failure
s	Dummy integration variable. See also Mathematical Symbols
s_0, s_1, s_2, ...	1, σ_1/σ_0, σ_2/σ_0, ...
s_i	σ_i/σ_0
s_i^1	Eigenfunction; Eq. (5.53)
s_{i2}	$= \sigma_{i2}/\sigma_0$
s_r	$= \sigma_r/\sigma_0$
s_{r2}	$= \sigma_{r2}/\sigma_0$
s_t	$= \sigma_t/\sigma_0$
t	Time
t_0	Time constant; 3) $= AE/kc$, 4) $= AE/kc$ or $(AE^2/2Kc^2\sigma_0)^{1/2}$, 5) $= M_J c/2EA$
t_J	Time representing length of joint $= 2L_J/c_J$
t_M	Time when bit penetration is maximum (in case of hammer drilling ~ during 1st stress wave reflection)
t_{M2}	Time when bit penetration is maximum during 2nd stress wave reflection

t_p	Time representing length of hammer = $2L_H/c_H$ and/or duration of incident stress wave
u	Particle velocity = $\partial w/\partial t$
u_0	Constant particle velocity component
u_n	Particle velocity associated with wave travelling in negative z-direction
u_p	Particle velocity associated with wave travelling in positive z-direction
V	Impact velocity
$\mathcal{V}$	Crater volume
W	Work performed by bit on rock (in case of hammer drilling ~ during 1st stress wave reflection)
W_2	Work performed by bit on rock during 2nd stress wave reflection
W_E	Elastic energy associated with stress waves
W_i	Impact energy and/or incident stress wave energy
W_K	Kinetic energy associated with stress waves
W_T	Total energy associated with stress waves = W_K+W_E
w	Particle displacement
w_0	Constant particle displacement component
w_1, w_2	Particle displacement components
w_n	Particle displacement associated with wave travelling in negative z-direction

w_p	Particle displacement associated with wave travelling in positive z-direction
x	Bit penetration into rock
x_0	Penetration constant; 2) = 0, 3) = $t_0 V$
$x_1, x_2, \ldots$	Discrete values of x; x_1 represents end of lst linear segment
x_d	Bit penetration due to destruction of rock
$x_{d1}, x_{d2}, \ldots$	Discrete values of x_d
x_e	Bit penetration due to elastic deformation of rock
x_M	Maximum bit penetration (in case of hammer drilling ~ during lst stress wave reflection)
x_m	Measured bit displacement ($\neq$ penetration)
$x_{m0}, x_{m1}, \ldots$	Discrete values of x_m
y	Function; Eqs. (2.32), (2.16), (2.10)
Z, Z_1, Z_2	Dynamic stiffnesses = AE/c, etc.
z	Axial position coordinate
z_0	Fixed value of z
α	$= 4kc^2 M_B / A^2 E^2$
β	$= t_p / t_0$
$\beta_0, \beta_1, \ldots$	Functions; 3) Eq. (3.120), 4) Eqs. (4.23)-(4.25) and (4.31) or Eqs. (4.57) and (4.48)
β_B	$= 2kL_B / A_B E_B$
Γ	$= (\alpha-1)^{1/2}$, $\alpha>1$
γ	$= k/k_e$
Δ	$= (1-\alpha)^{1/2}$, $0<\alpha<1$

Δ_1, Δ_2	Constants; Eqs. (3.116) and (3.117)
Δs_1, Δs_2, ...	$= s_0 - s_1$, $s_1 - s_2$, ...
$\Delta\eta$	Difference in efficiency
δ	$= kx_1/A\sigma_0$
ε	Strain $= \partial w/\partial z$
ε_0	Constant strain component
η	Efficiency
η^1	Largest eigenvalue; Eq. (5.53)
Θ	Stress wave shape parameter; Eq. (4.36)
θ	Half cone-angle or wedge-angle
θ_1, θ_2, ...	Discrete values of θ
θ_{cr}	Critical value of θ
κ_{co}	Lower bound of V/W for cone
κ_{we}	Lower bound of V/W for wedge
λ	$= t_p/t_0 = 4m/r$
ν	$= d\xi/d\tau$
ν_1	Constant $= d\xi(\beta)/d\tau$
ξ	$= x/x_0$
ξ_1	Constant $= \xi(\beta)$
ξ_M	$= x_M/x_0$
ρ	Density
Σ_1, Σ_2	Sums of squares; Eqs. (2.30) and (2.34)
σ	Stress wave or stress
σ_0	Stress constant and/or stress wave amplitude
σ_1, σ_2, ...	Stress wave amplitudes
σ_c	Compressive strength

σ_{cm}	Measured compressive strength
σ_i	Incident stress wave (in case of hammer drilling 1st incident stress wave)
σ_{i2}	2nd incident stress wave
σ_n, σ_{n1}	Stresses associated with waves travelling in negative z-direction
σ_p, σ_{p1}, σ_{p2}	Stresses associated with waves travelling in positive z-direction
σ_r	Reflected stress wave (in case of hammer drilling 1st reflected stress wave)
σ_{r2}	2nd reflected stress wave
σ_t	Transmitted stress wave
τ	$= t/t_0$
τ_e	Effective shear stress; Eq. (2.9)
τ_M	$= t_M/t_0$
τ_{M2}	$= t_{M2}/t_0$
τ_N	Normal stress acting on surface of failure
τ_S	Shear stress acting on surface of failure
ϕ	Internal angle of friction
ϕ_f	Angle of friction at rock/indentor interface
ψ	Failure angle
Ω	Function; Eq. (5.63)
ω	See Mathematical Symbols

Subscripts and Superscripts

B	Bit
H	Hammer
J	Joint
R	Rod
*	Chip formation

Mathematical Symbols

$L\{\xi(\tau)\} = \tilde{\xi}(s)$	Laplace transform of $\xi(\tau)$
$L^{-1}\{\tilde{\xi}(s)\} = \xi(\tau)$	Inverse Laplace transform of $\tilde{\xi}(s)$
$F\{\xi(\tau)\} = \hat{\xi}(\omega)$	Fourier transform of $\xi(\tau)$
$\bar{\xi}$	Complex conjugate of ξ
$D\xi(\tau) = \xi'(\tau) = d\xi(\tau)/d\tau$	Derivative with respect to the argument τ

1. INTRODUCTION

1.1. Purpose

There are often two opposite approaches to the theoretical solution of physical or technological problems. The first approach involves the establishment of a simple model which represents only the most essential properties of the actual physical system. From mathematical analysis, the most important behaviour of the actual system is obtained for a wide variety of conditions. The second approach involves the establishment of a more complete model which gives an accurate representation of the actual physical system. From mathematical analysis, the detailed behaviour of the actual system is obtained, sometimes under more restricted conditions. The first approach has, besides from generality and mathematical simplicity, the advantage of facilitating the physical understanding of many essential phenomena involved and will generally be adopted here in the study of some basic problems connected with percussive rock destruction.

Particular attention will be given to the mechanism of rock destruction and the conversion of kinetic impact energy to work in rock destruction. Some results obtained from the analyses of different models representing the same physical system will be compared. Some results of analyses will also be compared with results from experiments.

In the remainder of Chapter 1 a brief presentation of the techniques of percussive rock destruction and a literature review will be given. In Chapter 2 the problem of bit penetration into rock material will be considered and information regarding force-penetration relationship and ratio of crater volume to work will be obtained. In Chapter 3 three basic methods of percussive rock destruction will be compared mainly with regard to their efficiencies. In Chapter 4 a number of problems connected with one of the three methods, the hammer drilling method, will be treated separately while Chapter 5

will deal with the efficiency of transfer of stress wave energy through joints between drill rods. Finally, in Chapter 6, significant assumptions, results and conclusions will be summarized.

The problems have been chosen from those met by the author in his research work at the Central Physics Laboratory of Atlas Copco AB during 1967-1971 (LUNDBERG, 1967-1971, 1968).

1.2. Techniques of Percussive Rock Destruction

The percussive destruction of rock is very old as an art and well established as a technology. Yet fundamental understanding of many phenomena involved is quite young. Thus, for many centuries it has been possible to destroy rock by means of simple percussive tools and for more than one century pneumatic percussive rock drills have been used. In contrast to this, fundamental knowledge about the basic mechanics of percussive rock destruction was not significantly improved until recently.

If the various applications of percussive rock destruction are studied, it is found that they are often based upon one of the three basic methods briefly described below.

In the first method a hammer with a bit attached to its front impacts the rock, which is thereby crushed and chipped. In the second method a hammer impacts a bit, which before impact rests against the rock. In the third method a hammer impacts a rod, which is long in comparison with the hammer. During impact a stress wave is generated in the rod. This stress wave propagates towards the bit at the end of the rod, where it is partly reflected. Under the combined action of the incident and reflected stress waves the bit is forced into the rock, which is thereby crushed and chipped.

All three methods may be looked upon as methods of force transformation : The low level long duration force accelera-

ting the hammer is transformed by impact into a high level short duration force which facilitates destruction of rock (FISCHER, 1960).

Three main fields of application of these basic methods of percussive rock destruction are churn drilling, down-the-hole percussive drilling and hammer drilling respectively. Therefore, the methods will subsequently be referred to as the "churn drilling method", the "down-the-hole drilling method" and the "hammer drilling method" even if the complete process of "drilling" is not considered. The three methods are also frequently applied in different types of drop-hammers in rock drilling and rock mechanics research. They are schematically illustrated in Fig. 1.1.

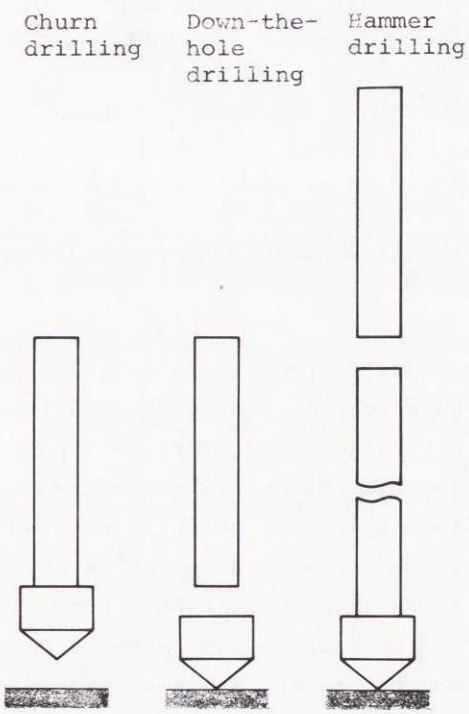

Fig. 1.1. Basic methods of percussive rock destruction.

The most important of the applications mentioned is hammer drilling, which is extensively utilized in the drilling of blast holes in medium hard and hard rock. Therefore, a brief description of hammer drilling is given below. Information about applications including hammer drilling can be found in several books (e.g. RYD & HOLDO, 1956; MCGREGOR, 1967; FINKEL, KALLDIN, LUNDBERG, LUNDQVIST & MEYER, 1969).

A schematic representation of a hammer drill system is illustrated in Fig. 1.2.

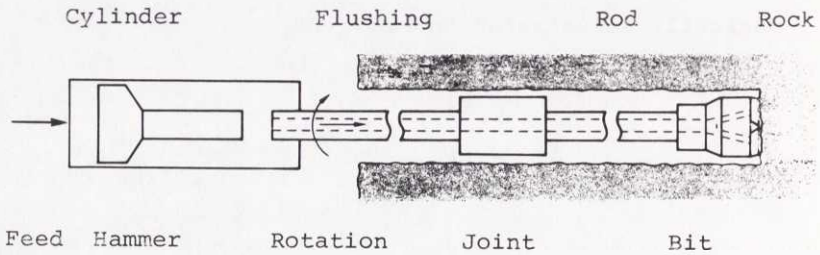

Fig. 1.2. A schematic representation of a hammer drill system.

A hammer drill comprises a cylinder with a reciprocating hammer. The source of energy is usually compressed air, but others are also used. Through impact, the kinetic energy of the accelerated hammer is transformed into stress wave energy in the drill rod, which is rotated at a certain angle between each blow. When deep holes are drilled there may be several rods joined together. Each of the joints usually gives rise to loss of energy, since stress wave energy is reflected and the joints are also heated as a result of friction. Finally, the stress wave reaches the bit and

causes one or several cutter elements to destroy the rock. The stress wave reflected from the bit gives rise to another stress wave, which is generated in the upper end of the drill rod. This stress wave may cause further rock destruction when it arrives at the bit.

To make drilling efficient it is important that the fragments of rock are continuously conveyed away from the hole bottom. This is done by the aid of a flushing fluid (usually air or water) which is conducted through a central hole in the drill rod and one or several holes in the bit. The fragments are then transported in the space between the drill rod and the wall of the bore hole to the rock surface.

To keep the rock drill in position it is necessary to exert a thrust force upon it. The thrust is also important in forcing the bit towards the rock and thus making transfer of energy to the rock efficient.

The technical development of pneumatic rock drills from 1857 to 1962 can be followed in a review by HOLDO (1962).

1.3. Literature Review

Discussions of literature in the field of percussive rock destruction have previously been presented e.g. by FISCHER (1960), HUSTRULID (1968) and HUSTRULID & FAIRHURST (1971).

Fundamental ingredients of percussive rock destruction are the phenomena of longitudinal impact and stress wave propagation. Some of the first treatments relevant to the situations in percussive rock destruction were given by DE SAINT-VENANT (1867, 1868) at approximately the same time as the first pneumatic rock drills came into use (see e.g. HOLDO, 1962). This elementary theory has later been applied by a large number of investigators. Thus the impact problem has been treated analytically (e.g. DONNELL, 1930; DAHL, 1932; ARNDT, 1960) as well as graphically (e.g. DE JUHASZ, 1942, 1949; FISCHER, 1960) and numerically (e.g. SIMON, 1963a; DUTTA, 1968; FU & PAUL, 1970).

In the elementary theory of elastic waves several restrictive assumptions are made which limit the applicability of the theory. A theory which is based on the fundamental equations of linear elasticity was developed by POCHHAMMER (1876) and CHREE (1889). However, their theory is limited to propagation of elastic waves in infinite cylindrical rods and therefore has been applied to only a few practical problems. Recently, however, it has become possible to solve linear elasticity impact problems by means of finite difference (e.g. BERTHOLF, 1966) or finite element (e.g. FU, 1970) methods. To avoid mathematical difficulties several approximate theories have also been developed. Thus LOVE (1927) introduced a one-dimensional theory which took radial inertia into consideration while MINDLIN & HERRMANN (1951) developed a one-dimensional theory in which radial shear was also taken into account. However, most theories of elastic waves, other than the elementary theory, have been only occasionally applied to problems connected with percussive destruction of rock, and in this respect their greatest value appears to be their ability to predict the range of applicability of the elementary theory and to explain certain phenomena (e.g. dispersion) which cannot be understood from the elementary theory alone. Information regarding elastic wave propagation in rods can be found in several reviews (e.g. ABRAMSON, PLASS & RIPPERGER, 1958; MIKLOWITZ, 1960; KOLSKY, 1963).

Another fundamental ingredient in percussive rock destruction is the interaction between a cutter element and rock. It includes for instance the mechanism of rock failure, the relationship between force and penetration and the relationship between crater volume and supplied energy. A large number of contributions have been given in this field during the last 20 years.

Experimental results from "static" (in presses) (e.g. FAIRHURST, 1961b; LUNDQVIST, 1968) as well as "dynamic" (in drop-hammers) (e.g. PENNINGTON, 1954; HARTMAN, 1959, 1962;

FAIRHURST, 1961b; STEPHENSON, 1963; HUSTRULID, 1968) tests performed for different types of cutters and rock materials have been reported. In the theoretical approaches some investigators have assumed the rock material to behave in a brittle manner (e.g. SINGH & HARTMAN, 1961; TANDANAND & HARTMAN, 1961; PAUL & SIKARSKIE, 1965; LUNDBERG, 1967; LUNDBERG, LUNDQVIST & MEYER, 1968; MILLER & SIKARSKIE, 1968; PAUL & GANGAL, 1969; BENJUMEA & SIKARSKIE, 1969) while others have assumed the rock material to behave in a ductile manner (e.g. CHEATHAM, 1958, 1964; PAONE & TANDANAND, 1966; PARISEAU & FAIRHURST, 1967; PARISEAU, 1971). The latter approach is often necessary when the rock material is subjected to a state of high hydrostatic pressure.

MILLER (1966) considered the influence of the duration of loading. According to Miller, the specific energy (ratio between supplied energy and crater volume) in percussive rock destruction, which is normally of the order of the compressive strength of the rock material (TEALE, 1965), could be considerably decreased if the duration of the load is decreased a few orders of magnitude. However, it should be observed that the specific energy obtained in conventional percussive rock destruction is generally much lower than the specific energies obtained in most suggested "exotic" methods of rock destruction (MAURER, 1968).

SIMON (1963b) studied the energy balance in percussive rock destruction and found that the energy associated with the formation of new surfaces is negligibly small. He concluded that most of the energy consumed is represented by elastic strain energy developed by the loading. This energy is largely dissipated in the form of stress waves generated by the high rate of unloading in front of propagating cracks.

Indexing, which is connected with the influence of previously formed craters on craters under formation, has been studied by several investigators and an extensive review

and discussion of their results was given by HUSTRULID (1968). Indexing appears to facilitate a considerable increase in the crater volume per blow if it takes place on a smooth and previously undamaged surface of rock. However, HARTMAN (1966) found that under real drilling conditions with indexing on a previously cratered surface, indexing does not play a major role in affecting the drilling process.

Little appears to have been published about the fundamentals of the churn drilling method even though it has been extensively applied in different types of drop-hammer experiments (e.g. PENNINGTON, 1954; HARTMAN, 1959; STEPHENSON, 1963; HUSTRULID, 1968). Sometimes, in such experiments, the hammer is short and thick and treated as a rigid mass, i.e. force and penetration are determined from the measured deceleration of the hammer and it is assumed that when the penetration velocity has dropped to zero, the hammer has completely delivered its kinetic energy to the rock. Sometimes, the hammer is a long slender rod, and force and penetration are then determined from stress wave measurements. Finally, sometimes the hammer can be considered to be neither a "lumped mass" nor a "long rod".

The difference between a "lumped mass" and a "long rod" drop-hammer was discussed by STEPHENSON (1963), who found the former type of drop-hammer preferable in his experiments. HUSTRULID (1968) observed that for such drop-hammers, energy transfer depends on hammer geometry and rock properties. He also developed a computer program which made energy transfer computations possible. In an example he showed that when the penetration resistance increases by a factor of 20/3 the efficiency of energy transfer to rock decreases from 98 to 87 per cent. Thus, he concluded, many experimental results obtained in different drop-hammers cannot be compared directly.

Recently, papers have appeared dealing with the down-the-hole method. PFLEIDER & LACABANNE (1961) discussed how to increase the power at the bottom of the drill hole in order to obtain an increased rate of penetration. However, they did not treat transfer of energy to the rock. This was later done by BAILEY (1967) who developed a computer program for the study of a down-the-hole percussive system, represented as a hammer and a bit each composed of two segments with constant cross sectional areas. As a result of the computations, he obtained efficiency of energy transfer to rock and maximum stress in hammer or bit. The quantity he tried to maximize is the ratio of efficiency and maximum stress rather than the efficiency. Bailey's paper was discussed by HUSTRULID & FAIRHURST (1967) who explained the relatively high and constant efficiency (73.5 - 83.5 per cent) obtained for the down-the-hole percussive system studied by Bailey. They concluded that the reason seems to be that the bit, in behaviour, approaches a "lumped" or rigid mass.

Another approach in the study of a similar system was employed by SCHMAUCK (1969), who studied a down-the-hole percussive system represented as a hammer with a constant cross sectional area and a bit composed of two segments, each with a constant cross sectional area. While Bailey described the interaction between bit and rock in terms of a force-penetration relation, Schmauck introduced a characteristic impedance, defined as the ratio between force and penetration velocity. Also, while Bailey studied the problem numerically, Schmauck used an essentially analytical method introduced by ARNDT (1959).

Of the three basic methods of percussive rock destruction, most attention has been paid to the hammer drilling method. An early attempt to analyse the transfer of energy to rock was made by DAHL (1932). However, he was prevented from completing his analysis because of insufficient experimental

information regarding the bit penetration process. Attempts were made later by TAKAOKA & HAYAMIZU (1956), who assumed that the penetration resistance was independent of penetration, and by FAIRHURST & KIM (1958). Further analysis was given by FAIRHURST (1961a, c) who assumed a linear force-penetration loading relationship (force proportional to penetration). He showed that if the stress wave incident to the bit is a certain exponential function of time (amplitude increasing), then the reflected stress wave is zero and consequently the efficiency of energy transfer to rock is 100 per cent. Later, SIMON (1964) extended Fairhurst's investigations by considering efficiency of energy transfer from drill rod to rock when the incident stress wave is of a type which is common in hammer drilling. For different types of incident stress waves he found that the efficiency assumes a maximum value for a certain length of the stress wave. Thus, for a rectangular stress wave, he obtained a maximum efficiency of 82 per cent provided that the force-penetration loading relationship is linear. Also, for a given incident stress wave, Simon determined what force-penetration relationship would allow complete energy transfer to rock, that is 100 per cent efficiency.

A common conclusion from the investigations by Fairhurst and Simon is that for obtaining complete transfer of energy to rock, either the stress wave or the force-penetration relationship or both must be different from that which it is normally possible to realise.

An unsuccessful attempt to obtain nearly complete energy transfer to rock was made by LONG (1966).

In the investigations discussed above, energy transfer only from the first incident stress wave of each blow was considered. However, the reflected stress wave at the bit is reflected again at the upper end of the drill rod and gives rise to a second incident stress wave towards the bit and so on. FURBY (1964) observed that some of these later

incident stress waves may give rise to further penetration of the bit into the rock and, consequently, all energy that is transferred to the rock is not necessarily transferred during the first reflection. This possibility was considered by HUSTRULID (1968), who showed that in many normal situations all energy that is transferred to the rock is transferred during the first two reflections. Normally, the drill system is so designed that the greatest part of this energy is transferred during the first interaction at the bit-rock interface.

Several investigators have paid attention to the need of thrust in hammer drilling (e.g. ARNDT, 1958; SIMON, 1964; HUSTRULID, 1968). Hustrulid obtained drilling rate as a function of thrust force and other parameters.

Lately, stability of motion has been considered for impact tools. This was done by e.g. FU & PAUL (1968) who studied a two-degree-of-freedom system where two rigid masses connected with a linear spring represented the tool case and the hammer. The delivery of energy from the hammer was described by means of an effective coefficient of restitution, and, thus, the system studied might as well represent any of the three methods of percussive rock destruction described above. The stability of the system was found to be very weak in the sense that a solution is stable only for extremely small perturbations.

The problem of energy transfer through joints between rods has been treated by FISCHER (1960), who assumed the joint to behave as an elastic swell on the rod. However, Fischer noticed that even a slight lack of contact between the rod surfaces seriously influences the joint behaviour. This was further demonstrated by means of photoelastic techniques by BABENKOV, IVANOV & HESIN (1965) who found that the efficiency of energy transfer through a joint decreased from 94 per cent to 81 per cent when, in a particular case, the

contact between the two drill rods disappeared. Also, TAKAOKA, HAYAMIZU & MISAWA (1958 in Japanese; see FAIRHURST, 1961a) found that frictional losses in the joint may be of the same order of magnitude as the losses due to reflected stress waves. However, the frictional losses depend to a large extent on the particular joint type and therefore they may be difficult to take into account in a general way. Few results regarding efficiency of energy transfer through a number of joints have been found in the literature. Thus, for example, FURBY (1964) simply assumed a constant relative portion of stress wave energy to be lost in each joint.

Some other reasons why the total kinetic energy of the hammer does not arrive at the bit as longitudinal stress wave energy are that (1) depending on hammer and rod geometry, the transfer of kinetic energy from hammer to rod may be incomplete (FISCHER, 1960), (2) if impact is eccentric, a part of the kinetic energy of the hammer generates flexural waves in the drill rod and (3) the stress waves are attenuated because of internal as well as external friction. Flexural waves in drill rods were considered by SHIMIZU & TAKATA (1960) as well as ROBERTS, HAWKES & FURBY (1962). The latter investigators found that the amplitude of strain in the flexural wave can be as high as 70 per cent of the amplitude in the desired longitudinal wave. Internal attenuation was briefly discussed by FAIRHURST (1961a) who found that, typically, attenuation would cause an energy reduction of 2 per cent in 10 ft. while TAKAOKA, HAYAMIZU & MISAWA (1958 in Japanese; see FAIRHURST 1961a) found a slightly higher value (3 per cent) when support losses were included. Thus, attenuation is a relatively unimportant source of energy loss in hammer drilling. On the other hand, since the time distance between two successive blows for normal percussive drills is normally as long as 20-30 ms, attenuation contributes to justify the usually made assumption, that no stress waves are present in the percussive system immediately before each impact.

Percussive drilling of rock is a complex process and the overall energy conversion involves many steps. Thus, the overall efficiency is determined by e.g. compressor efficiency, rock drill efficiency and the efficiency of transfer of hammer impact energy into work in rock breaking. These different steps and the overall efficiency in gold mining were considered by COOK & HUSTRULID (1970) who found that the overall efficiency (defined as the ratio of the power used in rock breaking to the electrical power input to the compressor motor) is about 9 per cent when pneumatic rock drills are employed. They also found that the energy consumption of the compressors for the rock drills (6 kWh/tonne of rock broken) represents a significant fraction of the total amount of energy absorbed by all mining, hoisting and milling operations (35 kWh/tonne of rock broken).

1.4. Acknowledgments

Atlas Copco AB - for permission to publish this work.

Professor Jan Hult, Chalmers University of Technology, Gothenburg - for guidance, encouragements and suggestions.

Mr. Jan Holdo, Dr. Nils Starfelt, Atlas Copco AB and Mr. Lennart Ottosson, Atlas Copco MCT AB - for support of this work.

Mr. Olaf Meyer, Atlas Copco AB - for support of this work, encouragements and suggestions.

Dr. Bo Lemcke, Institut CERAC S.A. - for support of the final phase of this work.

Professor Hans Christian Fischer, University of Uppsala - for a valuable discussion.

Dr. Lars-Erik Andersson, University of Linkoping - for advice and discussions regarding mathematical topics.

Mr. Gunnar Thuresson, The Royal Institute of Technology, Stockhom (now Atlas Copco AB) - for collaboration regarding a part of the investigations in this thesis.

Dr. Nick Hall-Taylor, Mr. Christopher Yates and Mrs. Susan Yates, Atlas Copco AB - for reading through the manuscript.

Mr. Stig Johansson, Atlas Copco AB - for photographic work.

Mrs. Radegundis Grach, Atlas Copco AB, and Mrs. Jacqueline Fosh, Institut CERAC S.A. - for drawing figures and typing respectively.

Many friends and colleagues at Atlas Copco AB, Atlas Copco MCT AB and Institut CERAC S.A. - for support and interest.

To all these people, and also to my wife Marit, I wish to express my sincere gratitude and thanks.

2. BIT PENETRATION

2.1. Introduction

A bit used in percussive rock destruction is usually equipped with one or several cutter elements. In order to obtain knowledge regarding the bit penetration process, it is therefore convenient to begin by studying the interaction between a single such cutter element and rock. Here the study will be restricted to wedge-shaped or cone-shaped indentors and to situations in which the rock behaves in a brittle manner.

In order to get a qualitative background, consider an indentor which is acted upon by a force F and which has penetrated a distance

$$x = x_d + x_e \tag{2.1}$$

into the rock material. x_d is considered to be the penetration due to rock destruction, while x_e is the penetration caused by elastic deformation of the rock.

If the indentor is sharp the destruction of rock occurs by crushing as well as chipping. This is illustrated in Fig. 2.1. If, on the other hand, the indentor is blunt, the chipping mode is not observed. This is illustrated in Fig. 2.2.

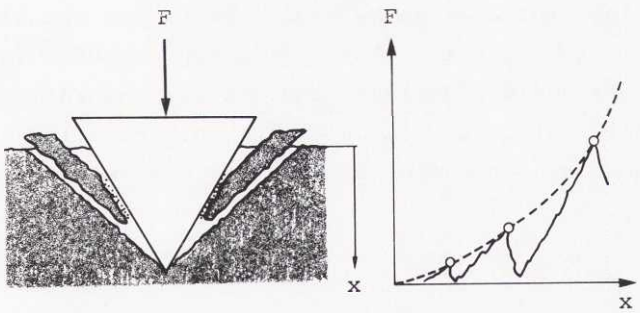

Fig. 2.1. Chipping and crushing when the indentor is sharp. Circles mark points of chip formation.

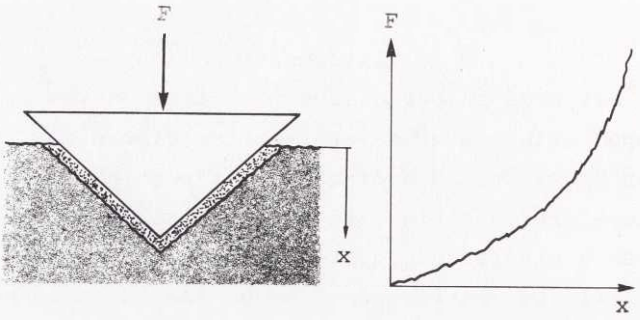

Fig. 2.2. Crushing when the indentor is blunt.

In general, in percussive rock destruction, the indentor penetrates into a rough and previously chipped surface, which complicates the penetration process to a large extent.

The same qualitative behaviour, as has already been described, can be observed if the process of loading and unloading takes place over a period of seconds (sometimes referred to as static penetration) or tenths of milliseconds (sometimes referred to as dynamic penetration). The latter order of duration of the penetration process is normal in percussive rock destruction.

Next, the analysis performed by PAUL & SIKARSKIE (1965) for a wedge-shaped indentor will be extended to a cone-shaped indentor (LUNDBERG, 1967; LUNDBERG, LUNDQVIST & MEYER, 1968). The results obtained will be compared with those obtained for a wedge by Paul & Sikarskie and with some experimental results. Also, with support of investigations made by HUSTRULID (1968) and others, the influence of penetration velocity will be discussed. Finally, bit penetration models for subsequent use in this work will be established.

2.2. Cone-shaped Indentor

2.2.1. Basic Assumptions

The basic assumptions closely correspond to those made by Paul & Sikarskie.

The indentor is assumed to be rigid and perfectly cone-shaped with a cone-angle 2θ. The friction between indentor and rock is described by a constant angle of friction ϕ_f and the rock surface is assumed to be plane. The elastic component of penetration x_e is neglected, which means that the penetration is due to destruction of rock only. Dynamic effects are also neglected.

When the indentor is forced towards the rock surface, it is assumed that radial cracks are formed as a result of tensile tangential stress and low tensile strength of the rock material. Chip failure then occurs on a conical surface of failure, which extends from the tip of the indentor to the free surface at angle of inclination ψ (failure angle). The idealized geometry of chip failure is illustrated in Fig. 2.3.

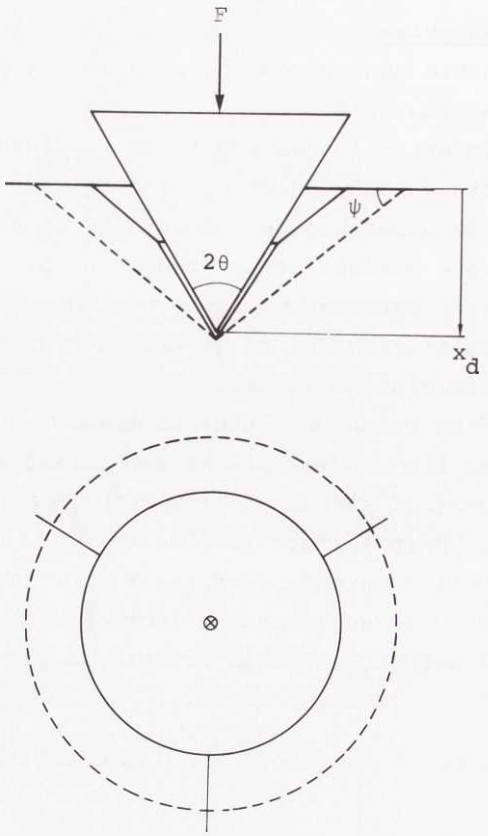

Fig. 2.3. Idealized geometry of chip failure.

Immediately before chip failure equilibrium prevails. Failure occurs when the stresses acting on the prescribed surface of failure satisfy everywhere the Coulomb-Mohr failure criterion, (COULOMB, 1776; MOHR, 1900). This criterion is illustrated in Fig. 2.4, where τ_S is the shear stress and τ_N is the normal stress acting on the surface of failure. C is the cohesive strength, σ_c is the compressive strength and ϕ is the internal angle of friction of the rock

material. The part of the envelope corresponding to tensile normal stress is dotted, since in the situation considered, the normal stress is assumed to be compressive.

The Coulomb-Mohr failure criterion was discussed by PAUL (1961), who also suggested a modification.

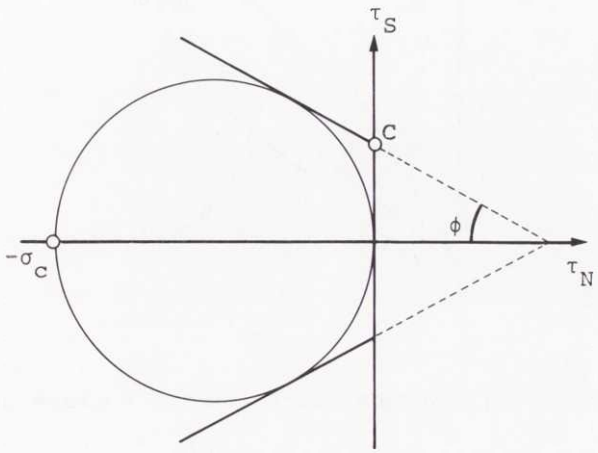

Fig. 2.4. Coulomb-Mohr failure criterion.

2.2.2. Analysis

2.2.2.1. Failure angle. - A chip is assumed to be formed when the force acting on the indentor is F^* and the penetration of the indentor into the rock material due to destruction of rock is x_d.

In Fig. 2.5 a sector of a chip is illustrated. Immediately before failure takes place the normal and shear stresses acting on the surface of failure are τ_N and τ_S respectively. These stresses are functions of position, however not of the circumferential position.

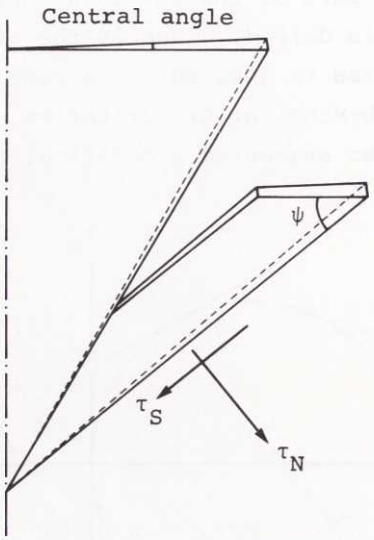

Fig. 2.5. Stresses acting on the surface of failure.

Failure occurs when the stresses τ_N and τ_S, for any possible surface of failure, satisfy everywhere the Coulomb-Mohr failure criterion, which can be expressed as

$$|\tau_S| + \tau_N \tan\phi = C \qquad (2.2)$$

where the cohesive strength C is related to the compressive strength σ_c and the internal angle of friction ϕ as

$$C = \sigma_c (1-\sin\phi)/2\cos\phi \qquad (2.3)$$

The stresses τ_N and τ_S result in forces per unit central angle N and S respectively. If it is assumed that $\tau_S \geq 0$, then by integration over the surface of failure, the failure criterion (2.2) can be transformed into a failure criterion in terms of the forces N and S, i.e.

$$\tau_e = C \tag{2.4}$$

where

$$\tau_e = 2\sin^2\psi(S+N\tan\phi)/x_d^2\cos\psi \tag{2.5}$$

τ_e can be considered as an effective shear stress with the property that failure occurs when it reaches the critical value C.

It should be observed that in the transformed failure criterion the forces N and S, as well as the failure angle ψ, are unknown quantities which remain to be determined.

As it is evident from Fig. 2.6, however, equilibrium of forces can be expressed by one equation for the indentor and two equations for the chips. These equations involve the force per unit central angle Q, which acts between indentor and chips and which, as a result of friction, deviates by an angle ϕ_f from the surface normals.

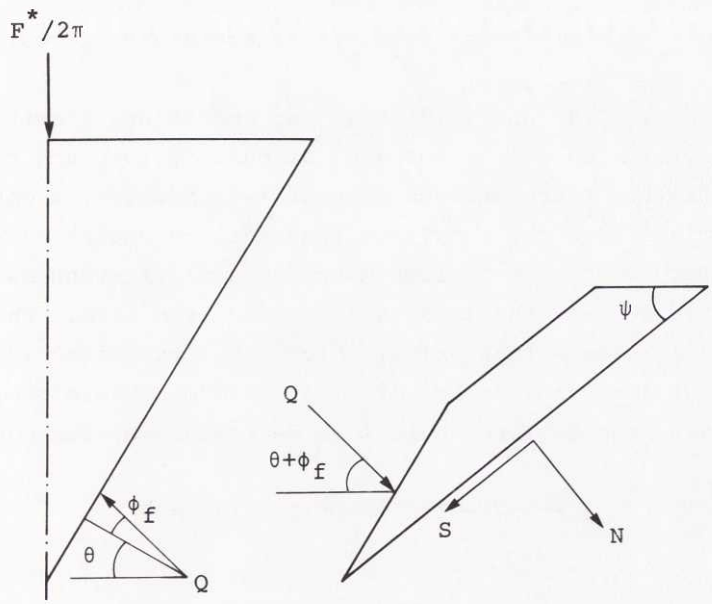

Fig. 2.6. Forces per unit of central angle acting on indentor and chips.

If Q is eliminated from these three equations of equilibrium, N and S can be expressed in terms of ψ and F^* as

$$N = -F^* \sin(\theta+\phi_f+\psi)/2\pi\sin(\theta+\phi_f) \qquad (2.6)$$

$$S = F^* \cos(\theta+\phi_f+\psi)/2\pi\sin(\theta+\phi_f) \qquad (2.7)$$

Since it has been assumed that $\tau_N \leq 0$ and $\tau_S \geq 0$, it is necessary that $N \leq 0$ and $S \geq 0$ respectively. Since $\theta < \pi/2$ and $\phi_f < \pi/2$, these conditions are satisfied provided that

$$\theta+\phi_f+\psi \leq \pi/2 \qquad (2.8)$$

Therefore, when ψ has been determined, it must be verified that, in accordance with these assumptions, the inequality (2.8) is satisfied.

When N and S, according to Eqs. (2.6) and (2.7), are substituted into Eq. (2.5) τ_e takes the form

$$\tau_e = F^* \sin^2\psi\cos(\theta+\phi_f+\phi+\psi)/\pi x_d^2 \cos\phi\sin(\theta+\phi_f)\cos\psi \qquad (2.9)$$

Now Eqs. (2.4) and (2.9) together constitute a criterion of failure in which the force F^* at chip failure and the angle of failure ψ are unknown quantities. However, ψ can be determined from the condition that failure occurs on the conical surface where the Coulomb-Mohr failure criterion is first satisfied when the load is increased from zero. This implies that ψ assumes that value, which makes the effective shear stress according to Eq. (2.9) a maximum. Therefore, as a result, the failure angle ψ is determined by the equation

$$-\tan^3\psi - 3\tan\psi + 2\cot(\theta+\phi_f+\phi) = 0 \qquad (2.10)$$

Since no chipping is possible unless $\psi>0$, a necessary condition for chip formation can be derived from Eq. (2.10). The result is

$$\theta+\phi_f+\phi<\pi/2 \tag{2.11}$$

Thus a critical half cone-angle with respect to chip formation is

$$\theta_{cr} = \pi/2-\phi_f-\phi \tag{2.12}$$

Subsequently it is assumed that $\theta<\theta_{cr}$ and that chipping also occurs.

From Eq. (2.10) it is also found that

$$\theta+\phi_f+\phi+\psi\leq\pi/2 \tag{2.13}$$

Therefore, and since $\phi\geq0$, the inequality (2.8) is satisfied in agreement with the initial assumptions that $\tau_N\leq0$ and $\tau_S\geq0$.

ψ versus $(\theta+\phi_f+\phi)$ according to Eq. (2.10) is shown in Fig. 2.7.

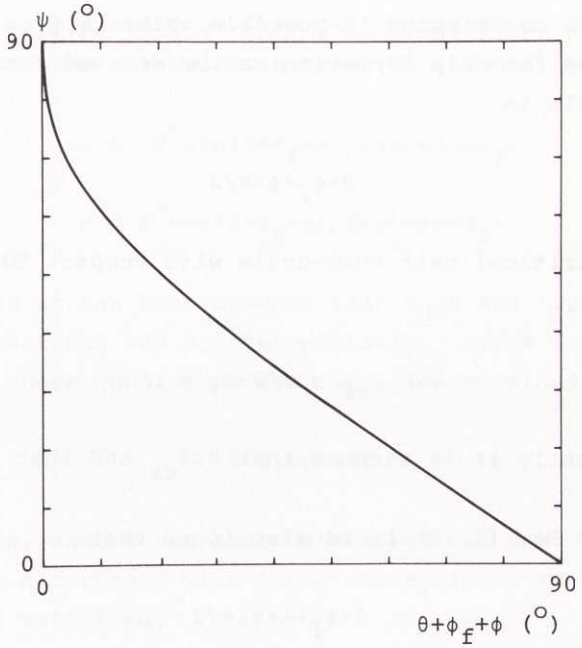

Fig. 2.7. Failure angle ψ versus $(\theta+\phi_f+\phi)$ for a cone.

For a wedge-shaped indentor Paul & Sikarskie obtained the corresponding failure angle

$$\psi = \pi/4-(\theta+\phi_f+\phi)/2 \qquad (2.14)$$

where θ now denotes the half wedge-angle. Further, with this notation, the same results as (2.11) and (2.12) were obtained also for a wedge.

ψ versus $(\theta+\phi_f+\phi)$ according to Eq. (2.14) is illustrated in Fig. 2.8.

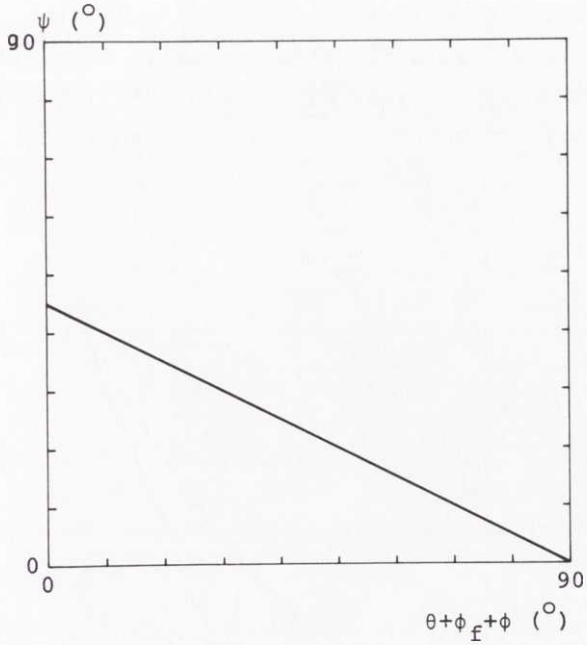

Fig. 2.8. Failure angle ψ versus $(\theta+\phi_f+\phi)$ for a wedge.

2.2.2.2. Force-penetration. - Now, when the failure angle ψ is determined, it is possible to determine also the relationship between the force F^* at chip failure and the penetration $x = x_d$. Substitution of Eqs. (2.3) and (2.9) into the failure criterion (2.4) yields

$$F^* = k_{co} x_d^2 \tag{2.15}$$

where

$$k_{co}/\sigma_c = \pi(1-\sin\phi)\sin(\theta+\phi_f)\cos\psi/2\sin^2\psi\cos(\theta+\phi_f+\phi+\psi) \tag{2.16}$$

In Fig. 2.9, a force-penetration characteristic according to Eq. (2.15) is illustrated, while Fig. 2.10 illustrates the relationship between k_{co}/σ_c and $(\theta+\phi_f)$ for different values of ϕ according to Eqs. (2.10) and (2.16).

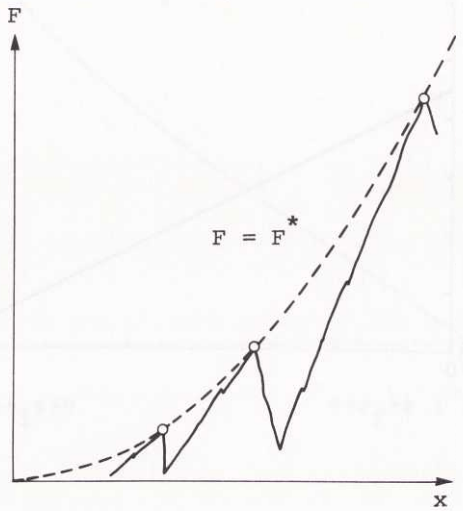

Fig. 2.9. Force-penetration characteristic for a cone. Circles mark points of chip formation.

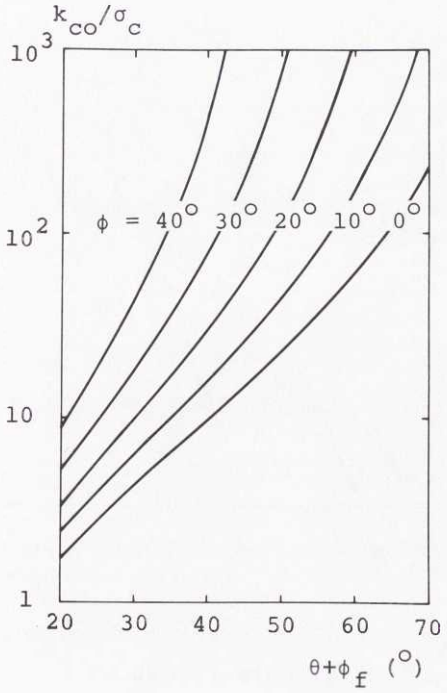

Fig. 2.10. k_{co}/σ_c versus $(\theta+\phi_f)$ for different values of ϕ.

For a wedge-shaped indentor with unit length, Paul & Sikarskie obtained the linear force-penetration envelope

$$F^* = k_{we}x_d \qquad (2.17)$$

where

$$k_{we}/\sigma_c = 2\sin(\theta+\phi_f)(1-\sin\phi)/\{1-\sin(\theta+\phi_f+\phi)\} \qquad (2.18)$$

In Fig. 2.11 a force-penetration characteristic according to Eq. (2.17) is illustrated, while Fig. 2.12 illustrates the relationship between k_{we}/σ_c and $(\theta+\phi_f)$ for different values of ϕ according to Eq. (2.18).

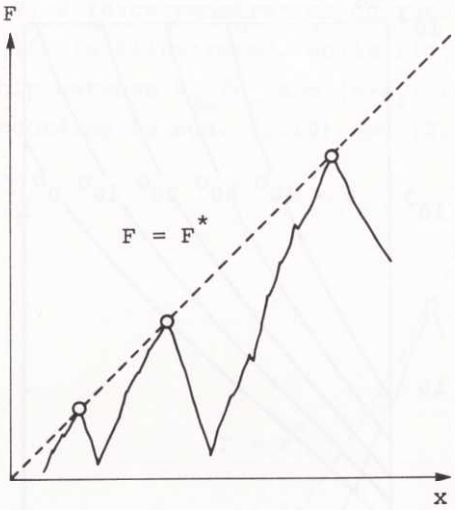

Fig. 2.11. Force-penetration characteristic for a wedge. Circles mark points of chip formation.

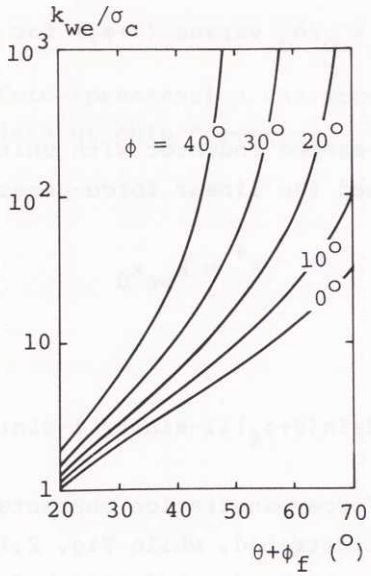

Fig. 2.12. k_{we}/σ_c versus $(\theta+\phi_f)$ for different values of ϕ.

2.2.2.3. Rock removal. - Immediately after the formation of a chip, the crater volume is

$$V = \pi x_d^3 \cot^2\psi/3 \tag{2.19}$$

Further, since during crushing and chipping $F \leq F^*$, the work performed by the force F is certainly

$$W \leq k_{co} x_d^3/3 \tag{2.20}$$

Thus, according to Eqs. (2.16), (2.19) and the inequality (2.20),

$$V/W \geq \kappa_{co} \tag{2.21}$$

where

$$\kappa_{co}\sigma_c = 2\cos\psi\cos(\theta+\phi_f+\phi+\psi)/(1-\sin\phi)\sin(\theta+\phi_f) \tag{2.22}$$

Fig. 2.13 illustrates the relationship between $\kappa_{co}\sigma_c$ and $(\theta+\phi_f)$ for different values of ϕ according to Eqs. (2.22) and (2.10).

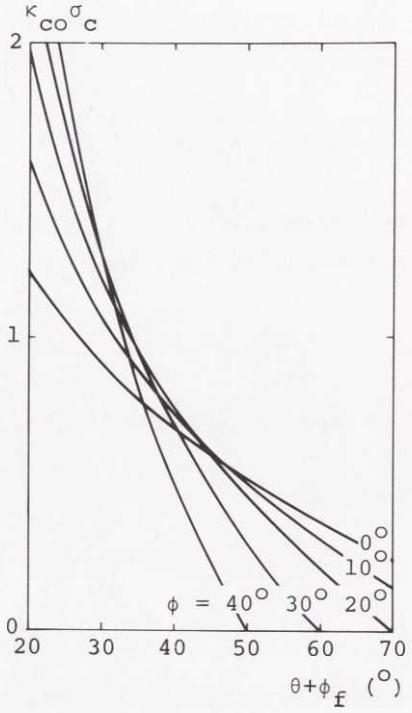

Fig. 2.13. $\kappa_{co}\sigma_c$ versus $(\theta+\phi_f)$ for different values of ϕ.

Paul & Sikarskie made certain assumptions regarding the force-penetration relationship during the crushing phase for a wedge and, based on these assumptions, they determined the work W and the crater volume V. Without making detailed assumptions regarding the force-penetration relationship during the crushing phase (except that $F<F^*$), it is, however, possible to obtain for a wedge the relation corresponding to the inequality (2.21). The result becomes

$$V/W \geq \kappa_{we} \qquad (2.23)$$

where

$$\kappa_{we}\sigma_c = \cot\psi\{1-\sin(\theta+\phi_f+\phi)\}/\sin(\theta+\phi_f)(1-\sin\phi) \qquad (2.24)$$

Fig. 2.14 illustrates the relationship between $\kappa_{we}\sigma_c$ and $(\theta+\phi_f)$ for different values of ϕ according to Eqs. (2.24) and (2.14).

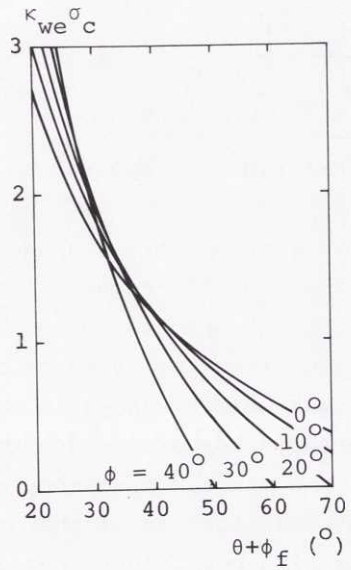

Fig. 2.14. $\kappa_{we}\sigma_c$ versus $(\theta+\phi_f)$ for different values of ϕ.

2.2.3. Experiment

2.2.3.1. Equipment. - The apparatus used in the penetration tests is illustrated in Fig. 2.15.

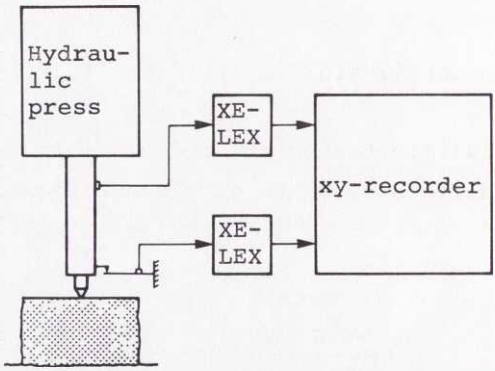

Fig. 2.15. Experimental apparatus.

The use of two sets of strain gauges, two XELEX carrier frequency bridges and one xy-recorder made it possible to record the force versus penetration when a conical indentor was forced into rock material by means of a hydraulic press.

The force-gauges were arranged in such a way that the signal was compensated for errors due to bending and changes in temperature. The carrier frequency was 25 kHz.

With a slight modification of the arrangement shown in Fig. 2.15, it was also possible to perform simple compressive strength tests on cylinders of rock material.

2.2.3.2. Procedure. - The measuring system was calibrated and, with the indentor and rock replaced by a special steel specimen, the rate of loading was adjusted to 1.6 kN/s. Then one conical indentor at a time was pressed into blocks of Swedish Bohus Granite having a plane upper surface and an approximate size of 0.25 m×0.25 m×0.10 m. Force versus penetration was recorded until a maximum value for the force of 40 kN was reached. For each cone-angle, 10-20 force-penetration curves were recorded (one for each crater). The craters were carefully

cleaned and filled with a synthetic clay, which was then removed and weighed. From the mass and density of the clay, the volume of each individual crater was determined. Tests were performed for indentors with cone-angles $2\theta = 60^{\circ}$, 75°, 90°, 110°, 125°, 135° and 150°.

Compressive strength tests were performed on 16 cylindrical specimens of the same rock material. The cylinder length was 44 mm and the diameter was 22 mm.

2.2.3.3. Evaluation. - A number of representative force-penetration records are reproduced in Appendix A. Generally they are similar to the one illustrated in Fig. 2.16.

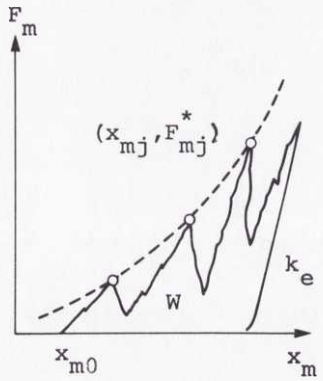

Fig. 2.16. Force-penetration record. Circles mark points of chip formation.

The penetration x of the indentor into the rock material can be expressed as

$$x_m - x_{m0} = x_d + x_e \qquad (2.25)$$

where x_m is the measured position of the indentor and x_{m0} is the value of x_m which corresponds to the first contact between indentor and rock.

In order to compare the experimental results with the theoretical results, the component x_d of the penetration, which is due to destruction of rock, must be determined. To facilitate this determination it is assumed that the elastic component x_e of the penetration can be expressed as

$$x_e = F_m/k_e \tag{2.26}$$

where F_m is the measured force and k_e is the slope of the unloading portion of the force-penetration curve (which is approximated by a straight line).

Consider now one of the points of chip formation. According to Eqs. (2.25) and (2.26), the penetration component x_{dj} can be expressed as

$$x_{dj} = x_{mj} - F^*_{mj}/k_e - x_{m0} \tag{2.27}$$

where index $j = 1, 2, \ldots$ refers to the jth point of chip formation for a single curve and F^*_{mj} is the measured force at that point.

On the other hand, from the theoretical result, Eq. (2.15), the value of the force F at the jth point of chip formation is expected to be

$$F^*_j = k_{co} x^2_{dj} \tag{2.28}$$

where k_{co} is a constant for given indentor and rock material. Therefore, a measure of the deviation of the theoretical results from the experimental results is given by the sum of squares

$$\Sigma_1 = \sum_{j=1}^{n} (F^*_{mj} - F^*_j)^2 \tag{2.29}$$

where n is the number of points of chip formation for a single curve. According to Eqs. (2.27) - (2.29), this sum can be

expressed as

$$\Sigma_1 = \sum_{j=1}^{n} \{F^*_{mj} - k_{co}(x_{mj} - F^*_{mj}/k_e - x_{m0})^2\}^2 \qquad (2.30)$$

and it is easily seen that the sum of squares Σ_1 for each single force-penetration curve is a function of the two unknown quantities x_{m0} and k_{co}.

To allow k_{co} to be determined, the coordinates (x_{mj}, F^*_{mj}) of points of chip formation were measured from the force-penetration records by means of a pencil follower and these coordinates were automatically punched on tape. Also, the slopes k_e of the unloading portion of the records were determined. Then, by means of a computer program, the parameters x_{m0} and k_{co} were determined to make the sum Σ_1 a minimum for each single curve. A direct determination of x_{m0} from the force-penetration records was considered to be too uncertain.

The energy consumed in crushing and chipping was determined as the area under the force-penetration curve, i.e.

$$W = \int F_m dx_m \qquad (2.31)$$

The determination of W according to Eq. (2.31) was made by means of a pencil follower and a computer program. By means of the same computer program also the ratio V/W between crater volume V and consumed energy W was computed.

Finally, average values of k_{co} and V/W were determined for each cone angle 2θ, 90 per cent confidence limits being determined using the assumption of a Students' distribution.

Numerical and statistical analyses as well as development of computer programs were performed by QVARNSTROM & SUNDQVIST (1968).

2.2.3.4. Results. - The average values of k_{co} and V/W are given in Table 2.1. 90 per cent confidence limits are also given in the table.

Table 2.1. Experimental values of k_{co} and V/W for Swedish Bohus Granite. 90 per cent confidence limits.

θ (^{o})	k_{co} (MN/m^2)	V/W ($10^{-8} m^2/N$)
30.0	1100±300	1.38±0.33
37.5	2300±400	1.01±0.26
45.0	4900±800	0.83±0.21
55.0	6300±2600	0.45±0.05
62.5	21000±4000	0.43±0.08
67.5	25000±18000	0.43±0.06
75.0	(No chipping)	0.47±0.01

The compressive strength of the rock material was determined to be

$$\sigma_{cm} = (180 \pm 3) MN/m^2$$

(90 per cent confidence limits).

2.2.3.5. Comparison of theory and experiment. - Now k_{co}, according to Eqs. (2.16) and (2.10), and V/W, according to the inequality (2.21), Eqs. (2.22) and (2.10), can be compared with the corresponding quantities as determined from experiments.

According to theory

$$k_{co} = \sigma_c y(\theta, \phi_f, \phi) \qquad (2.32)$$

where the function y is defined by Eqs. (2.16) and (2.10).

According to the experiments, on the other hand,

$$k_{co} = k_{co}(\theta) \tag{2.33}$$

has been obtained for a number of discrete values θ_j of θ (Table 2.1).

Therefore, a measure of the deviation of the theoretical results from the experimental results can be chosen as the sum of squares

$$\Sigma_2 = \sum_j \{k_{co}(\theta_j) - \sigma_c y(\theta_j, \phi_f, \phi)\}^2 \tag{2.34}$$

which is seen to be a function of the parameters σ_c, ϕ_f and ϕ. Since no attempt was made to directly measure ϕ_f or ϕ, the following two procedures could be employed in order to fit the theoretical results to the experimental results and indirectly determine ϕ_f and ϕ.

First, the experimentally determined value σ_{cm} is assigned to the compressive strength σ_c in Eq. (2.34) and those values of the parameters ϕ_f and ϕ that make the sum Σ_2 a minimum are determined. Then it is judged if the values obtained for ϕ_f and ϕ are reasonable and the theoretical functions k_{co} and κ_{co} are compared with the experimental values of k_{co} and V/W respectively for different values of θ.

Secondly, σ_c as well as ϕ_f and ϕ are determined in such a way that they make the sum Σ_2 a minimum. Then σ_c is compared with the measured value σ_{cm} and it is again judged if the values obtained for ϕ_f and ϕ are reasonable. Also, the theoretical functions k_{co} and κ_{co} are compared with the experimental values of k_{co} and V/W respectively for different values of θ.

The values obtained for σ_c, ϕ_f and ϕ according to the two procedures, are summarized in Table 2.2.

Table 2.2. Determination of σ_c, ϕ_f and ϕ according to the method of least squares.

Method	σ_c (MN/m^2)	ϕ_f (^{o})	ϕ (^{o})
1st	180	1	2
2nd	113	6	0

Fig. 2.17 shows theoretical ($\phi_f = 6^o$, $\phi = 0^o$, $\sigma_c = 113$ MN/m^2) and experimental values of k_{co} versus θ according to the second method of comparison. Fig. 2.18 shows κ_{co} according to theory and the experimental values of V/W versus θ for the same values of ϕ_f, ϕ and σ_c.

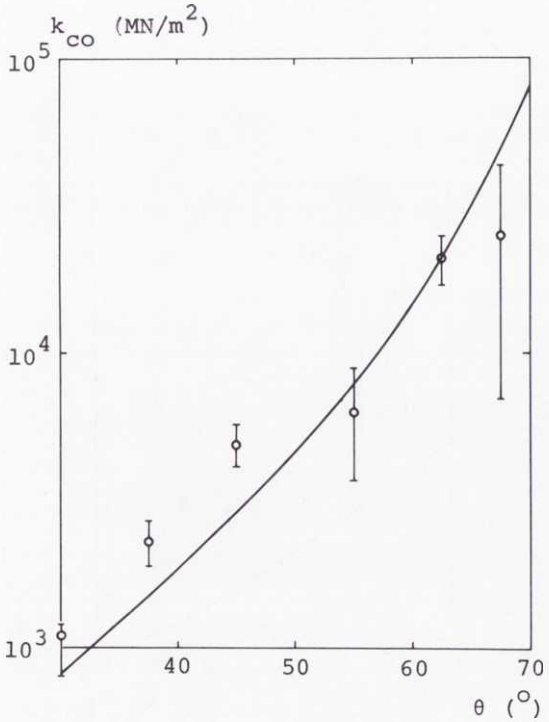

Fig. 2.17. k_{co} versus θ according to theory (σ_c = 113 MN/m^2, $\phi_f = 6^\circ$ and $\phi = 0^\circ$) and experiment.

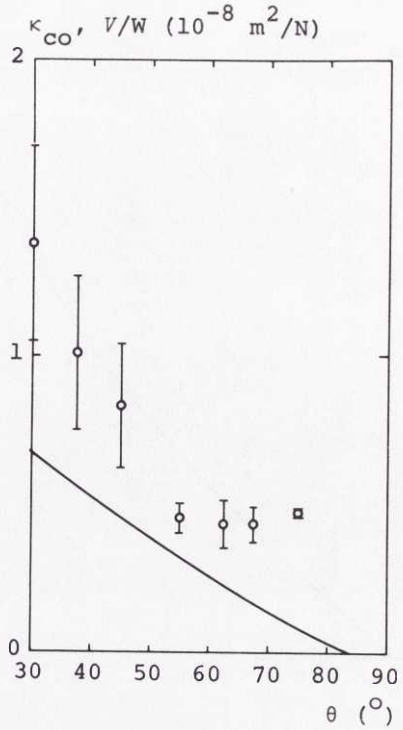

Fig. 2.18. κ_{co} according to theory (σ_c = 113 MN/m^2, $\phi_f = 6^\circ$ and $\phi = 0^\circ$) and V/W according to experiment versus θ.

According to Eq. (2.12) and the values obtained for ϕ_f and ϕ in the second procedure above, the critical half cone angle with respect to chipping is $\theta_{cr} = 84^\circ$. Thus, for consistency, chipping should not occur for $\theta > 84^\circ$.

In the experiments, chipping normally occurred for θ = = 30°-67.5° whereas chipping normally did not occur for $\theta = 75^\circ$. Also, it can be seen from Fig. 2.18 that the experimental values of V/W become essentially constant when θ is larger than approximately 60°. This can be interpreted as a gradual transition to only crushing behaviour.

2.2.4. Discussion

The results obtained here for a cone-shaped indentor are similar to those obtained by PAUL & SIKARSKIE (1965) for a wedge-shaped indentor. Considering the many common basic assumptions made, however, this agreement was to be expected.

Figs. 2.7 and 2.8 illustrate that the angle of failure ψ depends on $(\theta+\phi_f+\phi)$ in a similar way for the cone and for the wedge. However, the angle of failure is generally smaller for the wedge than for the cone. Also, the critical half cone-angle and the critical half wedge-angle with respect to chip formation are the same.

A significant difference between the cone and the wedge can be observed in the force-penetration relationships. Thus the force at chip formation for a cone is proportional to the square of penetration, whereas the force at chip formation for a wedge is proportional to penetration. However, it can be seen from Figs. 2.10 and 2.12 that the constants of proportionality k_{co} and k_{we} depend on σ_c, θ, ϕ_f and ϕ in similar ways.

Figs. 2.13 and 2.14 illustrate that rock removal behaviour is very much the same for the cone and the wedge.

According to Table 2.2 and Fig. 2.17, the best agreement (in the sense defined here) between theoretical and experimental results for cone penetration into Bohus Granite is obtained when σ_c = 113 MN/m^2, $\phi_f = 6^\circ$ and $\phi = 0^\circ$. The experimentally determined value of the compressive strength is σ_{cm} = 118 MN/m^2, while no attempt was made to determine directly the angle of friction ϕ_f and the angle of internal friction ϕ. However, the value $\phi = 0^\circ$ is certainly too low. Also, the value $\phi_f = 6^\circ$ is probably too low.

To summarize, the best agreement between theoretically determined and experimentally observed force-penetration envelopes for cones is obtained when lower values than the real values are given to the parameters σ_c, ϕ_f and ϕ. Since, according to Eqs. (2.16) and (2.10), the force-penetration

constant k_{co} is an increasing function of these parameters, it is obvious that for real values of the parameters σ_c, ϕ_f and ϕ, the theory gives an overestimation of the force F^* at chip formation.

Corresponding observations were made for a wedge by Paul & Sikarskie. With the assumption that $\phi_f = 0^\circ$, they obtained the best agreement between theoretically determined and experimentally observed force-penetration relations for wedges for very low values of ϕ (0°-10°) and a lower value of σ_c than was experimentally observed.

Paul & Sikarskie argue that there are two main reasons for the fact that the predicted values of the force-penetration constants are too high. First, the assumption that the Coulomb-Mohr failure criterion is simultaneously satisfied over the whole surface of failure contributes to the overestimation. Actually, the surface of failure is instead formed by cracks which are growing in size and therefore the required force is less. Secondly, the experimentally obtained value of the compressive strength σ_c may be too high because of lateral constraints at the ends of the test specimen. Since k_{co} as well as k_{we} is proportional to σ_c, corresponding errors result in the force-penetration constants.

Fig. 2.18 shows that for $\sigma_c = 113$ MN/m^2, $\phi_f = 6^\circ$ and $\phi = 0^\circ$ the theoretically determined relationship between κ_{co} and θ is consistent with the inequality (2.21) and the experimentally obtained relationship between V/W and θ.

Independently of the author, MILLER & SIKARSKIE (1968) extended the analysis by PAUL & SIKARSKIE (1965) to cone-shaped and also pyramid-shaped indentors. The first part of their analysis for cones is essentially identical with the analysis presented by the author previously (LUNDBERG, 1967; LUNDBERG, LUNDQVIST & MEYER, 1968) and in the present work. Thus, for example, for $\phi_f = 0^\circ$ they obtained the same relationship between the angle of failure ψ and $(\theta+\phi)$ as has been

obtained here between ψ and $(\theta+\phi_f+\phi)$. Also, they obtained the same quadratic relationship between the force F^* at chip formation and penetration x_d. Instead of determining a lower bound κ_{co} for the ratio of crater volume V and energy W, however, they made certain assumptions regarding the force-penetration relationship during the crushing phase and, based on these assumptions, they determined the work W and the crater volume V. They assumed a linear or a piece-wise linear force-penetration relationship during crushing and the ratio V/W became a function of penetration.

Another consequence of Miller & Sikarskie's assumptions regarding the crushing process is that when penetration exceeds a critical value chip formation is no longer possible. The reason is that the assumed crushing curve F(x) does not intersect the chip formation envelope $F^*(x)$, which rises steeper. Thus, even if the half cone-angle θ is less than the critical value θ_{cr}, chip formation may be impossible. This underlines that the inequality (2.11) is not a sufficient condition for chip failure and may be part of the explanation of the fact that, in the experimental results presented above, chip formation did not occur for θ greater than 60^o-75^o, whereas from theoretical and experimental results $\theta_{cr} = 84^o$. Another part of the explanation is, of course, that $\theta_{cr} = 84^o$ is a high value caused by the low values of ϕ_f and ϕ.

Miller & Sikarskie's experimental results did not prove or disprove conclusively the existence of a quadratic chipping envelope. The extent of the present experimental investigation has also been too small to make definite conclusions possible. However, the good qualitative agreement obtained here between thoery and experiment indicates that the quadratic chipping envelope is an essentially correct result. Attempts by Miller & Sikarskie to establish a relationship between specific energy (W/V) and penetration were rejected because of the large scatter exhibited by the data.

2.3. Dynamic Versus Static Loading

The conceptions "dynamic loading" and "static loading" are not unique and can be given different meanings. Here, dynamic loading of rock shall simply denote the type of loading that occurs in percussive rock destruction devices such as, for example, drop-hammers. The rate of loading may be typically of the order of, say 10^6 kN/s. Static loading of rock shall simply denote the type of loading that occurs in slow devices such as, for example, hydraulic presses. The rate of loading may typically be of the order of, say, 1 kN/s or less.

The question now arises as to whether the results obtained in Section 2.2 are applicable to percussive rock destruction even though no dynamic effects were taken into consideration. An indication may be obtained by studying whether there are significant differences between dynamic and static indentation experiments or not.

In Table 2.3, some results from different dynamic and static force-penetration experiments, which were collected by HUSTRULID (1968), are reproduced. In the table, k is the force per unit penetration for a wedge of unit length and θ is the half wedge-angle. The references given by Hustrulid are repeated in the table.

Table 2.3. Comparison of static and dynamic force-penetration constants using a sharp wedge bit (1 inch in length) in Indiana Limestone.

Wedge Angle 2θ (^{o})	Force-penetration Constant k (MN/m^2)		Peak Force (kN)	Investigator
	Static	Dynamic		
75	300	-	9	GNIRK (1962)
75	430	-	13	HUSTRULID (1968)
75	-	460	45	STEPHENSON (1963)
90	370	-	16	GNIRK
90	610	-	28	HUSTRULID
90	680	-	89	HAIMSON (1965)
90	-	690	58	STEPHENSON
105	530	-	16	GNIRK
105	870	-	27	HUSTRULID
105	-	1170	76	STEPHENSON
120	870	-	27	GNIRK
120	1060*	-	27	HUSTRULID
120	1090**	-	42	HUSTRULID
120	-	2070	107	STEPHENSON

102

* Indentation parallel to bedding.

** Indentation perpendicular to bedding.

As can be seen in Table 2.3, the results have been obtained by different investigators under different conditions (e.g. different peak forces). Therefore it is not surprising that there is a certain scatter even in static values obtained for the force-penetration constant k for the same half wedge-angle θ. Also, differences in dynamic and static values of k may, of course, be much influenced by these different conditions (it should be noticed that the dynamic peak forces have been considerably higher than the static peak forces when $2\theta = 75^{\circ}$, 105° and 120°). Therefore, the conclusions drawn from the results in Table 2.3 cannot be very extensive.

However, as was noticed by Hustrulid, the results in Table 2.3 do not indicate any large differences between dynamic and static values of k for the smaller wedge-angles, $2\theta = 75^{\circ}$ and 90°, whereas for the wedge-angle $2\theta = 120^{\circ}$ the dynamic force-penetration constant appears to be larger than the static one by a factor of two.

HUSTRULID (1968) performed force-penetration tests with winged bits on rough surfaces for different indexing angles and different types of rock. From these experiments he found that the average dynamic force-penetration constant is only slightly higher than the average static value. He concluded that the effect of rate of loading is reduced when the rock surface is rough.

STEPHENSON (1963) found for Indiana Limestone that the change of slope of the force-penetration curve is a very "slow" function of velocity. Thus, he found that when the penetration velocity is increased by five or six orders of magnitude, as from static to dynamic tests, the slope is increased by a factor of approximately two. For penetration velocities in the interval 0.4 m/s - 6.4 m/s, however, he found no influence of changes in penetration velocity. For a limited number of tests on three other rock types he did not find any significant difference even between static and dynamic tests.

As regards the ratio of crater volume and energy V/W for indentations on rough surfaces of Pink Tennessee Marble, White Tennessee Marble and Charcoal Granite, Hustrulid obtained higher values for the static tests than for the dynamic tests. Thus, in static tests, he generally obtained values of V/W higher than the inverse of the compressive strength $1/\sigma_c$ of the rock material, while in dynamic tests he generally obtained values of V/W lower than $1/\sigma_c$. The difference appears to be a factor of approximately two. This result is supported by results obtained by HAIMSON & FAIRHURST (1971) for Pink Tennessee Marble but is in direct contrast with results obtained by STEPHENSON (1963) for Indiana Limestone.

To summarize, the results obtained by several investigators indicate that certain differences may exist between static and dynamic penetration of an indentor into rock material. Thus, there are indications that the force-penetration constant k is higher and that the ratio V/W may be higher or lower in the dynamic tests than in the static tests. The differences may be a factor of two, but sometimes less. Therefore, to a certain extent but rather in a qualitative than quantitative sense, the results obtained in Section 2.2 should be applicable to situations in percussive rock destruction, even though dynamic effects were neglected in the analysis.

2.4. Bit Penetration Models

In Chapters 3 and 4, different methods of percussive rock destruction will be studied. A main interest in this study will be the transfer of impact energy (or stress wave energy) W_i to work W in rock destruction. In order to determine W/W_i, however, the force-penetration relationship, say $F(x,dx/dt)$, must be known. The ratio of crater volume V to impact energy (or stress wave energy) W_i can then be determined as $V/W_i = (V/W)(W/W_i)$ if the ratio V/W is known. Thus, ideally, the force-penetration relationship $F(x,dx/dt)$ and the ratio V/W should be known for the actual bit-rock combi-

nation (bit composed of several cutter elements, rough and previously damaged surface of rock etc.) under the actual conditions (water in the drill hole etc.).

In Section 2.2, some theoretical results were given regarding the penetration of a single cone or wedge into a piece of rock with a plane surface (upper bound of F and lower bound of V/W). Dynamic effects were neglected in the analysis but it was concluded in Section 2.3 that F as well as V/W seem to be somewhat different under static and dynamic conditions.

Obviously, the theoretical results in Section 2.2 will not be sufficient for the analyses in Chapters 3 and 4. It is not believed either that such sufficient theoretical results exist anywhere else. Therefore, the best thing to do is to idealize results which are obtained from measurements under conditions which are as much as possible realistic. Such measurements have been performed e.g. by HUSTRULID (1968).

Sometimes, at least for single impact devices, the detailed force-penetration relationship $F(x,dx/dt)$ and a particular value of V/W may be of interest. More often, however, rather a time average behaviour is of interest. In such cases it seems natural to represent $F(x,dx/dt)$ with a simple function and V/W with a constant value.

Below, three different force-penetration relationships are given. With reference to the results obtained by STEPHENSON (1963), it is assumed that the force F is independent of the absolute value $|dx/dt|$ of the penetration velocity. The force-penetration relationships are assumed to correspond either to a particular impact or to time average behaviour. V/W is assumed to be measured or else estimated as the inverse of the compressive strength $1/\sigma_c$.

The simplest force-penetration relationship that will be employed is shown in Fig. 2.19. Similar relationships were employed e.g. by FAIRHURST (1961c), SIMON (1964) and HUSTRULID (1968).

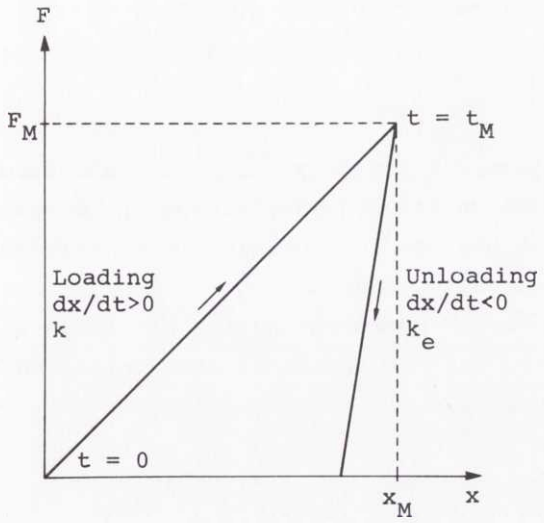

Fig. 2.19. Force-penetration curve with a linear loading section.

When $dx/dt \geq 0$ $(0 \leq t \leq t_M)$ the force is proportional to penetration , i.e.

$$F = kx \tag{2.35}$$

When $dx/dt < 0$ $(t > t_M)$ the force is proportional to the change in penetration, i.e.

$$F = F_M + k_e(x - x_M) \tag{2.36}$$

where x_M is the maximum penetration and

$$F_M = kx_M \tag{2.37}$$

is the corresponding maximum force.

Eq. (2.35) describes the loading phase and Eq. (2.36) describes the unloading phase. k and k_e represent properties

of the bit-rock combination. Thus,

$$\gamma = k/k_e \tag{2.38}$$

is a measure of the degree of elastic deformation of the rock for the given bit ($\gamma = 0$ corresponds to completely inelastic behaviour and $\gamma = 1$ to completely elastic behaviour). x_M and F_M depend on the load.

The work W performed by the bit is equal to the area bounded by the loading curve, the unloading curve and the x-axis. Thus,

$$W = (1-\gamma)F_M^2/2k \tag{2.39}$$

or

$$W = (1-\gamma)kx_M^2/2 \tag{2.40}$$

A simple representation of a force-penetration relationship with a non-linear loading section is illustrated in Fig. 2.20. This relationship was also employed e.g. by BERRY (1959).

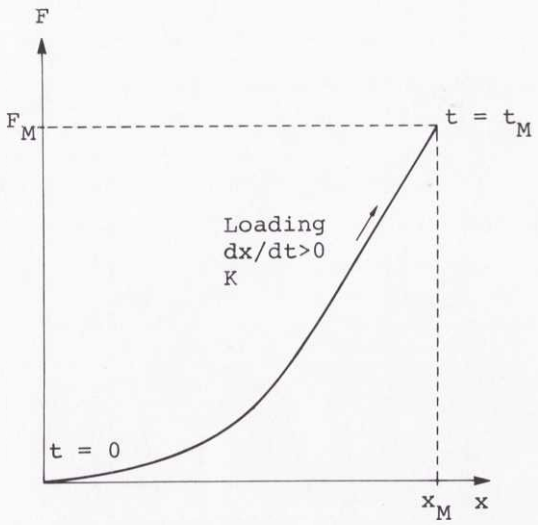

Fig. 2.20. Force-penetration curve with a parabolic loading section.

When $dx/dt>0$ ($0<t<t_M$) the force is proportional to the square of penetration, i.e.

$$F = Kx^2 \tag{2.41}$$

When $dx/dt\leq 0$ the contact between bit and rock is interrupted ($F = 0$), i.e. the behaviour of the rock is completely inelastic.

The work W performed by the bit is equal to

$$W = F_M^{3/2}/3K^{1/2} \tag{2.42}$$

where F_M is again the maximum force.

A detailed representation of a particular (measured) force-penetration relation by means of piece-wise linear segments is illustrated in Fig. 2.21. This relationship was

employed by THURESSON (1971a, b) in collaboration with the author. A similar relationship was also employed earlier e.g. by HUSTRULID (1968).

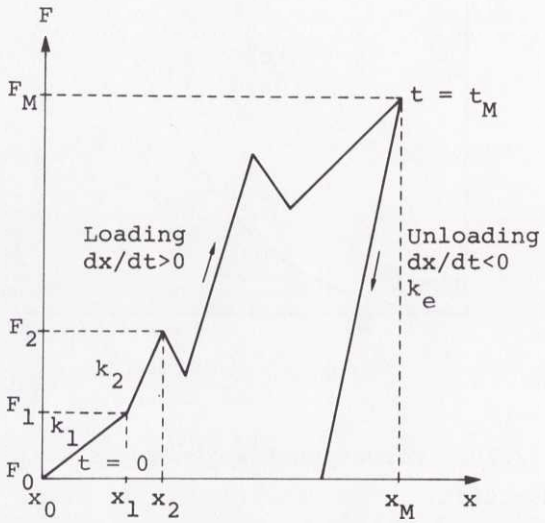

Fig. 2.21. Force-penetration curve with a piece-wise linear loading section.

The force-penetration relation illustrated in Fig. 2.21 is a generalization of the one illustrated in Fig. 2.19. Thus, the fundamental assumptions are the same, but the loading section is piece-wise linear and determined by the coordinates (x_j, F_j) $(j = 1, 2, \ldots)$ of the breaking points.

When $dx/dt \geq 0$ $(0 \leq t \leq t_M)$ the force F is given by

$$F(x) = F_{j-1} + k_j (x - x_{j-1}) \qquad (j = 1, 2, \ldots) \quad (2.43)$$

if x belongs to the interval

$$x_{j-1} \leq x < x_j \qquad (j = 1, 2, \ldots) \quad (2.44)$$

When $dx/dt<0$ ($t>t_M$), Eq. (2.36) is valid.

The work W performed by the bit is again equal to the area bounded by the loading curve, the unloading curve and the x-axis.

In general, the loads considered will be of such a nature that there is only one loading-unloading cycle. In Section 4.2, however, repeated loading will be considered. In such a case the reloading starts along the unloading curve and continues until $x = x_M$ and $F = F_M$. Then the loading continues the same way as during the first loading until the penetration velocity dx/dt again becomes negative etc.

3. BASIC METHODS IN PERCUSSIVE ROCK DESTRUCTION

3.1. Introduction

As was stated in Section 1.2, percussive rock destruction is often based upon one of the three basic methods illustrated in Fig. 1.1. It is convenient to name them the churn drilling method, the down-the-hole drilling method and the hammer drilling method respectively.

Even if many publications have dealt with problems connected with these three methods (Section 1.3), they do not appear to have been previously compared much with each other from an efficiency point of view. One reason for this may be that in many practical situations the geometrical proportions differ markedly between the methods. Thus, in down-the-hole drilling, the lengths of the bit and the hammer are usually approximately equal, whereas in hammer drilling, the bit is normally much shorter than the hammer.

It has not been found that the influence of bit mass in hammer drilling has been given much attention previously. Normally, it has been assumed that the bit is massless (e.g. FAIRHURST, 196lc; SIMON, 1964; HUSTRULID, 1968). One reason for this assumption is that in some situations of practical importance (integral steel drilling) zero bit mass is a good approximation. SIMON (1964) verified this by comparing the stress wave reflected from the bit with the stress wave incident towards the bit when the bit was free. Another reason is that the analysis becomes much simplified if bit mass is neglected.

In the following sections, the three methods of percussive rock destruction will be analysed and compared. As it is shown in Fig. 3.1, similar idealized conditions are assumed to prevail in all three cases.

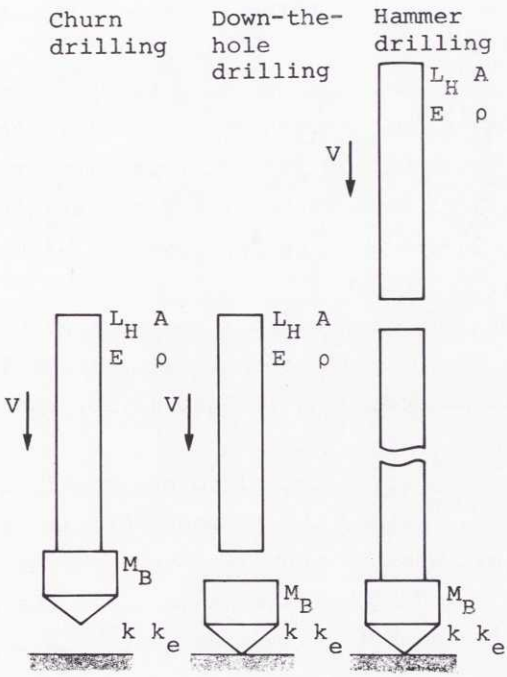

Fig. 3.1. Basic methods of percussive rock destruction.

The hammers and the drill rod are all assumed to be cylindrical and to have equal cross sectional areas $A_H = A_R = A$, equal Young's moduli $E_H = E_R = E$, and equal densities $\rho_H = \rho_R = \rho$. The length of the hammers is L_H and the length of the rod is $L_R >> L_H$.

The motions of the hammers and the rod are assumed to be governed by the elementary one-dimensional wave equation (Appendix B). This implies that the stress wave propagation in hammers and rod is non-dispersive and that the propagation velocity is equal to the sonic velocity

$$c = (E/\rho)^{1/2} \tag{3.1}$$

The same assumption has normally been made also by other investigators.

The bit is assumed to be rigid with a mass M_B. Therefore, its motion is governed by rigid body mechanics and the state of stress in its different parts is not considered. The complexity of this state of stress is illustrated by the photoelastic investigations performed by BABENKOV, IVANOV & HESIN (1965).

The interaction between bit and rock is characterized by a force-penetration relationship with linear loading and unloading sections according to Eqs. (2.35) and (2.36) respectively.

In order to justify the rigid bit model, two assumptions have been made. First, the propagation time for a stress wave through the bit must be much less than the propagation time for a stress wave through the hammer. If the propagation velocity is the same in hammer and bit this implies that

$$L_B/L_H \ll 1 \tag{3.2}$$

where L_B is the bit length. Secondly, when the bit penetrates into the rock, the elastic decrease in bit length must be much less than the penetration under the actual impact loading conditions. Under static loading conditions this condition can be easily formulated in mathematical terms. Then the decrease in bit length is $L_B F/A_B E_B$, where F is the static force, A_B is the cross sectional area of the bit and E_B is Young's modulus of the bit, while the bit penetration into the rock is F/k. Therefore, the condition becomes

$$kL_B/A_B E_B \ll 1 \tag{3.3}$$

under static loading conditions. In Section 3.2.3.2 it will be shown that the same condition is obtained also under certain impact loading conditions.

The condition (3.2) is usually satisfied in normal hammer drilling but not in normal down-the-hole drilling. However, this condition may be satisfied in drop-hammer devices, which are based on the down-the-hole drilling method.

The condition (3.3) can be tested by considering the following situation:

$A_B = 1.0\ 10^{-2}\ m^2$

$E_B = 2.0\ 10^{11}\ N/m^2$

$L_B = 0.10\ m$

0.10 m 120° wedge in contact with rock

Table 2.3: HUSTRULID (1968)

In this case, $kL_B/A_BE_B = 0.005$ and the condition (3.3) is satisfied.

Before impact the systems are free from stresses. This assumption is generally valid for single impact or low frequency impact devices. It is also often a good approximation in real rock drills, since the time between two successive blows is normally as long as 20-30 ms and there are internal as well as external sources of damping.

Before impact the systems are also at rest with the exceptions of the impacting elements which have the impact velocity V. The bits, in the cases of down-the-hole drilling and hammer drilling, are assumed to be initially in forceless contact with the rock. These assumptions are closely connected with the feeding systems (HUSTRULID, 1968) and are only to a certain extent fulfilled in actual down-the-hole or hammer rock drills. In different kinds of single impact devices, such as for example drop-hammers, they may be to a high degree fulfilled.

Effects of gravity are neglected since the forces due to gravity are very small compared to the impulsive forces caused by impact. It is also assumed that no flexural waves are generated.

In the cases of churn drilling and down-the-hole drilling, impact is assumed to occur at time $t = 0$, while in the case of hammer drilling, impact is assumed to occur at time $t = -L_R/c$. Therefore, the bit penetration into rock always starts when $t = 0$ in agreement with Fig. 2.19.

In the following sections the mechanical behaviour of the three systems will be studied.

The maximum forces F_M acting between bit and rock will be determined. F_M will be represented in non-dimensional form as

$$f_M = F_M/F_0 \tag{3.4}$$

where

$$F_0 = AEV/2c \tag{3.5}$$

F_0 is equal to the force acting at impact between two equal cylindrical rods, each with cross sectional area A, Young's modulus E and sonic velocity c, when the relative impact velocity is V (Appendix B.5).

The maximum forces are of importance in connection with the rock destruction process as well as with the bit life.

Also, the efficiencies η will be determined as

$$\eta = W/W_i \tag{3.6}$$

where W is the work performed by the bit on the rock and W_i is the impact energy.

The efficiencies are significant in optimization of rock drill performance as well as in the interpretation of different types of drop-hammer experiments (HUSTRULID, 1968).

The results obtained for the three methods will be compared with each other. Some results obtained from the theoretical analysis will also be compared with experimental results.

3.2. Churn Drilling Method

3.2.1. Penetration of the bit

3.2.1.1. Finite mass bit. - Consider first the situation when the mass M_B of the bit is finite. This situation is illustrated in Fig. 3.2.

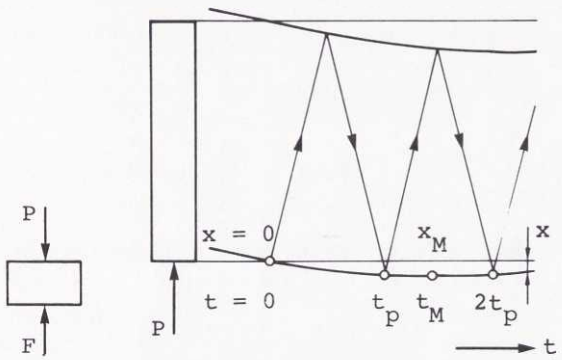

Fig. 3.2. Hammer and bit motion in churn drilling.

When at time t = 0 the bit impacts the rock, a compressive stress wave σ is generated at the hammer-bit interface, where it is denoted by $\sigma(t)$ (Appendix B). This stress wave propagates towards the free end of the hammer, where it is reflected as a tensile wave $-\sigma$. The front of this tensile wave arrives at the bit at time

$$t_p = 2L_H/c \qquad (3.7)$$

where for $t \geq t_p$ the resulting stress therefore becomes $\sigma(t)-\sigma(t-t_p)$. Under the combined action of the stress waves, the bit is accelerated towards the rock, and work W is performed.

The equation of motion of the bit is

$$M_B d^2x(t)/dt^2 = P(t)-F(t) \tag{3.8}$$

where, as illustrated in Fig. 3.2, x is the bit penetration into the rock, P is the force acting between hammer and bit and F is the force acting between bit and rock.

When

$$0 \leq t < t_p \tag{3.9}$$

the force P can be expressed as

$$P(t) = -A\sigma(t) \tag{3.10}$$

while the penetration velocity is (Appendix B)

$$dx(t)/dt = V+(c/E)\sigma(t) \tag{3.11}$$

Further, as long as the penetration velocity is non-negative, i.e.

$$dx(t)/dt \geq 0 \tag{3.12}$$

the force F and the penetration x are related according to Eq. (2.35), i.e.

$$F(t) = kx(t) \tag{2.35}$$

Elimination of P, F and σ in Eqs. (3.8), (3.10), (3.11) and (2.35) yields the differential equation

$$(M_B/k)d^2x(t)/dt^2+(AE/kc)dx(t)/dt+x(t) = (AE/kc)V \tag{3.13}$$

The initial conditions are

$$x(0) = 0 \tag{3.14}$$

and

$$dx(0)/dt = V \tag{3.15}$$

In Eqs. (3.13)-(3.15) it is convenient to introduce the non-dimensional time

$$\tau = t/t_0 \tag{3.16}$$

where

$$t_0 = AE/kc \tag{3.17}$$

Further, it is convenient to introduce the non-dimensional penetration

$$\xi = x/x_0 \tag{3.18}$$

where

$$x_0 = t_0 V \tag{3.19}$$

or according to Eq. (3.17),

$$x_0 = AEV/kc \tag{3.20}$$

If, finally, the non-dimensional bit mass

$$\alpha = 4kc^2 M_B/A^2E^2 \tag{3.21}$$

is introduced, Eqs. (3.13)-(3.15) can be transformed into

$$(\alpha/4)d^2\xi(\tau)/d\tau^2+d\xi(\tau)/d\tau+\xi(\tau) = 1 \tag{3.22}$$

$$\xi(0) = 0 \tag{3.23}$$

and

$$d\xi(0)/d\tau = 1 \tag{3.24}$$

respectively. The solution of Eqs. (3.22)-(3.24) is valid in the interval

$$0\leq\tau<\beta \tag{3.25}$$

where

$$\beta = t_p/t_0 \tag{3.26}$$

as long as

$$d\xi(\tau)/dt\geq 0 \tag{3.27}$$

When

$$t\geq t_p \tag{3.28}$$

Eqs. (3.10) and (3.11) are replaced by

$$P(t) = -A\{\sigma(t)-\sigma(t-t_p)\} \tag{3.29}$$

and

$$dx(t)/dt = V+(c/E)\sigma(t)+(c/E)\sigma(t-t_p) \tag{3.30}$$

respectively (Appendix B). If again the penetration velocity

is non-negative according to the inequality (3.12), then F and x are related according to Eq. (2.35).

Eqs. (2.35), (3.8), (3.11), (3.22), (3.29) and (3.30) and reintroduction of non-dimensional variables yield the differential equation

$$(\alpha/4)d^2\xi(\tau)/d\tau^2+d\xi(\tau)/d\tau+\xi(\tau) =$$
$$= -(\alpha/4)d^2\xi(\tau-\beta)/d\tau^2+d\xi(\tau-\beta)/d\tau-\xi(\tau-\beta) \qquad (3.31)$$

Since $\xi(\tau)$ and $d\xi(\tau)/d\tau$ must be continuous functions

$$\xi(n\beta) = \lim_{\tau\to n\beta-} \xi(\tau) \qquad (n = 1, 2, \ldots) \qquad (3.32)$$

and

$$d\xi(n\beta)/d\tau = \lim_{\tau\to n\beta-} d\xi(\tau)/d\tau \qquad (n = 1, 2, \ldots) \qquad (3.33)$$

respectively. The solution of Eqs. (3.31)-(3.33) is valid in the interval

$$\tau \geq \beta \qquad (3.34)$$

as long as the inequality (3.27) is satisfied.

The non-dimensional time

$$\tau_M = t_M/t_0 \qquad (3.35)$$

which makes the non-dimensional penetration ξ equal to its maximum value $\xi(\tau_M)$ or

$$\xi_M = x_M/x_0 \qquad (3.36)$$

can readily be obtained from the solution $\xi(\tau)$ of Eqs. (3.22)-(3.24) and Eqs. (3.31)-(3.33) for n = 1, 2, ... Then, according to the inequality (3.27), the solution $\xi(\tau)$ is valid in the interval

$$0 \leq \tau \leq \tau_M \tag{3.37}$$

Naturally, the solution can be extended to $\tau > \tau_M$ by employing the unloading section according to Eq. (2.36) of the force-penetration relationship. However, this will not be done here, since to determine the maximum force acting on the rock and the efficiency it is sufficient to know $\xi_M = \xi(\tau_M)$.

The details of the determination of $\xi(\tau)$ from Eqs. (3.22)-(3.24) and Eqs. (3.31)-(3.33) are given in Appendix C.

3.2.1.2. Zero mass bit. - According to Eq. (3.21) a bit of zero mass corresponds to $\alpha = 0$. Then Eqs. (3.22) and (3.23) yield

$$d\xi(\tau)/d\tau + \xi(\tau) = 1 \tag{3.38}$$

and

$$\xi(0) = 0 \tag{3.23}$$

respectively. The solution of Eqs. (3.38) and (3.23) is valid when $0 \leq \tau < \beta$ and $0 \leq \tau \leq \tau_M$.

Further, Eqs. (3.31) and (3.32) yield

$$d\xi(\tau)/d\tau + \xi(\tau) = d\xi(\tau-\beta)/d\tau - \xi(\tau-\beta) \tag{3.39}$$

and

$$\xi(n\beta) = \lim_{\tau \to n\beta-} \xi(\tau) \qquad (n = 1, 2, \ldots) \tag{3.32}$$

respectively. The solution of Eqs. (3.39) and (3.32) is valid when $\tau \geq \beta$ and $0 \leq \tau \leq \tau_M$.

The solution $\xi(\tau)$ of Eqs. (3.38), (3.23), (3.39) and (3.32) taken together is valid in the interval

$$0 \leq \tau \leq \tau_M \tag{3.37}$$

The condition (3.23) is now equivalent to the condition (3.24), whereas the condition (3.33) has been omitted, since when $\alpha = 0$, $d\xi(\tau)/d\tau$ need no longer be a continuous function.

Eqs. (3.38) and (3.23) yield

$$\xi = 1-e^{-\tau} \tag{3.40}$$

Since from Eq. (3.40) it is apparent that $d\xi(\tau)/d\tau > 0$ when $0 \leq \tau < \beta$, it is seen that $\tau_M \geq \beta$. Thus, the solution $\xi(\tau)$ can be extended to $\tau \geq \beta$.

Eqs. (3.39) and (3.40) yield

$$d\xi/d\tau+\xi = 2e^{-(\tau-\beta)}-1 \tag{3.41}$$

while Eqs. (3.32) and (3.40) yield

$$\xi(\beta) = 1-e^{-\beta} \tag{3.42}$$

The solution $\xi(\tau)$ of Eqs. (3.41) and (3.42) is valid when $\beta \leq \tau < 2\beta$ and $0 \leq \tau \leq \tau_M$. It takes the form

$$\xi = 2(\tau-\beta)e^{-(\tau-\beta)}+(2-e^{-\beta})e^{-(\tau-\beta)}-1 \tag{3.43}$$

Eq. (3.43) yields

$$d\xi/d\tau = e^{-(\tau-\beta)}\{e^{-\beta}-2(\tau-\beta)\} \tag{3.44}$$

Thus, it is seen that $d\xi(\tau)/d\tau > 0$ when

$$\beta \leq \tau < \beta + (1/2)e^{-\beta} \tag{3.45}$$

whereas $d\xi(\tau)/d\tau = 0$ when

$$\tau = \beta + (1/2)e^{-\beta} \tag{3.46}$$

Therefore,

$$\tau_M = \beta + (1/2)e^{-\beta} \tag{3.47}$$

and

$$\beta < \tau_M < 2\beta \tag{3.48}$$

provided

$$(1/2)e^{-\beta} < \beta \tag{3.49}$$

i.e.

$$\beta > 0.3517 \tag{3.50}$$

Finally, from Eqs. (3.43) and (3.47) the maximum non-dimensional penetration $\xi_M = \xi(\tau_M)$ is obtained as

$$\xi_M = 2e^{-(1/2)e^{-\beta}} - 1 \tag{3.51}$$

provided that the inequality (3.50) is satisfied.

By employing Eqs. (3.39) and (3.32) for n = 2, 3, ..., ξ_M can also be determined when $\beta \leq 0.3517$. However, as will be seen subsequently, this extension would be of only little interest.

.2.2. Bit force and efficiency

The maximum force F_M acting on rock is given by Eq. (2.37) while a non-dimensional maximum force f_M is defined by Eq. (3.4). According to Eqs. (3.5), (3.36) and (3.20), the latter can be expressed in terms of the non-dimensional maximum penetration $\xi_M(\alpha,\beta)$ as

$$f_M = 2\xi_M(\alpha,\beta) \tag{3.52}$$

Further, the efficiency η of energy transfer to rock is defined in Eq. (3.6) as

$$\eta = W/W_i \tag{3.6}$$

Here the work W performed on the rock is given by Eq. (2.40) whilst the impact energy is

$$W_i = (1/2)(M_H+M_B)V^2 \tag{3.53}$$

where

$$M_H = \rho A L_H \tag{3.54}$$

is the mass of the hammer. By combining Eqs. (2.40), (3.1), (3.6), (3.7), (3.17), (3.20), (3.21), (3.26), (3.36), (3.53) and (3.54), the efficiency can be expressed in terms of the non-dimensional quantities ξ_M, α, β and γ as

$$\eta = 4(1-\gamma)\xi_M^2(\alpha,\beta)/(\alpha+2\beta) \tag{3.55}$$

According to Eqs. (3.52) and (3.55), the efficiency can also be expressed as

$$\eta = (1-\gamma)f_M^2(\alpha,\beta)/(\alpha+2\beta) \tag{3.56}$$

In the case $\alpha = 0$ and $\beta > 0.3517$, $\xi_M(0,\beta)$ takes the simple form given by Eq. (3.51). Therefore, in this case

$$f_M = 2(2e^{-(1/2)e^{-\beta}} - 1) \tag{3.57}$$

and

$$\eta = 2(1-\gamma)(2e^{-(1/2)e^{-\beta}} - 1)^2/\beta \tag{3.58}$$

In Appendix C $\xi(\tau)$ is determined in the interval $0 \le \tau < 2\beta$ from Eqs. (3.22)-(3.24) and (3.31)-(3.33). The solution is valid (corresponds to the penetration) as long as $0 \le \tau \le \tau_M$ or $0 \le \xi \le \xi_M$. Therefore, when $\alpha > 0$ and

$$0 < \tau_M < 2\beta \tag{3.59}$$

ξ_M can be obtained from the solution $\xi(\tau)$ as a function of α and β. This has been achieved by numerical methods. Numerical results for f_M according to Eqs. (3.52) and (3.57) and for η according to Eqs. (3.55) and (3.58) are plotted in Figs. 3.3 and 3.4 respectively.

In the previous analysis it is natural to interprete β as a non-dimensional representation of t_p. According to Eqs. (3.7), (3.17) and (3.26), however, β can be expressed as

$$\beta = 2kL_H/AE \tag{3.60}$$

Therefore, particularly in the results of the analysis, it is sometimes convenient to interprete β also as a non-dimensional hammer length.

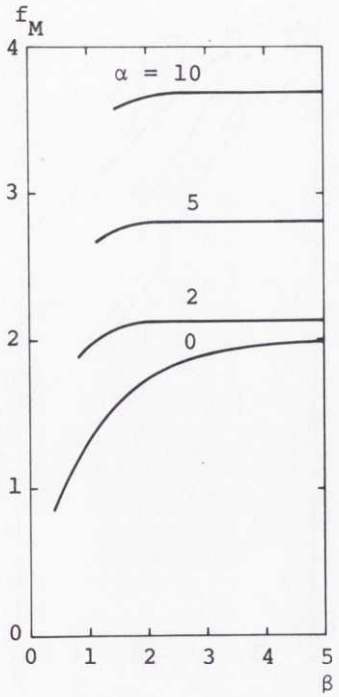

Fig. 3.3. f_M versus β for different values of α. $f_M = F_M/F_0$, $\alpha = 4kc^2M_B/A^2E^2$, $\beta = 2kL_H/AE$. Churn drilling method.

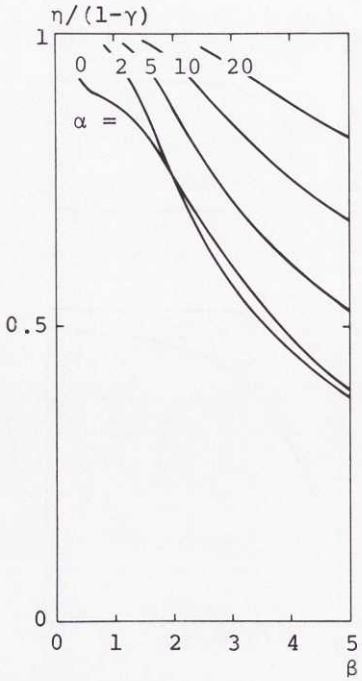

Fig. 3.4. $\eta/(1-\gamma)$ versus β for different values of α. $\eta = W/W_i$, $\alpha = 4kc^2M_B/A^2E^2$, $\beta = 2kL_H/AE$, $\gamma = k/k_e$. Churn drilling method.

3.2.3. Discussion

3.2.3.1. General. - The non-dimensional maximum force $f_M = F_M/F_0$, where $F_0 = AEV/2c$, has been determined as a function of the parameters $\alpha = 4kc^2M_B/A^2E^2$ and $\beta = 2kL_H/AE$. The relationship $f_M = f_M(\alpha,\beta)$ is illustrated in Fig. 3.3.

For high values of β, f_M approaches a constant value, which is equal to 2 when $\alpha = 0$. When $\alpha \geq 0$, the value of f_M for high values of β increases with α.

In physical terms this means that, for sufficiently long hammers, the maximum force F_M is at least $2F_0 = AEV/c$, which is the force obtained if the hammer without bit impacts a rigid wall longitudinally with the impact velocity V.

The efficiency $\eta = W/W_i$ has also been obtained as a function of α, β and $\gamma = k/k_e$. The relationship $\eta/(1-\gamma)$ versus α and β is illustrated in Fig. 3.4.

For a given value of α, $\eta/(1-\gamma)$ is a decreasing function of β. $\eta/(1-\gamma)$ approaches 1 for low values of β, and 0 for high values of β.

In physical terms this means that the highest efficiencies are obtained with short and stiff hammers in soft rock. This is natural, since in these situations, only little elastic and kinetic energy remain in the hammer at the end of the penetration process. Therefore, the transfer of the hammer impact energy to the rock must be almost complete and a high efficiency results.

In order to investigate when a hammer in a drop-tester acts as a rigid body, which is often assumed, and when it does not, HUSTRULID (1968) numerically studied a system similar to the one studied here. Since the rigid body description of the hammer can be a good approximation only when the efficiency of energy transfer to the rock is near 100 per cent (γ assumed to be zero), Hustrulid observed that one must be

extremely careful in applying this description, in particular when the rock is hard. From Fig. 3.4, it can be seen that similar conclusions result from the present analysis. See also Section 3.2.3.2, where a related problem, that of the rigid bit, is discussed.

3.2.3.2. The rigid bit assumption. - In order to justify the assumption that the bit behaves as a rigid body, the following two conditions were imposed in Section 3.1:

$$L_B/L_H << 1 \tag{3.2}$$

$$kL_B/A_B E_B << 1 \tag{3.3}$$

The meaning of the condition (3.2) is that the time required for a stress wave to travel through the bit is much less than the time taken by the wave to travel through the hammer.

The meaning of the condition (3.3) is that the elastic decrease in bit length when the bit penetrates into the rock is much less than the penetration.

The latter condition was formulated under static loading conditions. However, it is now possible to formulate a corresponding condition under impact loading conditions in a special situation. In order to do this, consider the situation when, in churn drilling, the bit is elastic with Young's modulus E_B, cross sectional area A_B and length L_B, whereas the length L_H of the hammer is zero. Then, according to Eq. (3.58), the efficiency of transfer of the bit kinetic energy to work performed on the rock is

$$\eta = 2(1-\gamma)(2e^{-(1/2)e^{-\beta_B}-1})^2/\beta_B \tag{3.61}$$

where from Eq. (3.60)

$$\beta_B = 2kL_B/A_BE_B \tag{3.62}$$

and where $\beta_B > 0.3517$.

For a perfectly rigid bit it is realized that

$$\eta = 1-\gamma \tag{3.63}$$

where γ can now be interpreted as the kinetic energy of the rebounding bit relative to the impact energy of the bit.

The reason that the efficiency is less when the bit is elastic than when it is rigid is that in the former case the bit deforms. Therefore, when the penetration is maximum, the bit contains elastic as well as kinetic energy.

It is now natural to state that, in the situation considered, the bit behaves like a rigid body when the efficiency η is not much less that $(1-\gamma)$. Since from Eq. (3.61) it is seen that $\eta/(1-\gamma) > 0.90$ when $\beta_B < 0.50$, the bit can be expected to behave almost as a rigid body when, say,

$$\beta_B << 2 \tag{3.64}$$

However, the condition (3.64) and Eq. (3.62) are equivalent to the condition (3.3).

With the introduction of the bit mass

$$M_B = \rho_B A_B L_B \tag{3.65}$$

and Eqs. (3.1), (3.21) and (3.60), the conditions (3.2) and (3.3) can also be expressed in terms of α and β as

$$\alpha/\beta << 2(A_B/A) \tag{3.66}$$

and

$$\alpha << 4(A_B/A)^2 \qquad (3.67)$$

respectively ($\rho_B = \rho$, $E_B = E$).

3.3. Down-the-hole Drilling Method

3.3.1. Penetration velocity of the bit

The situation when the bit mass M_B is zero, exactly corresponds to the churn drilling method and will therefore not be treated here. Consider instead the situation when the mass M_B of the bit is finite. This situation is illustrated in Fig. 3.5.

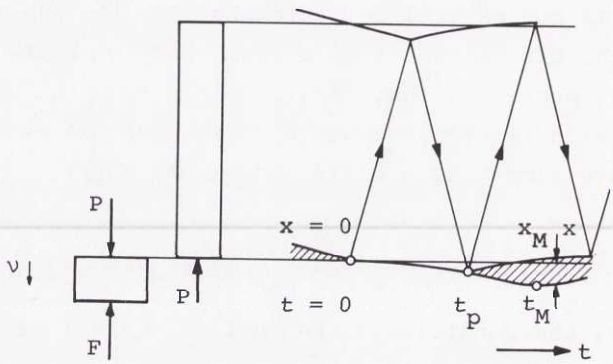

Fig. 3.5. Hammer and bit motion in down-the-hole drilling.

When at time t = 0, the hammer impacts the bit, a compressive stress wave σ is generated at the hammer-bit interface, where it is denoted by $\sigma(t)$ (Appendix B). This stress wave propagates towards the free end of the hammer, where it is reflected as a tensile wave $-\sigma$. Since the bit is initially at rest, the initially generated stress $\sigma(0)$ is the same as would have been obtained if the bit were replaced by a rigid wall, i.e. $-EV/c$. The front of this reflected tensile wave $-\sigma$ arrives at the bit at time $t = t_p$ in accordance with Eq.

(3.7). Then the hammer and bit separate, at least for some time. As a result of the bit's motion into the rock, work W is performed.

There may occur repeated impacts between the hammer and the bit. These repeated impacts may also cause further work to be performed on the rock. However, such repeated impacts will not be considered here.

In this case, Eqs. (3.8)-(3.14) and Eq. (2.35) remain unchanged. However, the initial condition (3.15) is replaced by

$$dx(0)/dt = 0 \tag{3.68}$$

Therefore, with the introduction of non-dimensional variables in accordance with Eqs. (3.16)-(3.21), Eqs. (3.22) and (3.23) apply, while Eq. (3.24) is replaced by

$$d\xi(0)/d\tau = 0 \tag{3.69}$$

It will be seen that it is convenient, in this case, to study the non-dimensional penetration velocity

$$\nu = d\xi/d\tau \tag{3.70}$$

rather than the penetration itself. Therefore, after differentiation, Eq. (3.22) is replaced by

$$(\alpha/4)d^2\nu/d\tau^2+d\nu/d\tau+\nu = 0 \tag{3.71}$$

Eqs. (3.69) and (3.70) yield

$$\nu(0) = 0 \tag{3.72}$$

while Eqs. (3.22), (3.23), (3.69) and (3.70) yield

$$d\nu(0)/d\tau = 4/\alpha \tag{3.73}$$

The solution of Eqs. (3.71)-(3.73) is valid in the interval

$$0 \leq \tau < \beta \tag{3.25}$$

as long as, according to Eqs. (3.27) and (3.70),

$$\nu(\tau) \geq 0 \tag{3.74}$$

β is given by Eq. (3.26) or (3.60).

The inequality (3.74) can also be replaced by

$$0 \leq \tau \leq \tau_M \tag{3.37}$$

where τ_M is the value of τ, which makes ξ equal to its maximum value ξ_M.

Naturally, the solution $\nu(\tau)$ can be extended to $\tau \geq \beta$ by studying the motions of hammer and bit after they have separated at $\tau = \beta$. This analysis may involve repeated impacts between the hammer and the bit. The solution $\nu(\tau)$ can also be extended to $\tau > \tau_M$ by employing the unloading section of the force-penetration relation in accordance with Eq. (2.36). These extensions will, however, not be made here.

The solution of Eq. (3.71) with the initial conditions (3.72) and (3.73) is

$$\nu = \begin{cases} (2/\Delta)e^{-2\tau/\alpha}\sinh(2\Delta\tau/\alpha), & 0<\alpha<1 \\ 4\tau e^{-2\tau}, & \alpha = 1 \\ (2/\Gamma)e^{-2\tau/\alpha}\sin(2\Gamma\tau/\alpha), & \alpha>1 \end{cases} \tag{3.75}$$

where

$$\Delta = (1-\alpha)^{1/2} \tag{3.76}$$

and

$$\Gamma = (\alpha-1)^{1/2} \tag{3.77}$$

The solution $\nu(\tau)$ is valid in the interval (3.25) when

$$0<\alpha\leq 1 \text{ or } \alpha>1 \text{ and } \beta\leq\pi\alpha/2\Gamma \tag{3.78}$$

and in the interval (3.37) with

$$\tau_M = \pi\alpha/2\Gamma \tag{3.79}$$

when

$$\alpha>1 \text{ and } \beta>\pi\alpha/2\Gamma \tag{3.80}$$

From Eq. (3.75) it can be verified that $\nu<1$, which means that the penetration velocity dx/dt is less than the impact velocity V.

3.3.2. Bit force and efficiency

If the condition (3.78) is satisfied, then the force P acting between hammer and bit is performing a positive work $\int P dx$ on the bit and rock when $0\leq t<t_p$. At time $t = t_p$, the contact between hammer and bit is interrupted. If there is no renewed contact between hammer and bit, the bit continues its motion into the rock, rebounds, and the total net work performed on the rock becomes equal to the work performed by the hammer on the bit and rock minus the kinetic energy of the rebounding bit, i.e.

$$W = (1-\gamma)\int_0^{t_p} P(dx/dt)dt \tag{3.81}$$

Since the energy W is also given by Eq. (2.39), the maximum force F_M acting between bit and rock can be determined from

$$F_M^2 = 2k\int_0^{t_p} P(dx/dt)dt \tag{3.82}$$

The impact energy is now

$$W_i = (1/2)M_H V^2 \tag{3.83}$$

where the mass of the hammer M_H is given by Eq. (3.54). Therefore, the efficiency η can be determined from Eqs. (3.81), (3.83) and (3.6), i.e.

$$\eta = W/W_i \tag{3.6}$$

If the contact between hammer and bit is renewed when $t>t_p$, then the work W, the maximum force F_M and the efficiency η as given by Eqs. (3.81) (3.82) and (3.6) respectively, may be exceeded. Therefore, when it is not known whether or not there is any renewed contact, these values of W, F_M and η must be considered as lower bounds of the actual values.

If the condition (3.80) is satisfied, then the force P acting between hammer and bit is performing a positive work $\int Pdx$ on the bit and rock when $0\leq t\leq t_M$. At time $t = t_M$ ($<t_p$) the penetration velocity and consequently the kinetic energy of the bit become zero. Therefore, the total net work performed on the rock can be obtained by replacing t_p by t_M in Eq. (3.81), i.e.

$$W = (1-\gamma)\int_0^{t_M} P(dx/dt)dt \tag{3.84}$$

Consequently the force F_M can be obtained from

$$F_M^2 = 2k\int_0^{t_M} P(dx/dt)dt \tag{3.85}$$

If now, according to Eqs. (3.10) and (3.11),

$$P = (AE/c)(V-dx/dt) \tag{3.86}$$

is substituted into Eqs. (3.81), (3.82), (3.84) and (3.85), and if further non-dimensional variables are introduced, then the non-dimensional maximum force f_M and the efficiency η can be obtained as functions of α, β and γ.

If the condition (3.78) is satisfied, $f_M(>0)$ can be obtained from the relationship

$$f_M^2 = 8\{I(\alpha,\beta)-J(\alpha,\beta)\} \tag{3.87}$$

where

$$I(\alpha,\beta) = \int_0^\beta \nu(\tau;\alpha)\,d\tau \tag{3.88}$$

and

$$J(\alpha,\beta) = \int_0^\beta \nu^2(\tau;\alpha)\,d\tau \tag{3.89}$$

The evaluated integrals (3.88) and (3.89) are given in Appendix D.

If instead, the condition (3.80) is satisfied, f_M can be obtained from the relationship

$$f_M^2 = 8\{I(\alpha,\pi\alpha/2\Gamma)-J(\alpha,\pi\alpha/2\Gamma)\} \tag{3.90}$$

which can be simplified to

$$f_M = 2(1+e^{-\pi/\Gamma}) \tag{3.91}$$

The efficiency η can be expressed in terms of f_M as

$$\eta = (1-\gamma)f_M^2(\alpha,\beta)/2\beta \tag{3.92}$$

Numerical results for f_M according to Eqs. (3.87)-(3.89) and (3.91) and for η, according to Eqs. (3.92), are plotted in Figs. 3.6 and 3.7 respectively.

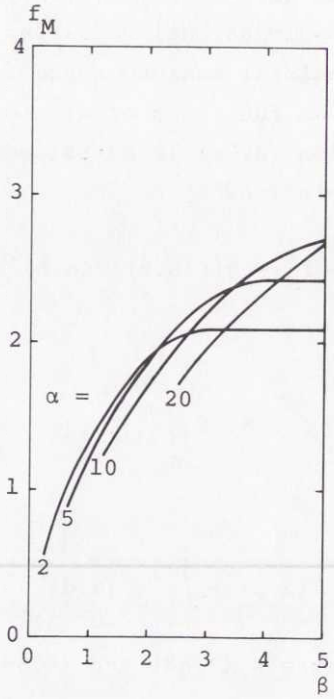

Fig. 3.6. f_M versus β for different values of α. $f_M = F_M/F_0$, $\alpha = 4kc^2M_B/A^2E^2$, $\beta = 2kL_H/AE$. Down-the-hole drilling method.

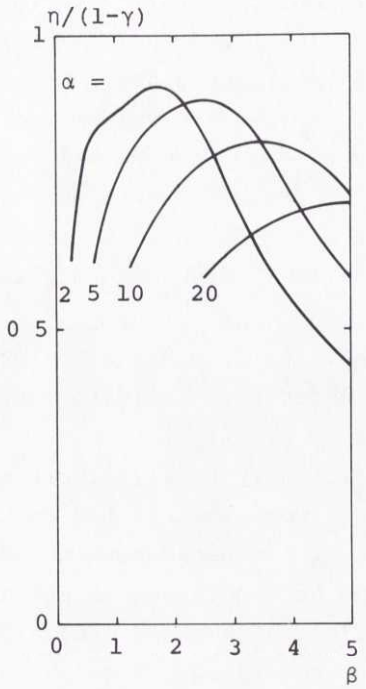

Fig. 3.7. $\eta/(1-\gamma)$ versus β for different values of α. $\eta = W/W_i$, $\alpha = 4kc^2M_B/A^2E^2$, $\beta = 2kL_H/AE$, $\gamma = k/k_e$. Down-the-hole drilling method.

3.3.3. Discussion

The non-dimensional maximum force $f_M = F_M/F_0$, where $F_0 = AEV/2c$, has been determined as a function of the parameters $\alpha = 4kc^2M_B/A^2E^2$ and $\beta = 2kL_H/AE$. The relationship $f_M = f_M(\alpha,\beta)$ is illustrated in Fig. 3.6.

For high values of β, f_M approaches a constant value, which is equal to 2 when $0<\alpha\leq 1$. When $\beta>\pi\alpha/2\Gamma$ and $\alpha>1$, f_M assumes the constant value given by Eq. (3.91), i.e. $2<f_M<4$.

In physical terms this means that, when the bit is light ($0<\alpha\leq 1$), the maximum force F_M never exceeds the value $2F_0 = AEV/c$, which is the force obtained if the hammer im-

pacts a rigid wall longitudinally with the impact velocity V. If the bit is heavy ($\alpha>1$) and the hammer is sufficiently long, this force AEV/c is exceeded. However, the maximum force never exceeds twice this value, i.e. 2AEV/c.

The efficiency $\eta = W/W_i$, where W is the work performed on rock as a result of the first impact between hammer and bit, has also been obtained as a function of α, β and $\gamma = k/k_e$. The relationship $\eta/(1-\gamma)$ versus α and β is illustrated in Fig. 3.7.

For a given value of α, η has a maximum for a certain value of β, which depends on α. Moreover, $\eta/(1-\gamma)$ approaches 0 for large values of β.

When γ is sufficiently small, it can be seen from Fig. 3.7 that efficiencies of more than 90 per cent can be obtained by a proper choice of the parameters α and β (say both of the order of 2). From the conditions (3.66) and (3.67) it can be seen that these values of α and β generally agree with the initial assumptions regarding bit behaviour. It can also be easily verified, and it will become apparent in Section 3.4.3.2, that these values of α and β correspond to values of the physical parameters M_B, k, A, L_H, c and E, that can be realized.

Thus, for such values of α and β, almost all impact energy is transferred to the rock as a consequence of the first impact between hammer and bit. If, in such cases, repeated impacts would occur, these impacts can only have a minor influence on the resulting efficiency.

When, on the other hand, the ratio of bit mass and hammer mass is very small, i.e. $\alpha/2\beta<<1$, and β is also small, say $\beta<<1$, the consideration of repeated impacts would influence the results to a large extent. When $\alpha/2\beta\rightarrow 0$, in fact, a treatment which takes repeated impacts into consideration would give the same results as were obtained for the churn drilling method when $\alpha = 0$.

From a physical point of view it is evident that during the impact kinetic energy is imparted to the bit which thereby performs work on the rock. When the penetration ceases, which may occur during as well as after impact, all kinetic energy of the bit has been transformed to work performed on the rock. From Fig. 3.7 it can be seen that the duration of impact ($t_p \sim \beta$) which gives rise to a maximum of energy transfer to the rock is an increasing function of the bit mass ($M_B \sim \alpha$).

A similar system was studied by FRANKLAND (1948), who analysed a one degree of freedom linear mass-spring system which is acted upon by different types of impulsive forces. For each type of load (rectangular, triangular, half-period sine pulse etc.) a dynamic load factor (roughly corresponding to f_M) was determined as a function of the ratio of pulse duration and period of the mass-spring system (corresponding to $\beta/\pi\alpha^{1/2}$). Results similar to those shown in Fig. 3.6 were obtained. However, Frankland did not study the type of impulsive force which is generated at impact by a cylindrical rod.

CHARLES & BRUYN (1956) studied experimentally the impact between a steel hammer and a pyrex glass rod, which was fixed in one end. The results obtained were compared with those obtained by Frankland for a half-period sine pulse and the agreement was satisfactory. In particular, Charles & Bruyn observed that the transfer of kinetic energy to strain energy in the glass rod assumed a maximum when the ratio of impact time and fundamental period of oscillation of the glass rod was 0.8. Then the fraction of energy transfer was 0.50. These results can be compared with the results obtained here. For example, $\alpha = 2.00$, $\beta = 1.70$ and $\gamma = 0$ result in the maximum efficiency $\eta = 0.91$ and the ratio of impact time and fundamental period of oscillation $\beta/\pi\alpha^{1/2} = 0.38$. Thus, an appreciably higher maximum efficiency is obtained for about half the impact time. This difference is not surprising,

however, since the difference between the pyrex glass rod employed by Charles & Bruyn and the system studied here appears to be appreciable.

3.4. Hammer Drilling Method

3.4.1. Stress wave reflection

3.4.1.1. Finite mass bit. - Consider first the situation when the mass M_B of the bit is finite. This situation is illustrated in Fig. 3.8.

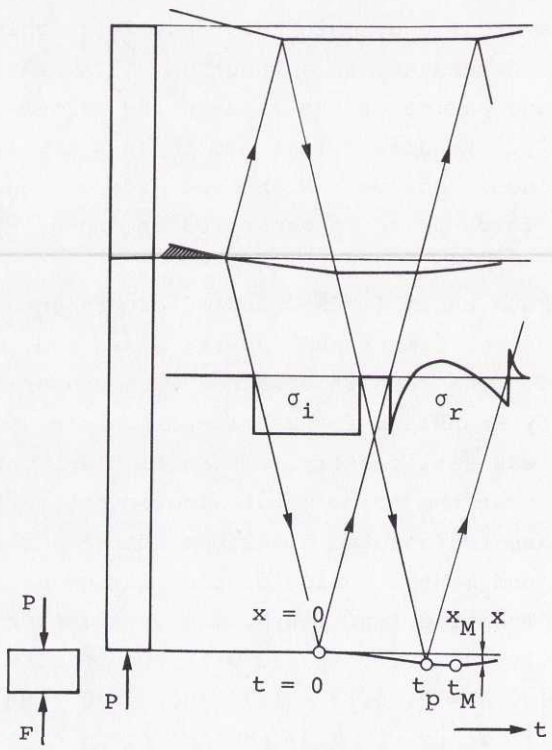

Fig. 3.8. Bit motion and stress wave generation and reflection in hammer drilling.

When at time $t = -L_R/c$ the hammer impacts the rod, a compressive stress wave σ_i is generated in the rod. This stress wave propagates towards the bit where it arrives at time $t = 0$ and is denoted by $\sigma_i(t)$ (Appendix B). At the bit a reflected stress wave σ_r is generated, which at the rod-bit interface is denoted by $\sigma_r(t)$. This reflected stress wave is determined by the boundary conditions at the rod-bit interface where the resultant stress becomes $\sigma_i(t)+\sigma_r(t)$. Under the combined action of the incident and reflected stress waves, the bit is accelerated towards the rock, and work W is performed.

When the reflected stress wave σ_r arrives at the rod hammer interface and the free end of the hammer, reflected stress waves are again generated which form a second incident stress wave σ_{i2}. Since $L_R >> L_H$, it is assumed that σ_{i2} does not interfere with σ_i or σ_r at the bit. Therefore, when the second incident stress wave arrives at the bit, where it is denoted by $\sigma_{i2}(t)$, it is assumed that $\sigma_i(t) = \sigma_r(t) = 0$, that the bit is at rest and that a second reflected stress wave σ_{r2} is generated. The bit is generally, at least temporarily, accelerated towards the rock again. Further work W_2 is therefore performed on the rock if the maximum force F_{M2} generated during the second stress wave reflection is larger than the maximum force F_M generated during the first stress wave reflection. This is illustrated in Fig. 3.9.

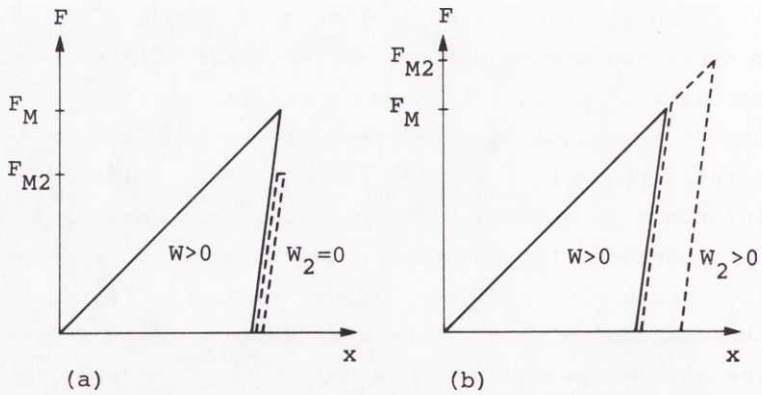

Fig. 3.9. Force-penetration relationships at the first (solid lines) and second (dotted lines) stress wave interactions at the bit. In (a) no work is performed on rock during the second stress wave interaction, whereas in (b), work W_2 is performed.

The events are repeated and, consequently, there are third and fourth stress wave interactions at the bit etc. Under normal operating conditions, however, HUSTRULID (1968) found that energy transfer to rock only occurs during the first and second stress wave interaction at the bit. Moreover, the main part of the energy transfer normally takes place during the first stress wave interaction. Sometimes, no energy transfer at all takes place during the second stress wave interaction.

From several points of view (e.g. fatigue of drill rods), it appears to be advantageous to transfer a maximum of energy to the rock during the first stress wave interaction at the bit. Therefore, the repeated reflections in the drill rod will not be further considered in this section. In Section 4.2, however, energy transfer from the second incident stress wave will be treated separately under somewhat more restricted conditions ($M_B = 0$).

The equation of motion of the bit is again given by Eq. (3.8), i.e.

$$M_B d^2x/dt^2 = P-F \tag{3.8}$$

where, as illustrated in Fig. 3.8, x is the bit penetration into the rock, P is the force acting between hammer and bit and F is the force acting between bit and rock.

The force P can be expressed as (Appendix B)

$$P = - A(\sigma_r+\sigma_i) \tag{3.93}$$

while the penetration velocity is (Appendix B)

$$dx/dt = (c/E)(\sigma_r-\sigma_i) \tag{3.94}$$

Further, as long as the penetration velocity is non-negative, i.e.

$$dx/dt \geq 0 \tag{3.12}$$

the force F and the penetration x are related in accordance with Eq. (2.35), i.e.

$$F = kx \tag{2.35}$$

To facilitate a subsequent comparison between theoretical and experimental stress wave forms (Section 3.6), it is convenient, in this case, to study the reflected stress wave $\sigma_r(t)$ rather than the penetration x(t) or the penetration velocity dx(t)/dt.

Elimination of P, F and x in Eqs. (3.8), (3.93), (3.94) and (2.35) yields the differential equation

$$(M_B/k)d^2\sigma_r/dt^2+(AE/kc)d\sigma_r/dt+\sigma_r =$$
$$= (M_B/k)d^2\sigma_i/dt^2-(AE/kc)d\sigma_i/dt+\sigma_i \qquad (3.95)$$

The initial conditions are

$$x(0) = 0 \qquad (3.96)$$

and

$$dx(0)/dt = 0 \qquad (3.97)$$

According to Eqs. (3.8), (3.93), (3.94) and (2.35), these initial conditions can be transformed into

$$(M_Bc/AE)d\sigma_r(0)/dt+\sigma_r(0) = (M_Bc/AE)d\sigma_i(0)/dt-\sigma_i(0) \qquad (3.98)$$

and

$$\sigma_r(0) = \sigma_i(0) \qquad (3.99)$$

respectively.

It is now convenient to introduce non-dimensional variables. Let therefore

$$s_i = \sigma_i/\sigma_0 \qquad (3.100)$$

and

$$s_r = \sigma_r/\sigma_0 \qquad (3.101)$$

where σ_0 is a normalizing stress. Using non-dimensional stresses, and introducing these stresses together with the non-dimensional time τ, defined by Eqs. (3.16) and (3.17), and the parameter α, defined by Eq. (3.21), into Eqs. (3.95),

(3.98) and (3.99) gives

$$(\alpha/4)d^2s_r/d\tau^2+ds_r/d\tau+s_r = (\alpha/4)d^2s_i/d\tau^2-ds_i/d\tau+s_i \tag{3.102}$$

$$(\alpha/4)ds_r(0)/d\tau+s_r(0) = (\alpha/4)ds_i(0)/d\tau-s_i(0) \tag{3.103}$$

and

$$s_r(0) = s_i(0) \tag{3.104}$$

Eq. (3.94) and the condition (3.12) can also be tranformed into

$$s_r(\tau)-s_i(\tau)\geq 0 \tag{3.105}$$

The solution of Eqs. (3.102)-(3.104) is valid for $\tau\geq 0$ as long as the condition (3.105) is satisfied. The inequality (3.105) is equivalent with

$$0\leq\tau\leq\tau_M \tag{3.37}$$

where τ_M is the value of τ, which makes ξ equal to its maximum value ξ_M. Therefore, when $\alpha>0$ or $s_i(\tau)$ is a continuous function, τ_M (>0) can be determined from the equation

$$s_r(\tau_M)-s_i(\tau_M) = 0 \tag{3.106}$$

When $\alpha = 0$ and $s_i(\tau)$ is not a continuous function, however, τ_M must be determined as the value of τ for which s_r-s_i changes sign from positive to negative.

Naturally, the solution $s_r(\tau)$ can be extended to $\tau>\tau_M$ by employing the unloading section of the force-penetration relationship according to Eq. (2.36). This extension, however, will not be made here.

By introduction of the Laplace transforms $\tilde{s}_i(s)$ and $\tilde{s}_r(s)$ of $s_i(\tau)$ and $s_r(\tau)$ respectively, Eqs. (3.102)-(3.104) yield

$$\tilde{s}_r(s) = H_B(s)\tilde{s}_i(s) \tag{3.107}$$

where

$$H_B(s) = \{(\alpha/4)s^2-s+1\}/\{(\alpha/4)s^2+s+1\} \tag{3.108}$$

Thus, the solution $s_r(\tau)$ can be obtained as the inverse Laplace transform of $H_B(s)\tilde{s}_i(s)$, i.e.

$$s_r(\tau) = L^{-1}\{H_B(s)\tilde{s}_i(s)\} \tag{3.109}$$

The incident stress wave $s_i(\tau)$ is generally determined by the material and geometry of the hammer and rod. In the simple situation considered here

$$\sigma_i(t) = \begin{cases} -EV/2c\ , & 0\le t<t_p \\ 0\ , & t_p\le t \end{cases} \tag{3.110}$$

Therefore, if the normalizing stress σ_0 is chosen as

$$\sigma_0 = EV/2c \tag{3.111}$$

$s_i(\tau)$ becomes

$$s_i(\tau) = \begin{cases} -1\ , & 0\le\tau<\beta \\ 0\ , & \beta\le\tau \end{cases} \tag{3.112}$$

Eqs. (3.102)-(3.104) and (3.112) or Eqs. (3.108), (3.109) and (3.112) yield

$$s_r = -g(\tau)+g(\tau-\beta) \tag{3.113}$$

where $g(\tau) = 0$ when $\tau<0$ and

$$g(\tau) = \begin{cases} 1-(4/\Delta)e^{-2\tau/\alpha}\sinh(2\Delta\tau/\alpha), & 0<\alpha<1 \\ 1-8\tau e^{-2\tau}, & \alpha = 1 \\ 1-(4/\Gamma)e^{-2\tau/\alpha}\sin(2\Gamma\tau/\alpha), & \alpha>1 \end{cases} \tag{3.114}$$

when $\tau\geq 0$. Δ and Γ are given by Eqs. (3.76) and (3.77), i.e.

$$\Delta = (1-\alpha)^{1/2} \tag{3.76}$$

and

$$\Gamma = (\alpha-1)^{1/2} \tag{3.77}$$

$\tau_M(>0)$ can be determined from Eq. (3.106) and Eqs. (3.112)-(3.114).

When

$$0<\alpha\leq 1 \text{ or } \alpha>1 \text{ and } \beta\leq\pi\alpha/2\Gamma \tag{3.78}$$

$\tau_M(\geq\beta)$ is obtained as

$$\tau_M = \begin{cases} (\alpha/4\Delta)\ln(\Delta_1), & 0<\alpha<1 \\ \beta e^{2\beta}/(e^{2\beta}-1), & \alpha = 1 \\ (\alpha/2\Gamma)\{\arctan(\Delta_2)+n\pi\}, & \alpha>1 \end{cases} \tag{3.115}$$

where

$$\Delta_1 = (e^{2\beta(1+\Delta)/\alpha}-1)/(e^{2\beta(1-\Delta)/\alpha}-1) \tag{3.116}$$

$$\Delta_2 = \sin(2\Gamma\beta/\alpha)/\{\cos(2\Gamma\beta/\alpha)-e^{-2\beta/\alpha}\} \tag{3.117}$$

and where the number n = 0, 1, 2, ... is determined by the zeros β_0, β_1, β_2, ... ($0 = \beta_0 < \beta_1 < \ldots$) of the denominator in Eq. (3.117). Thus

$$n = j \tag{3.118}$$

when

$$\beta_j \leq \beta < \beta_{j+1} \tag{3.119}$$

where

$$\cos(2\Gamma\beta_j/\alpha)-e^{-2\beta_j/\alpha} = 0 \tag{3.120}$$

When

$$\alpha > 1 \text{ and } \beta > \pi\alpha/2\Gamma \tag{3.80}$$

$\tau_M (< \beta)$ is obtained as

$$\tau_M = \pi\alpha/2\Gamma \tag{3.121}$$

3.4.1.2. Zero mass bit. - According to Eq. (3.21) a bit of zero mass corresponds to $\alpha = 0$. Then Eqs. (3.102) and (3.103) yield

$$ds_r/d\tau+s_r = -ds_i/d\tau+s_i \tag{3.122}$$

and

$$s_r(0) = -s_i(0) \tag{3.123}$$

The condition (3.104) is omitted, since when $\alpha = 0$, the penetration velocity dx/dt need no longer be a continuous function.

The solution of Eqs. (3.122) and (3.123) is valid for $\tau \geq 0$ as long as the condition (3.105) is satisfied.

By Laplace transformation again the solution $s_r(\tau)$ can be obtained from Eq. (3.109), where now

$$H_B(s) = (1-s)/(1+s) \tag{3.124}$$

When $s_i(\tau)$ is given by Eq. (3.112) then $s_r(\tau)$ is given by Eq. (3.113), where now

$$g(\tau) = 1-2e^{-\tau} \tag{3.125}$$

when $\tau \geq 0$.

It is readily verified that the condition (3.105) is satisfied when $0 \leq \tau < \beta$. However, when $0 < \gamma \leq 1$, the force acting on the bit is a continuous function of time. Therefore, $s_i(\tau)+s_r(\tau)$ must also be a continuous function and it is realized that, since $s_i(\beta) = 0$,

$$s_r(\beta) = \lim_{\tau \to \beta-} \{s_i(\tau)+s_r(\tau)\} \tag{3.126}$$

From Eqs. (3.112), (3.113), (3.125) and (3.126) then

$$s_r(\beta) = -2(1-e^{-\beta}) \tag{3.127}$$

Therefore, $s_r(\beta) < 0$, and since $s_i(\beta) = 0$, then

$$s_r(\beta)-s_i(\beta) < 0 \tag{3.128}$$

To summarize, the penetration velocity is positive when $0 \leq \tau < \beta$, but suddenly becomes negative when $\tau = \beta$. Therefore, the solution obtained is valid only in the interval $0 \leq \tau < \beta$, i.e.

$$s_r = -1+2e^{-\tau} \tag{3.129}$$

when

$$0 \leq \tau < \beta \tag{3.130}$$

Since τ_M is defined as the value of τ, which makes ξ equal to its maximum value ξ_M, and since $\xi(\tau)$ is a continuous function

$$\tau_M = \beta \tag{3.131}$$

(Notice that $d\xi(\tau_M)/d\tau \neq 0$).

3.4.2. Bit force and efficiency

According to Eqs. (3.8), (3.93) and (3.94), the maximum force acting on rock is

$$F_M = -A\{\sigma_r(t_M)+\sigma_i(t_M)\}-(M_B c/E)\{d\sigma_r(t_M)/dt-d\sigma_i(t_M)/dt\} \tag{3.132}$$

or if non-dimensional variables are introduced according to Eqs. (3.4), (3.16), (3.21), (3.100) and (3.101),

$$f_M = -\{s_r(\tau_M)+s_i(\tau_M)\}-(\alpha/4)\{ds_r(\tau_M)/d\tau-ds_i(\tau_M)/d\tau\} \tag{3.133}$$

When the condition (3.78) is satisfied, then $\tau_M \geq \beta$, $s_r(\tau_M) = s_i(\tau_M) = ds_i(\tau_M)/d\tau = 0$ and Eq. (3.133) can be simplified to

$$f_M = -(\alpha/4)ds_r(\tau_M)/d\tau \tag{3.134}$$

Eqs. (3.113), (3.114) and (3.134) yield

$$f_M = \begin{cases} (1/\Delta)\left[(1-\Delta)e^{-2(1-\Delta)\tau_M/\alpha} - (1+\Delta)e^{-2(1+\Delta)\tau_M/\alpha} - \right. \\ \left. -(1-\Delta)e^{-2(1-\Delta)(\tau_M-\beta)/\alpha} + (1+\Delta)e^{-2(1+\Delta)(\tau_M-\beta)/\alpha}\right] \\ \qquad\qquad 0<\alpha<1 \\ 2\left[2\tau_M e^{-2\tau_M} - e^{-2\tau_M} - 2(\tau_M-\beta)e^{-2(\tau_M-\beta)} + e^{-2(\tau_M-\beta)}\right] \\ \qquad\qquad \alpha = 1 \\ 2e^{-2\tau_M/\alpha}\{-\cos(2\Gamma\tau_M/\alpha) + (1/\Gamma)\sin(2\Gamma\tau_M/\alpha) + \\ + e^{2\beta/\alpha}\cos\left[2\Gamma(\tau_M-\beta)/\alpha\right] - \\ -(1/\Gamma)e^{2\beta/\alpha}\sin\left[2\Gamma(\tau_M-\beta)/\alpha\right]\} \\ \qquad\qquad \alpha>1 \end{cases} \qquad (3.135)$$

When the condition (3.80) is satisfied, then $\tau_M < \beta$, $s_r(\tau_M) = s_i(\tau_M) = -1$, $ds_i(\tau_M)/d\tau = 0$ and Eq. (3.133) can be simplified to

$$f_M = 2-(\alpha/4)ds_r(\tau_M)/d\tau \qquad (3.136)$$

Eqs. (3.113), (3.114), (3.121) and (3.136) yield

$$f_M = 2(1+e^{-\pi/\Gamma}) \qquad (3.137)$$

This result is identical with the result (3.91) in the case of down-the-hole drilling.

Finally, when $\alpha = 0$, $s_i(\tau_M) = 0$ and Eq. (3.133) is simplified to

$$f_M = -s_r(\tau_M) \qquad (3.138)$$

Eqs. (3.127), (3.131) and (3.138) yield

$$f_M = 2(1-e^{-\beta}) \qquad (3.139)$$

Eqs. (3.115), (3.135), (3.137) and (3.139) yield f_M as a function $f_M(\alpha,\beta)$.

Again the efficiency η is given in terms of $f_M(\alpha,\beta)$ by Eq. (3.92), i.e.

$$\eta = (1-\gamma) f_M^2(\alpha,\beta)/2\beta \qquad (3.92)$$

Thus, when $\alpha = 0$, the simple result

$$\eta = 2(1-\gamma)(1-e^{-\beta})^2/\beta \qquad (3.140)$$

is obtained.

Numerical results for f_M according to Eqs. (3.115), (3.135), (3.137) and (3.139) and for η according to Eq. (3.92) are plotted in Figs. 3.10 and 3.11 respectively.

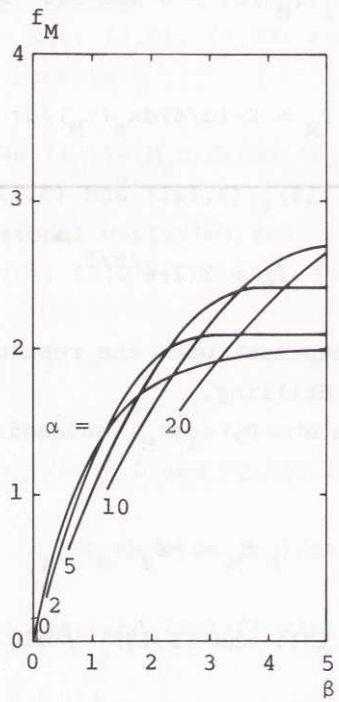

Fig. 3.10. f_M versus β for different values of α. $f_M = F_M/F_0$, $\alpha = 4kc^2M_B/A^2E^2$, $\beta = 2kL_H/AE$. Hammer drilling method.

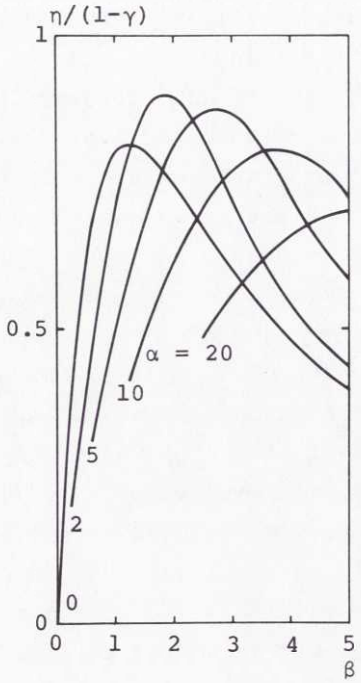

Fig. 3.11. $\eta/(1-\gamma)$ versus β for different values of α. $\eta = W/W_i$, $\alpha = 4kc^2M_B/A^2E^2$, $\beta = 2kL_H/AE$, $\gamma = k/k_e$. Hammer drilling method.

3.4.3. Discussion

3.4.3.1. General. - The non-dimensional maximum force $f_M = F_M/F_0$, where $F_0 = AEV/2c$, has been determined as a function of the parameters $\alpha = 4kc^2M_B/A^2E^2$ and $\beta = 2kL_H/AE$. The relationship $f_M = f_M(\alpha,\beta)$ is illustrated in Fig. 3.10.

For high values of β, f_M approaches a constant value, which is equal to 2 when $0 \leq \alpha \leq 1$. When $\beta > \pi\alpha/2\Gamma$ and $\alpha > 1$, f_M assumes the constant value given by Eq. (3.137), i.e. $2 < f_M < 4$.

In physical terms this means that, when the bit is light ($0 \leq \alpha \leq 1$), the maximum force F_M never exceeds the value $2F_0$ =

= AEV/c, which is the force obtained, if the hammer impacts a rigid wall longitudinally with the impact velocity V. If the bit is heavy ($\alpha>1$) and the hammer is sufficiently long, this force AEV/c is exceeded. However, the maximum force never exceeds twice this value, i.e. 2AEV/c.

The efficiency $\eta = W/W_i$, where W is the work performed on rock during the first stress wave interaction at the bit, has also been obtained as a function of α, β and $\gamma = k/k_e$. The relationship $\eta/(1-\gamma)$ versus α and β is illustrated in Fig. 3.11.

For a given value of α, $\eta/(1-\gamma)$ has a maximum for a certain value of β, which depends on α. Moreover, $\eta/(1-\gamma)$ approaches 0 for small and large values of β.

When $\alpha = 0$, the maximum value of $\eta/(1-\gamma)$ is 0.815 for $\beta = 1.26$. Further, $\eta/(1-\gamma)>0.50$ when $0.35<\beta<3.85$, i.e. when $\gamma = 0$, the efficiency is higher than 50 per cent when β varies with a factor between 1 and 11. These observations are in agreement with results presented earlier by SIMON (1964) (Simon's parameter $\pi_1 = \beta$) and, according to Eq. (3.60) they imply that with given values of the parameters L_H, A and E, it is possible to obtain high efficiency in very different types of rock. Also, if during drilling the parameter k, describing the interaction between cutters and rock, varies between extremes differing as much as a factor of 11, it is still possible to obtain an efficiency which is always higher than 50 per cent.

The highest possible value of $\eta/(1-\gamma)$ for any combination of α and β is 0.902 and this value is assumed when $\alpha = 2.329$ and $\beta = 1.970$. From the conditions (3.66) and (3.67) it can be seen that these values of α and β generally agree with the initial assumptions regarding bit behaviour. It can also easily be verified, and it will become apparent in Section 3.4.3.2 that these values of α and β correspond to values of the physical parameters k, M_B, A, L_H, c and E, that can be

realized in hammer drilling. When γ is sufficiently small, it is therefore possible to transfer more than 90 per cent of the impact energy to the rock during the first stress wave interaction at the bit. Thus, the energy that may be delivered during subsequent stress wave interactions at the bit is only of minor importance. Also, since it is not desirable that repeated stress wave reflections take place in the rod, there seems to be no reason to increase by only a few per cent the total efficiency by decreasing the relative amount of energy delivered to the rock during the first stress wave interaction. Therefore, even with respect to repeated stress wave interactions at the bit, $\alpha = 2.329$, $\beta = 1.970$ (and $\gamma = 0$) appear to be a convenient choice of parameters. It must however be stressed that this conclusion is drawn when the force-penetration relationship is linear during loading (k constant) and when it is possible to choose $\alpha > 0$. HUSTRULID (1968) showed that when the force-penetration relationship is non-linear during loading, and when $\alpha = 0$ ($M_B = 0$), there may be a considerable amount of energy transferred to the rock during the second stress wave interaction.

In physical terms, the following can be stated:

If the bit mass M_B is small (α low) and the rock is soft (β low), then the end of the rod behaves as approximately free and the reflected stress wave σ_r differs from the incident stress wave σ_i essentially only in sign. If, on the other hand, the rock is hard (β high), then the end of the rod behaves as approximately fixed and the reflected stress wave σ_r is approximately equal to the incident stress wave σ_i. Therefore, when $\alpha = 0$ and β is either low or high, only little energy is delivered to the rock and the efficiency η is low. For some intermediate value of β the efficiency becomes maximum.

If the bit is heavy (α high), then because of the inertia of the bit, the rod end behaves as fixed during the first stress wave interaction. Therefore, the efficiency η becomes low again.

For intermediate values of the bit mass (intermediate values of α), however, an essential part of the kinetic energy gained by the bit during the presence of the incident stress wave, can be transferred to the rock. Therefore, in this case, the inertia of the bit has a favourable influence on the energy transfer to the rock.

3.4.3.2. Maximum efficiency conditions. - Eqs. (3.21) and (3.60) can be combined to give

$$M_B = \alpha(A^2E^2/4c^2)/k \tag{3.141}$$

and

$$M_B = (\alpha/\beta^2)(L_H^2/c^2)k \tag{3.142}$$

When $\alpha = 2.329$ and $\beta = 1.970$, Eqs. (3.141) and (3.142) provide two necessary conditions for maximum efficiency, $\eta = 0.902$. If it is assumed that the hammer and rod material is steel, then $E = 2.0\ 10^{11} N/m^2$ and $c = 5.1\ 10^3 m/s$ are given, and Eq. (3.141) relates M_B and k for a given value of A, while Eq. (3.142) relates M_B and k for a given value of L_H. Therefore, if two of the four parameters M_B (characterizing the bit), k (characterizing bit-rock interaction), A (characterizing rod and hammer) and L_H (characterizing hammer) are arbitrarily chosen, then the remaining parameters can be determined from Eqs. (3.141) and (3.142). This is illustrated in Fig. 3.12, where maximum efficiency combinations of M_B, k, A and L_H are given.

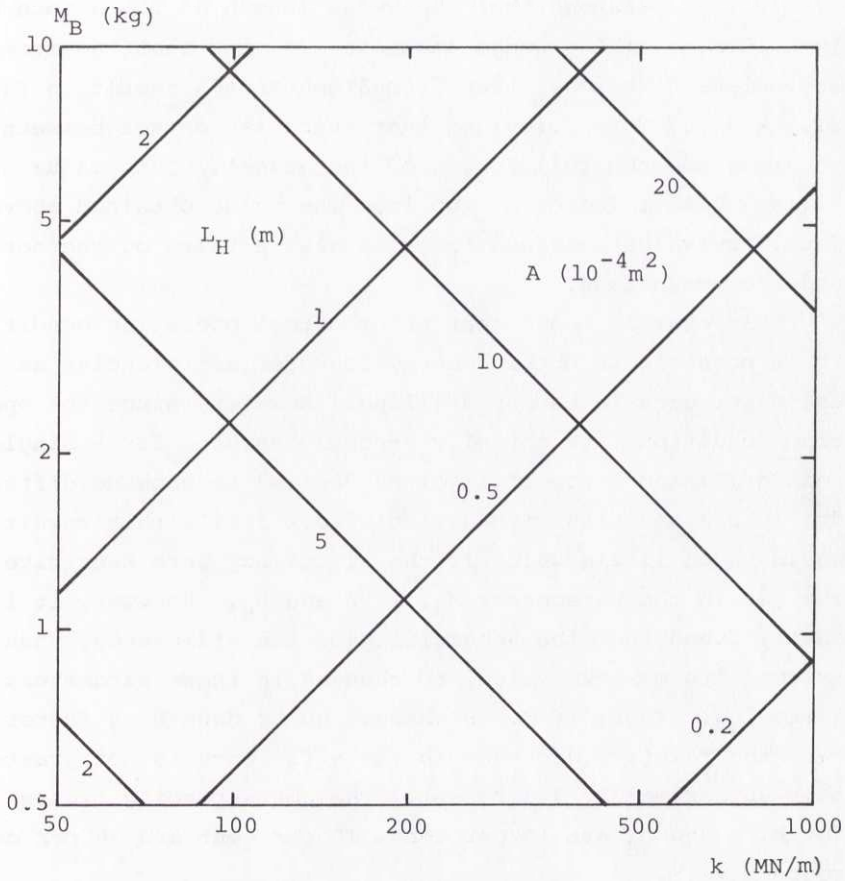

Fig. 3.12. Combinations of M_B, k, A and L_H giving maximum efficiency η.

For example, it is found that when A = 1.0 $10^{-3}m^2$ and L_H = 0.50 m, then for maximum efficiency M_B = 2.3 kg and k = 390 MN/m.

The rod cross section A = 1.0 $10^{-3}m^2$ approximately corresponds to a 1½ inch drill steel. If it is assumed that the bit is cylindrical with a diameter of 3 inches (0.075 m) and a density of 7.8 $10^3 kg/m^3$, then it is found that the bit mass M_B = 2.3 kg corresponds to a bit length of L_B = 0.067 m, which is a normal value.

If it is assumed that the wedge length of the 3 inch bit is 0.10 m, that the wedge angle is 120° and that the rock is Indiana Limestone, then from Stephenson's result in Table 2.3, k = 207 MN/m (provided that there is contact between the rock and the full length of the wedge). This value only differs with a factor of two from the value obtained above. Thus, the value obtained for k is also a value of the normal order of magnitude.

This example shows that under normal operating conditions it is possible to obtain energy transfer efficiencies as high as 90 per cent in hammer drilling. However, since the operating conditions are normally strongly varying for a single rock drill and since it is often desired to combine different drill rods and bits with a single rock drill, this result would be of little value if the efficiency were sensitive to changes in the parameters M_B, k, A and L_H. However, it is easily found that the sensitivity of the efficiency, when it assumes its maximum value, to changes in these parameters is quite low. Thus, if M_B is changed up or down by a factor of two, the relative decrease in the efficiency is not greater than approximately 9 per cent. The corresponding figures for k, A and L_H are 19 per cent, 10 per cent and 36 per cent respectively.

It is seen that the hammer length L_H is the parameter that influences the efficiency to the highest degree. Still the sensitivity to changes in hammer length is not very high. This latter result is in agreement with e.g. the early observation made by RYD (1938) that within certain limits the result of drilling does not depend very much on whether a given work has been performed using a light or heavy hammer. In the example it is also seen that the sensitivity to changes in bit mass M_B or rod and hammer cross sectional area A is low.

From this example, the conclusion can be drawn that from an efficiency point of view only, the detailed choice of design parameters for a percussive drill is not very critical. Also, it can be concluded that, even if there are large variations of the conditions at the bottom of the drill hole and even if there are large variations in the different layers of rock, it should still be possible to keep the average efficiency high. This is in agreement with observations made by COOK & HUSTRULID (1970).

3.5. Comparison of the Methods

Figs. 3.13 and 3.14 illustrate some differences and similarities between the three methods of percussive rock destruction that have been analysed. It must, however, be remembered that the values of f_M and $\eta/(1-\gamma)$ for the down-the-hole and hammer drilling methods are based on a single impact and a single stress wave interaction respectively. Therefore, in general, these values represent lower bounds of the values which would be obtained if the phenomena of repeated impact and repeated stress wave interactions, respectively, were taken into consideration.

Fig. 3.13 illustrates that generally

$$f_M(\text{hammer}) \leq f_M(\text{down-the-hole}) \leq f_M(\text{churn}) \qquad (3.143)$$

and Fig. 3.14 illustrates that generally

$$\eta(\text{hammer}) \leq \eta(\text{down-the-hole}) \qquad (3.144)$$

For sufficiently small values of β, however,

$$\eta(\text{hammer}) < \eta(\text{down-the-hole}) < \eta(\text{churn}) \qquad (3.145)$$

Identical results (f_M and $\eta/(1-\gamma)$) are obtained for the down-the-hole and hammer drilling methods, when $\alpha > 1$ and $\beta > \pi\alpha/2\Gamma$.

Similar conclusions that were obtained in Section 3.4.3.2. regarding maximum efficiency conditions for the hammer drilling method can be obtained also for the other methods. Thus, for example, efficiencies higher than 90 per cent can be obtained for proper values of α, β and γ. Furthermore, these high efficiencies are not very sensitive to changes in the parameters M_B, k, A and L_H and they can be realized in conventional designs.

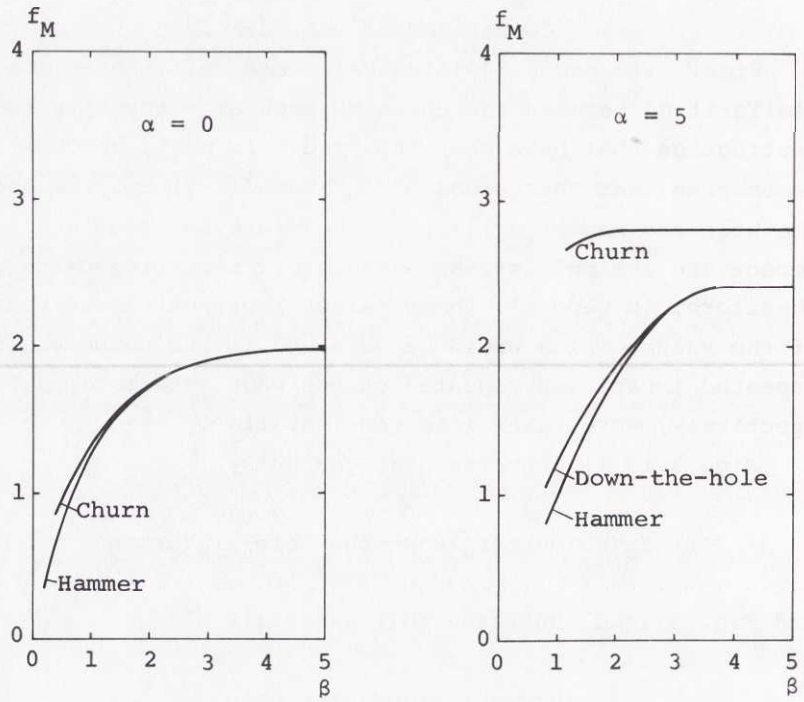

Fig. 3.13. f_M versus β for $\alpha = 0$ and $\alpha = 5$.
$\alpha = 4kc^2M_B/A^2E^2$, $\beta = 2kL_H/AE$.

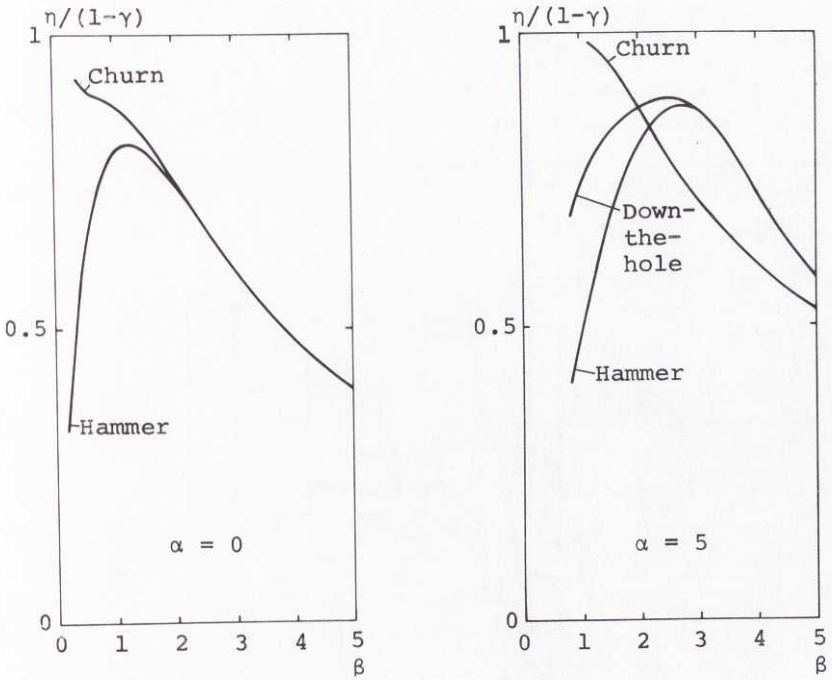

Fig. 3.14. $\eta/(1-\gamma)$ versus β for $\alpha = 0$ and $\alpha = 5$. $\alpha = 4kc^2M_B/A^2E^2$, $\beta = 2kL_H/AE$, $\gamma = k/k_e$.

3.6. Experiment

3.6.1. Equipment

The apparatus used in the tests is illustrated in Fig. 3.15.

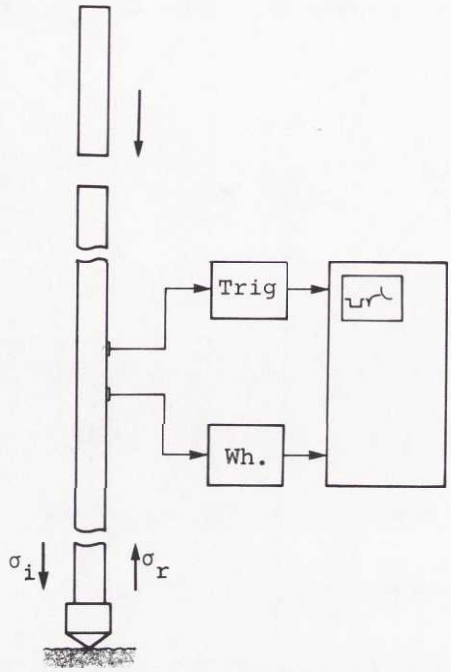

Fig. 3.15. Experimental apparatus.

Different artificial bits were attached to a drill rod in a drop-hammer. The hammers were cylindrical with approximately the same cross sectional area as the rod and different lengths. Therefore, on impacting the rod, the hammers produced rectangular stress waves with different lengths. Before impact, the bits were either resting on a cubical block of Swedish Bohus Granite, approximately 1 m^3, or they were free.

Two sets of strain gauges, compensated for bending, were mounted on the rod. The upper gauges were connected via a trigger unit to the trig input of a Tektronix oscilloscope and the lower gauges were connected to the input of one of the channels of the oscilloscope via a conventional Wheatstone bridge circuit. The trigger unit was adjusted to give

a single output triggering pulse a short time before the arrival of the incident stress wave σ_i, which was recorded together with the reflected stress wave σ_r by means of a camera.

The design of the bits and their attachment to the rod are illustrated in Fig. 3.16. The cutter was a single conical pin, and the bits differed in diameter and therefore also in mass.

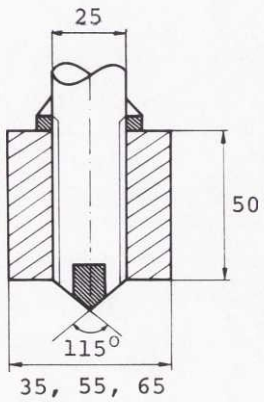

Fig. 3.16. Bits for the experiments.

3.6.2. Procedure.

Incident (σ_i) and reflected (σ_r) stress waves were recorded for eight combinations of three hammers (t_p = 0.20 ms, 0.40 ms and 0.60 ms), four bits (M_B = 0 kg, 0.38 kg, 0.93 kg and 1.30 kg) and two different end conditions (k = 0 MN/m and 5.6 MN/m). The pulse lengths t_p were determined from the incident stress wave records and the bit masses M_B (including the part of the rod inside the bit body) were calculated (density 7.8 10^3kg/m^3, length 50 mm, diameters 35 mm, 55 mm and 65 mm respectively). The value of the force-penetration constant k was determined from the reflected stress wave record and theoretical results when M_B = 0. The method of

achieving this will be shown below. In the tests where $k>0$, the bit was moved to an undamaged piece of rock surface before each impact.

The eight combinations of t_p, M_B and k are given in Table 3.1. In the same table are also given corresponding values of

$$\alpha = 4kc^2M_B/A^2E^2 \tag{3.21}$$

and according to Eqs. (3.17) and (3.26)

$$\beta = kct_p/AE \tag{3.146}$$

as well as L_B/L_H and kL_B/A_BE_B ($A = 4.90\ 10^{-4}m^2$, $E = E_B = 2.0\ 10^{11}N/m^2$, $c = 5.1\ 10^3m/s$). It can be seen that for all the eight combinations the inequalities (3.2) and (3.3) are well satisfied. Thus, from a theoretical point of view, the bits are expected to approach rigid masses in behaviour.

Table 3.1. Combinations of t_p, M_B and k in the tests.

Test Number	t_p (ms)	M_B (kg)	k (MN/m)	α	β	L_B/L_H	kL_B/A_BE_B
1	0.60	0	0	0	0	0.03	0
2	0.60	0.38	0	0	0	0.03	0
3	0.60	0.93	0	0	0	0.03	0
4	0.20	1.30	0	0	0	0.10	0
5	0.40	1.30	0	0	0	0.05	0
6	0.60	1.30	0	0	0	0.03	0
7	0.60	0	5.6	0	0.17	0.03	0
8	0.60	1.30	5.6	0.079	0.17	0.03	0.0004

3.6.3. Results and comparison of theory and experiment

The experimental results are shown in Figs. 3.17 and 3.18.

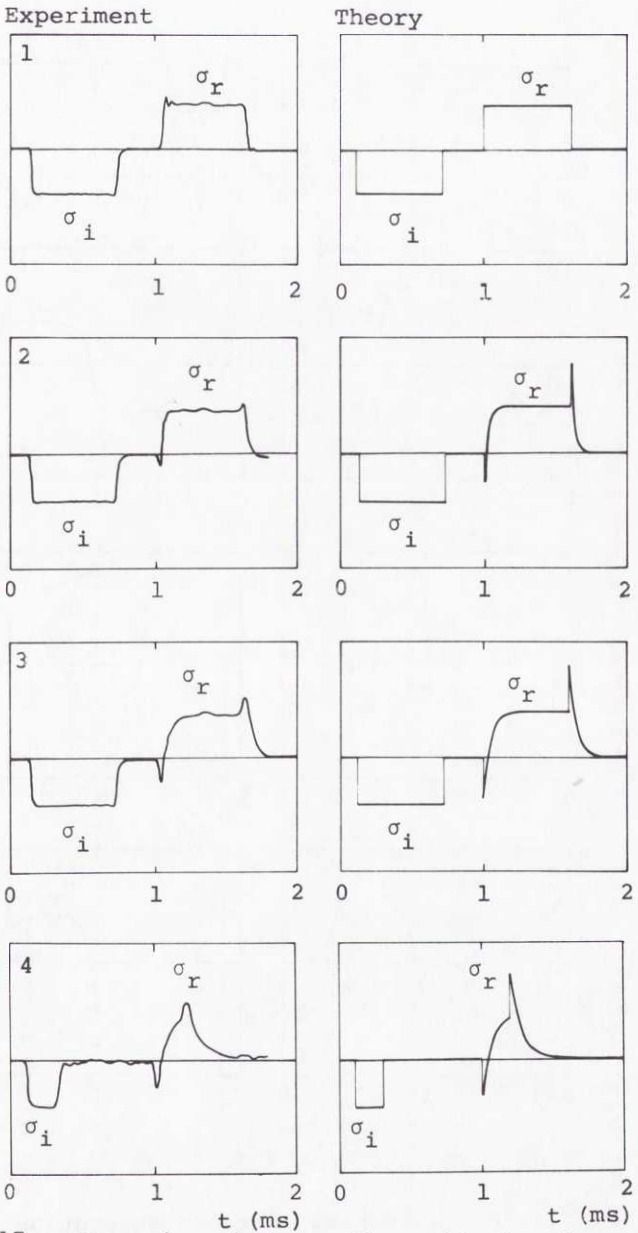

Fig. 3.17. Comparison between theoretical and experimental results. Tests 1-4.

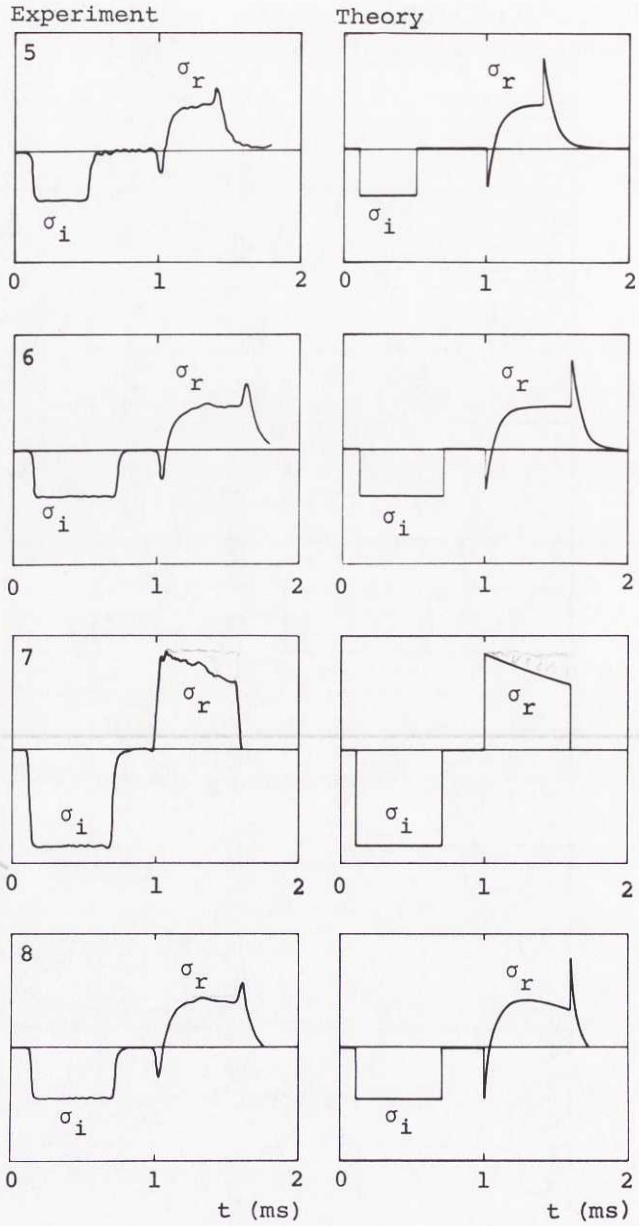

Fig. 3.18. Comparison between theoretical and experimental results. Tests 5-8.

The theoretical results also shown in Figs. 3.17 and 3.18 are obtained as follows:

The incident stress wave is approximated with a rectangular pulse with amplitude σ_0:

$$\sigma_i/\sigma_0 = \begin{cases} -1 & , \quad 0 \le t < t_p \\ 0 & , \quad t_p \le t \end{cases} \tag{3.147}$$

Then, according to Eqs. (3.100), (3.101), (3.112), (3.113), (3.16) and (3.26)

$$\sigma_r/\sigma_0 = -G(t)+G(t-t_p) \tag{3.148}$$

where

$$G(t) = g(t/t_0) \tag{3.149}$$

and where $g(t/t_0)$ is given by Eqs. (3.114) and (3.125).

When $M_B = 0$ and $k \to 0$ (Test 1), the end is free and Eqs. (3.149), (3.125), (3.16) and (3.17) yield in the limit

$$G(t) = -1 \tag{3.150}$$

Thus, σ_r differs from σ_i only by the sign.

When $M_B > 0$ and $k \to 0$ (Tests 2-6), $\alpha \to 0$ and Eqs. (3.149), (3.114), (3.76), (3.16), (3.17) and (3.21) yield in the limit

$$G(t) = 2e^{-(AE/M_B c)t}-1 \tag{3.151}$$

When $M_B = 0$ and $k > 0$ (Test 7), Eqs. (3.149), (3.125) and (3.16) yield

$$G(t) = 1-2e^{-t/t_0} \tag{3.152}$$

where

$$t_0 = AE/kc \tag{3.17}$$

When finally $M_B>0$ and $k>0$ (Test 8), Eqs. (3.149), (3.114) and (3.16) yield

$$G(t) = 1-(4/\Delta)e^{-(2/\alpha)t/t_0}\sinh\{(2\Delta/\alpha)t/t_0\} \tag{3.153}$$

From Test 7, it is found that

$$\sigma_r(t_p-)/\sigma_0 = 0.68 \tag{3.154}$$

while according to Eqs. (3.148) and (3.152),

$$\sigma_r(t_p-)/\sigma_0 = -1+2e^{-t_p/t_0} \tag{3.155}$$

Eqs. (3.155), (3.154) and $t_p = 0.60$ ms then yield $t_0 = 3.45$ ms. With this value of t_0, Eq. (3.152) is fitted to the experimental result in Test 7. The same value of t_0 is, however, substituted into Eq. (3.153) to allow a comparison between theory and experiment in Test 8. From Eq. (3.17) and the determined value of t_0, $k = 5.6$ MN/m is also obtained.

3.6.4. Discussion

The agreement between theory and experiment, as illustrated by Figs. 3.17 and 3.18 is for many practical purposes quite satisfactory. However, there are essentially two types of deviation between theory and experiment.

First, there are small oscillations in the measured stresses without correspondence in theory. This deviation is caused by the limitations of the elementary stress wave theory (Appendix B).

Secondly, experimentally observed peaks in $\sigma_r(t)$ at $t = 0$ and $t = t_p$ have lower amplitudes and are smoother than the

peaks obtained from theory. This deviation can readily be explained as follows: The theoretical peaks result from the two basic assumptions that the incident stress wave is a perfect rectangular pulse and that the bit behaves as a perfectly rigid body. However, in the experiments, the rise and decay times of the incident stress wave are seen to be approximately 20 μs. Furthermore, the widths of the theoretically determined peaks are of the order 10 μs (M_B = 0.38 kg) to 50 μs (M_B = 1.30 kg), while the travelling time for a stress wave twice the length of the bit is approximately 20 μs. Thus, during these short time intervals that correspond to the width of the theoretically determined peaks in σ_r, there is not sufficient time to allow the bit to behave like a rigid body. Therefore, the experimentally determined stress peaks are not as high and as sharp as those obtained theoretically.

The second deviation discussed above is essential with respect to considerations regarding e.g. fatigue of drill rods. However, the deviation is not very significant in connection with the determination of maximum bit force or efficiency of energy transfer to rock.

The comparison between theory and experiment was performed in a situation corresponding to the hammer drilling method. However, it is reasonable to believe that similar agreement would also be obtained for the churn drilling and down-the-hole drilling methods.

4. SUPPLEMENTARY PROBLEMS CONNECTED WITH HAMMER DRILLING

4.1. Introduction

In Section 3.4 the hammer drilling method was analysed, and in Section 3.5 it was compared with two other methods of percussive rock destruction, viz. the churn drilling method and the down-the-hole drilling method. However, there are several important aspects of hammer drilling which were not covered by the analysis in Section 3.4. A few of these aspects will be treated separately in the present chapter.

In Section 3.4 the determination of the work performed on the rock was entirely based on the energy delivered during the first stress wave reflection at the bit during each cycle. However, as was shown by HUSTRULID (1968), there may be repeated transfer of energy to the rock caused by repeated stress wave reflections in the drill rod. In Section 4.2 it will be shown, in a situation similar to the one studied in Section 3.4, under what conditions there is or is not energy transfer to the rock during the second stress wave interaction at the bit. For the sake of simplicity, however, it is assumed that the bit mass $M_B = 0$, i.e. $\alpha = 0$.

In Section 3.4 the analysis was limited to the situation when the hammer is cylindrical and the hammer and rod cross sectional areas and material properties are equal, i.e. when the incident stress wave is a rectangular pulse. However, FAIRHURST (1961c) and SIMON (1964) have shown that the shape of the incident stress wave influences the efficiency of energy transfer to the rock to a large extent. ARNDT (1960), FISCHER (1960), SIMON (1963a) and DUTTA (1968) have also shown how the shape of the incident stress wave can be determined if hammer and rod material and geometrical properties are known. In order to demonstrate in greater detail the influence of stress wave shape on the energy transfer to the

rock, energy transfer from a stress wave shaped as a triangular pulse will be studied in Section 4.3. Also, in the same section, the efficiency will be studied when the incident stress wave is generated by a cylindrical hammer with greater dynamic stiffness than the rod. Except for the shapes of the incident stress waves, the situations studied in Section 4.3 are similar to the one studied in Section 3.4. For the sake of simplicity, however, it is assumed that the bit mass $M_B = 0$, i.e. $\alpha = 0$.

In Sections 3.4, as well as 4.2 and 4.3, the loading section of the force-penetration characteristic is assumed to be linear as is illustrated in Fig. 2.19. In Section 4.4, however, the influence of a non-linear loading section of the force-penetration characteristic will be considered by first assuming a parabolic relation as is illustrated in Fig. 2.20. In this case it is assumed that the incident stress wave is a rectangular pulse and that the bit mass $M_B = 0$. Then, also, a more general type of non-linear loading section of the force-penetration characteristic will be considered by assuming a piece-wise linear relation as is shown in Fig. 2.21. In that case it is assumed that the incident stress wave is a piece-wise linear function of time, while the bit mass $M_B (>0)$ may be arbitrary.

4.2. Energy Transfer from the Second Incident Stress Wave

4.2.1. Introduction

Consider hammer drilling as it is illustrated in Figs. 3.1 and 3.8 and assume that the bit is massless, $M_B = 0$. Let the notation and basic assumptions be the same as in Chapter 3.

Then, according to the results obtained in Section 3.4, the incident stress wave

$$s_i = \begin{cases} -1 , & 0 \le \tau < \beta \\ 0 , & \beta \le \tau \end{cases} \qquad (3.112)$$

gives rise to the generation of a reflected stress wave at the bit

$$s_r = -1+2e^{-\tau} \qquad (3.129)$$

when

$$0 \le \tau < \beta \qquad (3.130)$$

This has been referred to as the first stress wave reflection or interaction at the bit. During this first stress wave reflection, the maximum force acting on the bit is

$$f_M = 2(1-e^{-\beta}) \qquad (3.139)$$

and the efficiency of energy transfer to the rock is

$$\eta = 2(1-\gamma)(1-e^{-\beta})^2/\beta \qquad (3.140)$$

The first part of the reflected stress wave s_r is tensile, i.e. $s_r > 0$. Therefore, when the reflected stress wave arrives at the rod-hammer interface, it separates the rod from the hammer and is, at least as long as it is tensile, reflected from the free upper end of the rod as a compressive second incident stress wave $s_{i2} = -s_r < 0$. When this second incident stress wave s_{i2} arrives at the bit, it is assumed that the force F acting between bit and rock has dropped to zero (the rod is sufficiently long). Therefore, the force-penetration characteristic met by s_{i2} takes the form (2.36) as long as the force F acting on the rock is less than the maximum force F_M obtained during the first stress wave reflection. If F becomes

greater than F_M, then the force-penetration relationship is given by Eq. (2.35) as long as the penetration velocity is non-negative. At the bit s_{i2} gives rise to a second reflected stress wave s_{r2}. At the bit these stress waves are denoted by $s_{i2}(\tau)$ and $s_{r2}(\tau)$ respectively (Appendix B).

If the maximum force F_{M2} reached at the bit, during the second stress wave reflection, is less than F_M, then no further work is performed on the rock. This is illustrated in Fig. 3.9a. If, on the other hand, F_{M2} is greater than F_M, then work W_2 is performed on the rock during the second stress wave reflection in addition to the work W performed during the first stress wave reflection. This is illustrated in Fig. 3.9b. In the latter case, the values of f_M and η as given by Eqs. (3.139) and (3.140) respectively, may be considered as lower limits of the actual values obtained, when repeated reflections are taken into account.

Next, the maximum force F_{M2} attained during the second stress wave reflection will be determined. Then, by studying when

$$F_{M2} \leq F_M \tag{4.1}$$

a criterion will be obtained, which tells when no work is performed on the rock by the second incident stress wave. If the criterion is not satisfied, such work is performed.

4.2.2. Second stress wave reflection

For brevity, it is convenient to redefine time so that $\tau = 0$ corresponds to the time when the second incident stress wave s_{i2} arrives at the bit. Thus, at the bit

$$s_{i2} = 1-2e^{-\tau} \tag{4.2}$$

for $0 \leq \tau < \beta$, at least as long as s_{i2} is compressive, i.e.

$$s_{i2}(\tau)<0 \tag{4.3}$$

Some time after s_{i2} has become tensile, i.e. $s_{i2}>0$, s_{i2} may be different from the expression given by Eq. (4.2) because of a reestablished contact between hammer and rod. Eqs. (4.2) and (3.127) show that s_{i2} changes from compressive to tensile when $0<\tau\leq\beta$. However, the force F acting on the rock must attain its maximum value F_{M2} at some time $\tau = \tau_{M2}$ when the incident stress wave is compressive or when it changes from compressive to tensile. This is realized since $F>0$ and $s_{i2}>0$ implies $dx/dt<0$, i.e. a negative penetration velocity. Consequently, $0<\tau_{M2}\leq\beta$ and s_{i2} is given correctly by Eq. (4.2) in the interval $0\leq\tau\leq\tau_{M2}$ when $0<\tau_{M2}<\beta$ and in the interval $0\leq\tau<\tau_{M2}$ when $\tau_{M2} = \beta$.

For brevity, it is also convenient to redefine the penetration x in such a way that x = 0 corresponds to the penetration when the second incident stress wave arrives at the bit. Thus, it is assumed that x(0) = 0 and that

$$F = k_e x \tag{4.4}$$

as long as in agreement with Eq. (4.1) $F_{M2}\leq F_M$. The case $F_{M2}>F_M$ need not be considered. The force-penetration relationship thus met by the second incident stress wave is illustrated in Fig. 4.1.

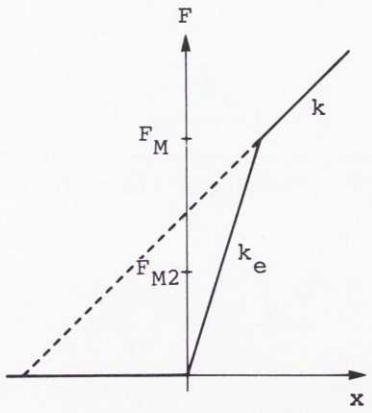

Fig. 4.1. Force-penetration relationship at second stress wave reflection.

From Eqs. (3.95) and (3.98) respectively (with $M_B = 0$), the differential equation

$$(AE/k_e c)d\sigma_{r2}/dt+\sigma_{r2} = -(AE/k_e c)d\sigma_{i2}/dt+\sigma_{i2} \quad (4.5)$$

and the initial condition

$$\sigma_{r2}(0) = -\sigma_{i2}(0) \quad (4.6)$$

are obtained. If, in accordance with earlier definitions, the non-dimensional stresses

$$s_{i2} = \sigma_{i2}/\sigma_0 \quad (4.7)$$

and

$$s_{r2} = \sigma_{r2}/\sigma_0 \quad (4.8)$$

are introduced, where σ_0 is defined in Eq. (3.111), and if

also the parameter γ in agreement with Eq. (2.38) and the non-dimensional time τ in agreement with Eqs. (3.16) and (3.17) are introduced, then Eqs. (4.5) and (4.6) take the forms

$$\gamma ds_{r2}/d\tau+s_{r2} = -\gamma ds_{i2}/d\tau+s_{i2} \tag{4.9}$$

and

$$s_{r2}(0) = -s_{i2}(0) \tag{4.10}$$

respectively.

From Eqs. (4.2), (4.9) and (4.10) the solution

$$s_{r2} = 1+2\{(1+\gamma)/(1-\gamma)\}(e^{-\tau/\gamma}-e^{-\tau}) \tag{4.11}$$

for $s_{r2}(\tau)$ is obtained. This solution is valid in the interval $0\leq\tau\leq\tau_{M2}$ when $0<\tau_{M2}<\beta$ and in the interval $0\leq\tau<\tau_{M2}$ when $\tau_{M2} = \beta$.

4.2.3. Energy transfer

In accordance with the definition (3.4) of f_M, the non-dimensional maximum force f_{M2} at the second stress wave reflection is defined as

$$f_{M2} = F_{M2}/F_0 \tag{4.12}$$

where F_0 is given by Eq. (3.5). Since with $f = F/F_0$ and $0<\gamma\leq 1$ $f(\tau)$ is a continuous function, it is realized that $f(\tau)\rightarrow f(\tau_{M2}) = f_{M2}$ when $\tau\rightarrow\tau_{M2}-$. Therefore (Cf. Eq. 3.133),

$$f_{M2} = -\lim_{\tau\rightarrow\tau_{M2}-}\{s_{r2}(\tau)+s_{i2}(\tau)\} \tag{4.13}$$

where τ_{M2} can be determined as the value of τ for which $(s_{r2}-s_{i2})$ changes sign from positive to negative when $0\leq\tau\leq\beta$.

From Eqs. (4.2), (4.11) and (4.13), the following results are obtained:

When

$$\beta>\{\gamma/(1-\gamma)\}\ln\{(1+\gamma)/2\gamma\} \tag{4.14}$$

then

$$\tau_{M2} = \{\gamma/(1-\gamma)\}\ln\{(1+\gamma)/2\gamma\} \tag{4.15}$$

and

$$f_{M2} = 2\left[-1+\{2/(1-\gamma)\}\{2\gamma/(1+\gamma)\}^{\gamma/(1-\gamma)} - \right.$$
$$\left. -\{(1+\gamma)/(1-\gamma)\}\{2\gamma/(1+\gamma)\}^{1/(1-\gamma)}\right] \tag{4.16}$$

In this case, according to Eqs. (3.139) and (4.16),

$$f_{M2}\leq f_M \tag{4.17}$$

provided that

$$e^{-\beta}\leq 2-\{2/(1-\gamma)\}\{2\gamma/(1+\gamma)\}^{\gamma/(1-\gamma)} +$$
$$+\{(1+\gamma)/(1-\gamma)\}\{2\gamma/(1+\gamma)\}^{1/(1-\gamma)} \tag{4.18}$$

When

$$\beta\leq\{\gamma/(1-\gamma)\}\ln\{(1+\gamma)/2\gamma\} \tag{4.19}$$

then

$$\tau_{M2} = \beta \tag{4.20}$$

and

$$f_{M2} = 2\left[-1+\{2/(1-\gamma)\}e^{-\beta}-\{(1+\gamma)/(1-\gamma)\}e^{-\beta/\gamma}\right] \tag{4.21}$$

In this case, according to Eqs. (3.139) and (4.21), the inequality (4.17) is satisfied provided that

$$\{(3-\gamma)/(1-\gamma)\}e^{-\beta}-\{(1+\gamma)/(1-\gamma)\}e^{-\beta/\gamma}\leq 2 \qquad (4.22)$$

For brevity, it is convenient to introduce functions $\beta_1(\gamma)$, $\beta_2(\gamma)$ and $\beta_3(\gamma)$ defined for $0<\gamma<1$ as

$$\beta_1 = \{\gamma/(1-\gamma)\}\ln\{(1+\gamma)/2\gamma\} \qquad (4.23)$$

$$\beta_2 = -\ln\left[2-\{2/(1-\gamma)\}\{2\gamma/(1+\gamma)\}^{\gamma/(1-\gamma)}+\right.$$
$$\left.+\{(1+\gamma)/(1-\gamma)\}\{2\gamma/(1+\gamma)\}^{1/(1-\gamma)}\right] \qquad (4.24)$$

and implicitly as

$$\{(3-\gamma)/(1-\gamma)\}e^{-\beta}3-\{(1+\gamma)/(1-\gamma)\}e^{-\beta}3^{/\gamma} = 2 \qquad (4.25)$$

Then the condition for no energy transfer to the rock at the second stress wave reflection, i.e. $f_{M2}\leq f_M$, can be summarized as follows:

$$\beta>\beta_1(\gamma) \text{ and } \beta\geq\beta_2(\gamma) \qquad (4.26)$$

or

$$\beta\leq\beta_1(\gamma) \text{ and } \beta\geq\beta_3(\gamma) \qquad (4.27)$$

However, $\beta_1(1/2) = \beta_2(1/2) = \beta_3(1/2) = \ln(3/2)$ and

$$\beta_1(\gamma)\leq\beta_3(\gamma)\leq\beta_2(\gamma) \qquad (4.28)$$

when $0<\gamma\leq 1/2$, whereas

$$\beta_3(\gamma)<\beta_2(\gamma)<\beta_1(\gamma) \tag{4.29}$$

when $1/2<\gamma<1$. Therefore, the conditions (4.26) and (4.27) can be summarized as

$$\beta\geq\beta_0(\gamma) \tag{4.30}$$

where

$$\beta_0(\gamma) = \begin{cases} \beta_2(\gamma) & , \quad 0<\gamma\leq 1/2 \\ \beta_3(\gamma) & , \quad 1/2<\gamma<1 \end{cases} \tag{4.31}$$

Thus, if the condition (4.30) is satisfied, there is no energy transfer to the rock during the second stress wave reflection at the bit. If, on the other hand, the condition (4.30) is not satisfied, then such energy transfer occurs. This is illustrated in Fig. 4.2.

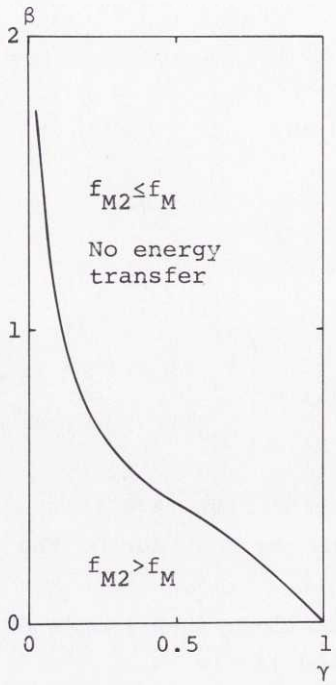

Fig. 4.2. Combinations of the parameters γ and β for which energy transfer does or does not take place at the second stress wave reflection at the bit. $\beta = 2kL_H/AE$, $\gamma = k/k_e$.

4.2.4. Discussion

According to the condition (4.30), no energy transfer to the rock occurs at the second stress wave reflection if the parameter $\beta = 2kL_H/AE$ is greater than or equal to a certain value β_0 which is a function of the parameter $\gamma = k/k_e$. This is illustrated in Fig. 4.3. Fig. 4.2 illustrates that β_0 is a decreasing function of γ and that $\beta_0 \to \infty$ when $\gamma \to 0$ and $\beta_0 \to 0$ when $\gamma \to 1$.

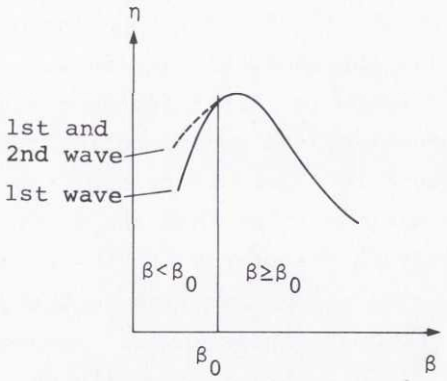

Fig. 4.3. For $\beta \geq \beta_0$ no energy is transferred to the rock by the second incident stress wave.

When $0<\gamma<1$, energy is not transferred to the rock by the second incident stress wave if the rock is sufficiently hard (k large) and/or if the hammer is sufficiently long (L_H large). This is explained by the fact that in such cases the tensile part of the first reflected stress wave is relatively small. Consequently, the compressive part of the second incident stress wave is also relatively small. If, on the other hand, the rock is sufficiently soft and/or the hammer is sufficiently short, then an essential part of the second incident stress wave is compressive, and additional work is performed on the rock.

When the deformation of rock is completely inelastic, i.e. $\gamma \to 0$, a certain amount of energy is always delivered by the second incident stress wave. This is explained by the fact that if, in this case, the second incident stress wave gives rise to any penetration at all, then additional work is performed. When, on the other hand, the deformation of rock is completely elastic, i.e. $\gamma \to 1$, then the maximum force due to the second incident stress wave is always less than the maximum force due to the first incident stress wave. This is

explained by the fact that the force-penetration relationships faced by the first and second incident stress waves are identically the same, the stress wave energies are also the same, but while the first incident stress wave is completely compressive, the second incident stress wave is to a certain extent tensile. Therefore, the second wave gives rise to less maximum force than the first wave.

When energy is transferred to the rock by the second incident stress wave, energy may also be transferred by the third, fourth etc. incident stress waves. However, as was noticed by HUSTRULID (1968), this is normally not the case in hammer drilling. When, on the other hand, no energy is transferred to the rock by the second incident stress wave, it seems likely that no energy is transferred by the third, fourth etc. stress waves either. The reason for this is that the amplitude of the compressive part in the beginning of the third incident stress wave is smaller than that of the second incident stress wave, while the force-penetration relationship remains unchanged etc.

In Section 3.4.3 it was concluded that since the maximum efficiency based on energy transfer from the first incident stress wave only is as high as 0.902 (for $\alpha = 2.329$, $\beta = 1.970$ and $\gamma = 0$), the energy that may be delivered by subsequent incident stress waves is only of minor importance. Here it is moreover seen that when $\alpha = 0$ and $\beta \geq \beta_0(\gamma)$, there is no further energy at all delivered by the second incident stress wave (and probably not by any other subsequent stress wave). This further strengthens the feeling that from a rock drill design point of view it may be sufficient to consider energy transfer by the first incident stress wave.

4.3. Influence of Incident Stress Wave Shape

4.3.1. Introduction

Consider hammer drilling when the hammer material (Young's modulus E_H, sonic velocity c_H) is not necessarily the same as the rod material (Young's modulus $E_R = E$, sonic velocity $c_R = c$) and when the hammer geometry is arbitrary. Assume that the rod is cylindrical with cross sectional area $A_R = A$ and that there may be an anvil between the hammer and rod.

In this case, the stress wave σ_i, which is generated at impact, will not generally have the simple form of a rectangular pulse as in Section 3.4. Instead, the shape of the generated stress wave is determined by an infinite number of reflections in the hammer and anvil, and it may often become quite complex. This has been shown by several investigators, e.g. ARNDT (1960), FISCHER (1960), SIMON (1963a) and DUTTA (1968). Also, the energy of the generated stress wave (Appendix B)

$$W_i = (Ac/E)\int \sigma_i^2(t)dt \qquad (4.32)$$

may be less than or equal to the impact energy. In other words, the hammer may possibly rebound without being influenced by the reflected stress wave σ_r from the bit end of the rod. Normally, however, no such rebound occurs and the impact energy and the generated stress wave energy are equal (provided that the rod is long enough). This is also the case in the situation considered in Section 3.4.

The work performed on the rock at the first stress wave reflection at the bit is again given by Eq. (2.39), i.e.

$$W = (1-\gamma)F_M^2/2k \qquad (2.39)$$

and, as in Section 3.1, an efficiency of energy transfer to the rock is defined as

$$\eta = W/W_i \tag{3.6}$$

Provided that the impact energy of the hammer is completely converted into stress wave energy, W_i here and in Section 3.1 have the same meaning and, consequently, the definitions of the efficiency η are the same. If, however, the impact energy of the hammer is not completely converted into stress wave energy in the rod, then the definition of efficiency given here results in a higher efficiency than the definition in Section 3.1.

If the non-dimensional stresses s_i and s_r in accordance with Eqs. (3.100) and (3.101), the non-dimensional time τ in accordance with Eqs. (3.16) and (3.17) and the non-dimensional maximum force

$$f_M = F_M/F_0 \tag{3.4}$$

where now in agreement with earlier definitions (Eqs. (3.5) and (3.111))

$$F_0 = A\sigma_0 \tag{4.33}$$

are introduced, then Eqs. (4.32), (2.39) and (3.6) yield

$$\eta = (1-\gamma) f_M^2 / 2\int s_i^2(\tau)\,d\tau \tag{4.34}$$

Since for the rectangular stress wave considered in Section 3.4 the value of the integral in Eq. (4.34) is β, it can be seen that Eq. (3.92) is a special case of Eq. (4.34).

For many types of stress waves $s_i(\tau)$ the penetration velocity $d\xi/d\tau$ is non-negative until the time τ_M when the

maximum force f_M is attained. Then, according to Eq. (3.133),

$$f_M = -\{s_r(\tau_M)+s_i(\tau_M)\}-(\alpha/4)\{ds_r(\tau_M)/d\tau-ds_i(\tau_M)/d\tau\} \tag{3.133}$$

where τ_M is the value of τ, which makes ξ equal to its maximum value ξ_M.

Since, as was shown in Section 3.4, the penetration velocity $d\xi/d\tau$ is proportional to (s_r-s_i), this quantity changes sign when $\tau = \tau_M$. Therefore, when $\alpha>0$ or $s_i(\tau)$ is a continuous function τ_M can be determined from the equation

$$s_r(\tau_M)-s_i(\tau_M) = 0 \tag{3.106}$$

When $\alpha = 0$ and $s_i(\tau)$ is not a continuous function, however, τ_M must be determined as the value of τ for which (s_r-s_i) changes sign from positive to negative.

As long as the penetration velocity is non-negative, i.e.

$$0\leq\tau\leq\tau_M \tag{3.37}$$

and when $\alpha>0$ the reflected stress wave $s_r(\tau)$ is related to the incident stress wave $s_i(\tau)$ by the differential equation

$$(\alpha/4)d^2s_r/d\tau^2+ds_r/d\tau+s_r = (\alpha/4)d^2s_i/d\tau^2-ds_i/d\tau+s_i \tag{3.102}$$

and the initial conditions

$$(\alpha/4)ds_r(0)/d\tau+s_r(0) = (\alpha/4)ds_i(0)/d\tau-s_i(0) \tag{3.103}$$

and

$$s_r(0) = s_i(0) \tag{3.104}$$

When $\alpha = 0$, Eqs. (3.102)-(3.104) are replaced by Eqs. (3.122) and (3.123), i.e. the initial condition (3.104) is omitted.

To sum up, if the incident stress wave $s_i(\tau)$ is known, it is often possible to determine the efficiency η, defined as the ratio of the work performed on the rock at the first stress wave reflection and the incident stress wave energy, by use of Eqs. (3.102)-(3.104), (3.106), (3.133) and (4.34). It is therefore realized that the efficiency η is unaffected by σ_0, which represents the stress wave amplitude.

If the complete incident and reflected stress waves $s_i(\tau)$ and $s_r(\tau)$ are known, the efficiency η can be determined more simply as

$$\eta = (\int s_i^2 d\tau - \int s_r^2 d\tau) / \int s_i^2 d\tau \qquad (4.35)$$

Next, the influence of incident stress wave shape on efficiency will be illustrated by two examples. First it will be assumed that the incident stress wave is an arbitrary triangular pulse. Such a pulse is not normally generated at impact, but the example illustrates perfectly some fundamental properties of the relationship between efficiency and incident stress wave shape. Then the incident stress wave is assumed to be of such a type as is generated by impact, when the hammer is cylindrical and of greater dynamic stiffness (Appendix B) than the rod (when the hammer and rod materials are the same, this implies that the hammer has a larger cross sectional area than the rod). In both examples, it is assumed for the sake of simplicity that the bit mass $M_B = 0$, i.e. $\alpha = 0$.

4.3.2. Triangular incident stress wave

4.3.2.1. Stress wave reflection. - The incident stress wave is assumed to be given by

$$s_i = \begin{cases} -\tau/2\Theta\beta & , \quad 0 \le \tau < 2\Theta\beta \\ (\tau-2\beta)/2(1-\Theta)\beta & , \quad 2\Theta\beta \le \tau < 2\beta \end{cases} \qquad (4.36)$$

and is illustrated in Fig. 4.4. In accordance with the definition of β in Section 3.4, β is the non-dimensional half-width of $s_i(\tau)$, while Θ $(0 \le \Theta \le 1)$ determines the position along the τ-axis of the peak amplitude. Therefore, β and Θ represent the duration and shape of the stress wave respectively.

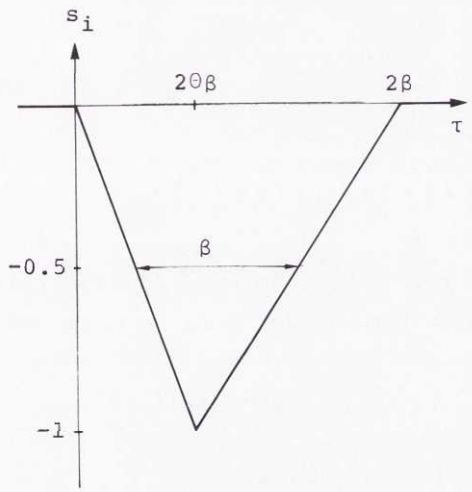

Fig. 4.4. Incident stress wave $s_i(\tau)$.

When $0<\Theta<1$, Eqs. (3.122), (3.123) and (4.36) yield

$$s_r = \begin{cases} (1-e^{-\tau}-\tau/2)/\theta\beta & , \quad 0\leq\tau<2\theta\beta \\ -e^{-\tau}/\theta\beta+e^{-(\tau-2\theta\beta)}/\theta\beta(1-\theta)- & \\ -(1+\beta)/\beta(1-\theta)+\tau/2\beta(1-\theta) & , \quad 2\theta\beta\leq\tau<2\beta \end{cases} \tag{4.37}$$

The solution (4.37) is valid in the interval (3.37), i.e. $0\leq\tau\leq\tau_M$, where according to Eqs. (3.106), (4.36) and (4.37) $2\theta\beta\leq\tau_M<2\beta$ and

$$\tau_M = \ln\{(e^{2\theta\beta}-1+\theta)/\theta\} \tag{4.38}$$

When $\theta\to 0$ and $\theta\to 1$ Eq. (4.38) yields

$$\lim_{\theta\to 0}\tau_M = \ln(1+2\beta) \tag{4.39}$$

and

$$\lim_{\theta\to 1}\tau_M = 2\beta \tag{4.40}$$

respectively.

4.3.2.2. Efficiency. - According to Eqs. (3.133) (with $\alpha = 0$), (3.106) and (4.36) the maximum force f_M is obtained as

$$f_M = (2\beta-\tau_M)/\beta(1-\theta) \tag{4.41}$$

Further, Eq. (4.36) yields

$$\int s_i^2(\tau)d\tau = 2\beta/3 \tag{4.42}$$

and the efficiency η is obtained by substitution of Eqs. (4.41) and (4.42) into Eq. (4.34) as

$$\eta = 3(1-\gamma)(2\beta-\tau_M)^2/4\beta^3(1-\theta)^2 \tag{4.43}$$

When $\theta \to 0$ Eqs. (4.43) and (4.38) yield

$$\lim_{\theta \to 0} \eta = 3(1-\gamma)\{2\beta - \ln(1+2\beta)\}^2/4\beta^3 \tag{4.44}$$

and when $\theta \to 1$ the same equations yield

$$\lim_{\theta \to 1} \eta = 3(1-\gamma)\{2\beta - 1 + e^{-2\beta}\}^2/4\beta^3 \tag{4.45}$$

From Eqs. (4.43)-(4.45) and (4.38) it is seen that the efficiency η is a function of the parameters β, θ and γ. β represents the length of the stress wave while θ represents the shape of the stress wave. In dimensional units β can be expressed as

$$\beta = t_p/t_0 \tag{3.26}$$

where t_p is the half-width of the triangular pulse and

$$t_0 = AE/kc \tag{3.17}$$

Numerical results for η according to Eqs. (4.43)-(4.45) and (4.38) are plotted in Fig. 4.5.

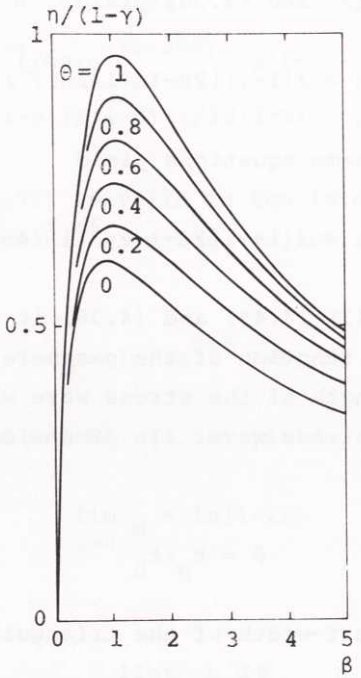

Fig. 4.5. $n/(1-\gamma)$ versus β for different values of Θ. $\beta = t_p/t_0$, where t_p is the half-width of the triangular pulse and $t_0 = AE/kc$, $\gamma = k/k_e$.

4.3.3. Incident stress wave generated by a cylindrical hammer with dynamic stiffness greater than or equal to the dynamic stiffness of the rod

4.3.3.1. Stress wave reflection. - The incident stress wave is given by (e.g. FISCHER, 1960)

$$s_i = -s_n \quad , \quad n\beta \leq \tau < (n+1)\beta \quad (n = 0, 1, 2, \ldots) \qquad (4.46)$$

where

$$s_n = q^n \tag{4.47}$$

$$q = (R-1)/(R+1) \tag{4.48}$$

$$R = A_H E_H c/AEc_H \quad (\geq 1) \tag{4.49}$$

$$\beta = t_p/t_0 \tag{4.50}$$

$$t_p = 2L_H/c_H \tag{4.51}$$

and is illustrated in Fig. 4.6. A_H, E_H and c_H denote the cross sectional area, the Young's modulus and the sonic velocity respectively for the hammer, while $A = A_R$, $E = E_R$ and $c = c_R$ denote the corresponding quantities for the rod (subscripts R are dropped). t_0 is given by Eq. (3.17). $A_H E_H/c_H$ and $AE/c = A_R E_R/c_R$ are sometimes referred to as the dynamic stiffness of the hammer and rod respectively. Therefore, R will be referred to as the dynamic stiffness ratio.

According to Eq. (4.46), β is the non-dimensional duration of each constant amplitude segment of the stress wave, while, according to Eqs. (4.46)-(4.48), R determines the ratio q of the amplitudes of two successive segments s_{n+1} and s_n of the stress wave. Therefore, β and R represent the duration and shape of the stress wave respectively.

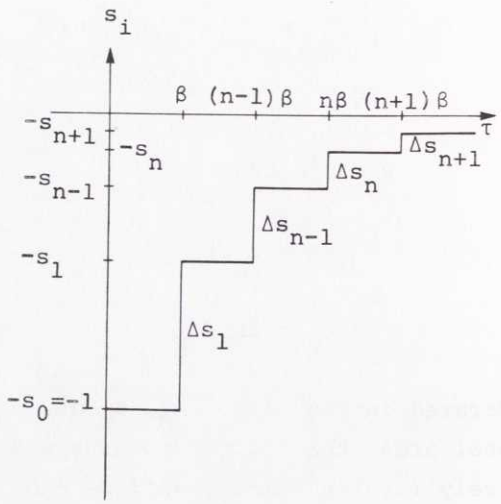

Fig. 4.6. Incident stress wave $s_i(\tau)$.

When $R \geq 1$, as it is assumed here, the impact energy is completely transformed into stress wave energy. When $R<1$, however, the stress wave energy is less than the impact energy, and the hammer rebounds after the time t_p given by Eq. (4.51). When $R>1$ the stress wave duration is infinite, according to Eq. (4.46), whereas when $R \leq 1$, the stress wave is a rectangular pulse as in Section 3.4.

It is also seen that when the hammer and rod materials are the same, then $R = A_H/A \geq 1$, i.e. the cross sectional area of the hammer is larger than the cross sectional area of the rod, and $\beta = 2kL_H/AE$, i.e. β is given by Eq. (3.60).

When $R \geq 1$ and $\tau \geq \beta$ the incident stress wave $s_i(\tau)$ can also be expressed as

$$s_i = -1 + \sum_{j=1}^{n} \Delta s_j \quad , \quad n\beta \leq \tau < (n+1)\beta \quad (n = 1, 2, \ldots) \tag{4.52}$$

where, according to Eqs. (4.46) and (4.47),

$$\Delta s_j = (1-q)q^{j-1} \tag{4.53}$$

Eqs. (3.122), (3.123) and (4.52) yield

$$s_r = 2e^{-\tau} - 1 + \sum_{j=1}^{n} \Delta s_j (-2e^{-(\tau - j\beta)} + 1)$$
$$n\beta \le \tau < (n+1)\beta \qquad (n = 1, 2, \ldots) \tag{4.54}$$

The solution (4.54) is valid as long as $s_r(\tau) - s_i(\tau) \ge 0$, i.e. in the interval (3.37) or $0 \le \tau \le \tau_M$, where τ_M is the value of τ, for which $s_r(\tau) - s_i(\tau)$ changes sign from positive to negative.

Eqs. (4.52)-(4.54) yield

$$s_r - s_i = 2e^{-\tau}\{1 - (1-q) \sum_{j=1}^{n} q^{j-1} e^{j\beta}\}$$
$$n\beta \le \tau < (n+1)\beta \qquad (n = 1, 2, \ldots) \tag{4.55}$$

Since it is known from the analysis in Section 3.4 that $s_r(\tau) - s_i(\tau)$ does not change sign in the interval $0 \le \tau < \beta$, it can be seen that $s_r(\tau) - s_i(\tau)$ can change sign only when $\tau = n\beta$, $n = 1, 2, \ldots$. From Eq. (4.55) τ_M can therefore be determined as follows: Let the functions $\beta_n(R)$ be defined by

$$1 - (1-q) \sum_{j=1}^{n} q^{j-1} e^{j\beta_n} = 0 \tag{4.56}$$

i.e. if $\beta_n \neq -\ln(q)$

$$1 - e^{\beta_n} + (1-q) q^n e^{(n+1)\beta_n} = 0 \tag{4.57}$$

for $n = 1, 2, \ldots$ and let $\beta_0(R) \to \infty$. Then

$$\tau_M = j\beta \tag{4.58}$$

if β satisfies the inequality

$$\beta_j(R) < \beta \le \beta_{j-1}(R) \qquad (j = 1, 2, \ldots) \tag{4.59}$$

This is illustrated in Fig. 4.7.

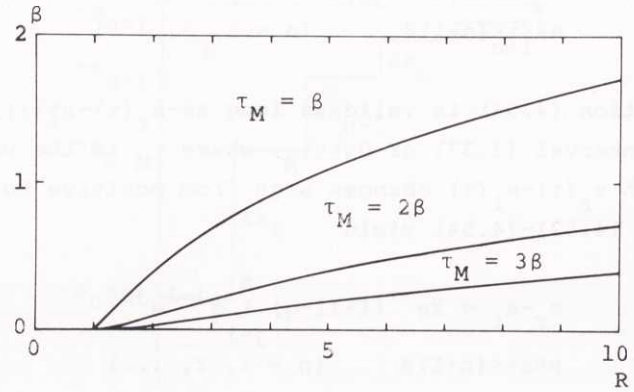

Fig. 4.7. τ_M versus β and R.

4.3.3.2. Efficiency. - According to Eqs. (3.133) (with $\alpha = 0$), (4.52)-(4.54) and (4.58), the maximum force f_M is obtained as

$$f_M = 2e^{-j\beta}(e^{\beta}-1)\{1-(qe^{\beta})^j\}/(1-qe^{\beta}) \qquad (4.60)$$

provided that β belongs to the interval given by the inequality (4.59).

Further, Eqs. (4.46) and (4.47) yield

$$\int s_i^2(\tau)d\tau = \beta/(1-q^2) \qquad (4.61)$$

and the efficiency η is obtained by substitution of Eq. (4.61) into Eq. (4.34) as

$$\eta = (1-\gamma)(1-q^2)f_M^2/2\beta \qquad (4.62)$$

When R = 1, Eqs. (4.48) and (4.57) yield q = 0 and $\beta_n = 0$, n = 1, 2, ... Therefore, always $\beta_1 < \beta < \infty$ and, according to

Eqs. (4.59) and (4.60), j = 1 and

$$f_M = 2(1-e^{-\beta}) \tag{4.63}$$

Eqs. (4.62) and (4.63) yield the efficiency

$$\eta = 2(1-\gamma)(1-e^{-\beta})^2/\beta \tag{4.64}$$

Eqs. (4.63) and (4.64) agree with Eqs. (3.139) and (3.140), which were derived for $\alpha = 0$ when $s_i(\tau)$ is a rectangular pulse.

Numerical results for η according to Eqs. (4.60) and (4.62) are plotted in Fig. 4.8.

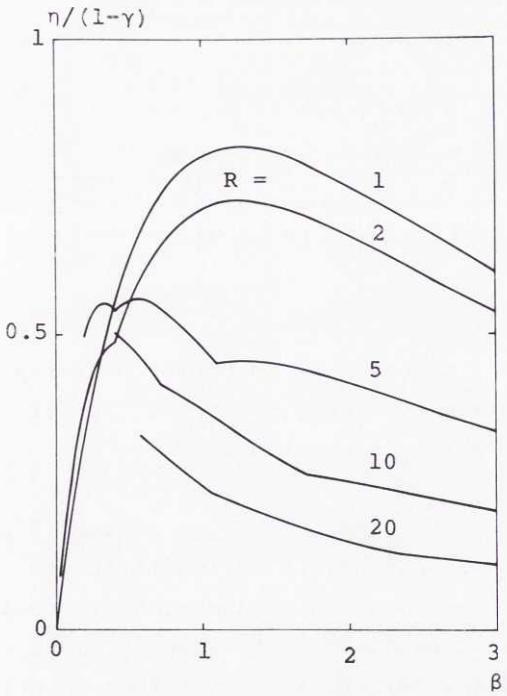

Fig. 4.8. $\eta/(1-\gamma)$ versus β for different values of R. $\eta = W/W_i$, $\beta = t_p/t_0$ where $t_p = 2L_H/c_H$ and $t_0 = AE/kc$, $R = A_H E_H c/AEc_H$, $\gamma = k/k_e$.

4.3.4. Discussion

For two different types of incident stress waves the influence of stress wave shape on the efficiency of energy transfer to the rock has been studied. In both cases the duration of the stress wave was represented by the parameter β, while the shape of the stress wave was represented by the parameters Θ ($0 \leq \Theta \leq 1$) and R ($R \geq 1$) respectively.

The influence of Θ and R on the stress wave shape is illustrated in Fig. 4.9.

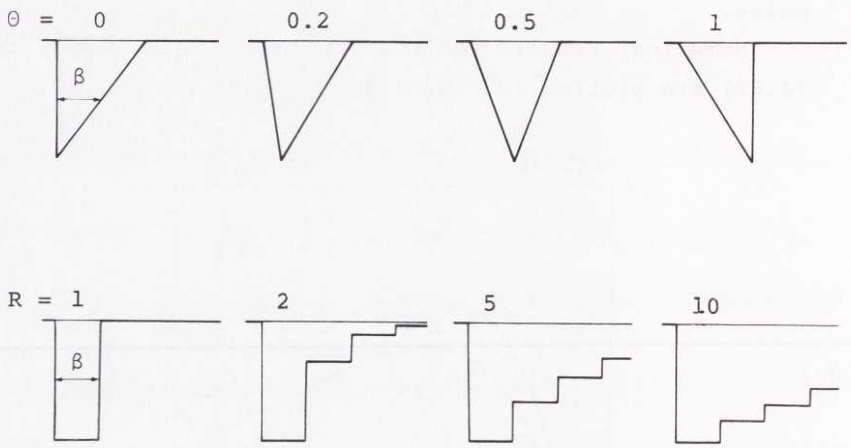

Fig. 4.9. Stress wave shape for different values of Θ and R respectively. The duration of the stress waves is represented by β, which is constant.

Before the influence of the parameters Θ and R on the efficiency is discussed, it is legitimate to ask what incident stress wave shape would give the highest possible efficiency. The answer to this question is readily found as follows: According to Eq. (4.35), it is possible to obtain the efficiency $\eta = 1$ if $s_r(\tau) \equiv 0$. Therefore, the efficiency $\eta = 1$ can be obtained provided that $\gamma = 0$ and, according to Eq. (3.122), $s_i(\tau)$ is determined from the differential equation

$$-ds_i/d\tau+s_i = 0 \tag{4.65}$$

If the initial condition (3.123) is replaced by the condition that $s_i(\tau)\to -s_r(\tau)=0$ when $\tau\to-\infty$, then

$$s_i(\tau) = \begin{cases} -e^{\tau} & , \quad \tau<\tau_M \\ 0 & , \quad \tau\geq\tau_M \end{cases} \tag{4.66}$$

where τ_M is arbitrary. In this case, the penetration velocity drops to zero when $\tau = \tau_M$, since $s_r(\tau)-s_i(\tau) = 0$ when $\tau\geq\tau_M$. It is also seen that the half-width of the stress wave s_i given by Eq. (4.66) is

$$\beta = \ln 2 \tag{4.67}$$

i.e. the half-width $\beta = 0.693$ is constant and independent of τ_M. If $\gamma>0$, a reflected stress wave is generated for $\tau\geq\tau_M$ and the efficiency is reduced to $\eta = 1-\gamma$.

The result given by Eq. (4.66) was earlier obtained by FAIRHURST (1961c) and is illustrated in Fig. 4.10.

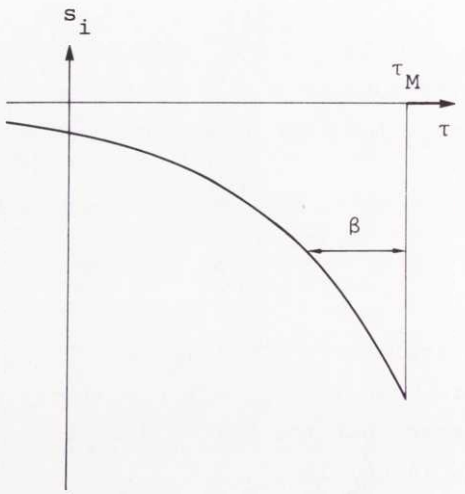

Fig. 4.10. Incident stress wave $s_i(\tau)$ for maximum efficiency ($\eta = 1-\gamma$).

When the incident stress wave is a triangular pulse with a given value of Θ ($0 \leq \Theta \leq 1$), $\eta/(1-\gamma)$ assumes its maximum value for a certain value of β. This value of β, which is approximately equal to 1, and the corresponding maximum value of $\eta/(1-\gamma)$ depend on Θ. Thus, when Θ increases from 0 to 1, the maximum value of $\eta/(1-\gamma)$ increases from 0.61 when $\Theta = 0$ to 0.97 when $\Theta = 1$. Moreover, $\eta/(1-\gamma)$ approaches 0 for low and high values of β. Also, for any given value of β, $\eta/(1-\gamma)$ is an increasing function of Θ.

That a higher value of Θ results in a higher efficiency than a lower value of Θ may be expected from the fact that the stress wave given by Eq. (4.66), which has an increasing amplitude, is the most favourable incident stress wave from an efficiency point of view. This, in turn, can qualitatively be understood from the fact that the force F is an increasing function of the penetration x.

When the incident stress wave is of the type which is generated by a cylindrical hammer and the dynamic stiffness

ratio R ($R \geq 1$) is given, $\eta/(1-\gamma)$ in general again assumes its maximum value for a certain value of β. This value of β and the corresponding maximum value of $\eta/(1-\gamma)$ depend on R. Thus, when $R = 1$, the maximum value of $\eta/(1-\gamma)$ is 0.815 for $\beta = 1.26$. For $R > 1$ the maximum value of $\eta/(1-\gamma)$ becomes less and for sufficiently large values of R the corresponding value of β also becomes less. However, it should be noted that for certain values of R, the value of β corresponding to the maximum value of $\eta/(1-\gamma)$ may not be unique.

From a comparison of Figs. 4.9 and 4.10, it can be seen that the stress wave generated by the cylindrical hammer when $R > 1$ has properties which are in a sense opposite to those of the most favourable stress wave with respect to efficiency. This is illustrated in the analysis by the fact that when $\beta_j(R) < \beta \leq \beta_{j-1}(R)$, then $\tau_M = j\beta$ and consequently, the stress wave energy corresponding to the tail $\tau \geq j\beta$ of $s_i(\tau)$ represents wasted energy (the work performed on the rock would have been the same without that tail part of the stress wave). On the other hand, it is evident from the analysis that for certain low values of β and certain values of R, the efficiency may be increased by increasing the value of R, i.e. by increasing the relative part of the stress wave energy, which is contained in the tail of the wave.

4.4. Influence of Non-Linear Loading Section of the Force-Penetration Characteristic

4.4.1. Parabolic force-penetration characteristic

4.4.1.1. Introduction. - Consider hammer drilling when the force-penetration characteristic is parabolic according to Eq. (2.41). Assume also for the sake of simplicity that the elastic deformation of the rock is negligible in agreement with

Fig. 2.20 ($k_e \to \infty$) and that the bit mass is zero ($M_B = 0$). Let the notation and other basic assumptions be the same as in Chapter 3.

4.4.1.2. Stress wave reflection. - From Eqs. (2.41), (3.8), (3.93) and (3.94) it is found that during loading the reflected stress wave σ_r is related to the incident stress wave σ_i by the differential equation

$$(AE^2/4Kc^2)(d\sigma_r/dt+d\sigma_i/dt)^2+(\sigma_r+\sigma_i)(\sigma_r-\sigma_i)^2 = 0 \tag{4.68}$$

The initial condition is obtained from Eq. (3.98) as

$$\sigma_r(0) = -\sigma_i(0) \tag{4.69}$$

Assume that, in agreement with Eqs. (3.110) and (3.111), the incident stress wave is given by

$$\sigma_i(t) = \begin{cases} -\sigma_0 , & 0 \le t < t_p \\ 0 , & t_p \le t \end{cases} \tag{4.70}$$

and introduce non-dimensional stresses according to Eqs. (3.100) and (3.101).

Introduce the non-dimensional time according to Eq. (3.16) where the normalizing time t_0 is now defined by

$$t_0^2 = AE^2/2Kc^2\sigma_0 \tag{4.71}$$

Then Eqs. (4.68)-(4.70) are transformed into

$$(ds_r/d\tau+ds_i/d\tau)^2+2(s_r+s_i)(s_r-s_i)^2 = 0 \tag{4.72}$$

$$s_r(0) = -s_i(0) \tag{4.73}$$

and

$$s_i(\tau) = \begin{cases} -1 & , \quad 0 \leq \tau < \beta \\ 0 & , \quad \beta \leq \tau \end{cases} \tag{3.112}$$

where

$$\beta = t_p/t_0 \tag{3.26}$$

The solution of Eqs. (4.72) and (4.73) is valid as long as the penetration velocity is positive, i.e.

$$s_r(\tau) - s_i(\tau) > 0 \tag{4.74}$$

or

$$0 \leq \tau < \tau_M \tag{4.75}$$

Therefore, the solution

$$s_r = 1 - 2\tanh^2(\tau) \tag{4.76}$$

is valid in the interval $0 \leq \tau < \beta$. Since it is further realized that $s_r(\tau) \equiv 0$ when $\tau \geq \beta$, it is seen that the penetration becomes maximum when $\tau \to \beta-$, i.e.

$$\tau_M = \beta \tag{4.77}$$

4.4.1.3. Efficiency. - The efficiency of energy transfer to the rock is again defined as

$$\eta = W/W_i \tag{3.6}$$

where the work W performed on the rock is given by Eq. (2.42)

and where the stress wave energy W_i is given by Eqs. (4.32) and (4.70).

If the non-dimensional maximum force f_M is introduced according to Eqs. (3.4) and (4.33) and if the non-dimensional variable β is introduced, Eq. (3.6) can be expressed as

$$\eta = 2^{1/2} f_M^{3/2} / 3\beta \tag{4.78}$$

Further, it is easily found that

$$f_M = \lim_{\tau \to \beta-} \{ s_r(\tau) + s_i(\tau) \} \tag{4.79}$$

i.e.

$$f_M = 2\tanh^2(\beta) \tag{4.80}$$

Substitution of Eq. (4.80) into Eq. (4.78) finally results in

$$\eta = 4\tanh^3(\beta)/3\beta \tag{4.81}$$

Numerical results for η according to Eq. (4.81), are plotted in Fig. 4.11.

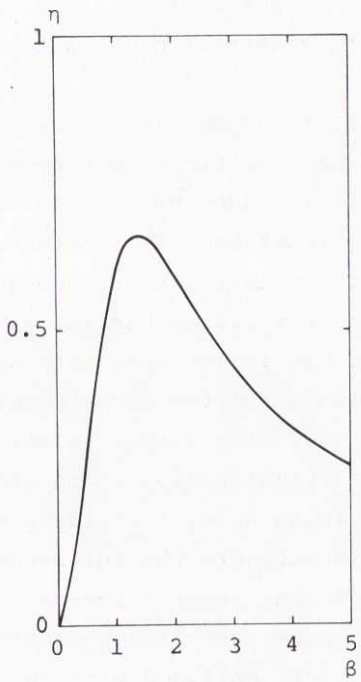

Fig. 4.11. η versus β. $\eta = W/W_i$, $\beta = t_p/t_0$ where $t_p = 2L_H/c$ and $t_0^2 = AE^2/2Kc^2\sigma_0$.

4.4.1.4. Discussion. - The relation between η and β when the force-penetration characteristic is parabolic has the same general features as the corresponding relation when the force-penetration characteristic is linear (Section 3.4). However, the maximum efficiency, $\eta = 0.66$, is lower than in the linear case, and a basic difference is that in the linear case β is independent of the stress wave amplitude σ_0. Therefore, the efficiency depends on the stress wave amplitude in the non-linear case but not in the linear case.

4.4.2. Piece-Wise Linear Force-Penetration Characteristic

4.4.2.1. Introduction. - From the results presented in Chapter 2, it is evident that when the bit is equipped with a single cone-shaped (Fig. 2.9) or wedge-shaped (Fig. 2.11) indentor, the force-penetration relationship is often not very well represented for a single penetration by the quadratic relationship (2.41) or the linear relationship (2.35). This may also be the case when the bit is equipped with several cutter elements. A truer representation of the force-penetration characteristic is given by the piece-wise linear relationship according to Eq. (2.43). This relationship, which can be accurately fitted to experimental data, is illustrated in Fig. 2.21.

In order to investigate the influence on efficiency of different types of non-linear force-penetration relations, the treatment of hammer drilling presented in Chapter 3 was extended to the above-mentioned piece-wise linear force-penetration relationship. It was also assumed that the incident stress wave is a piece-wise linear function of time. Other basic assumptions were the same as in Chapter 3.

For each linear segment of the force-penetration relationship, a differential equation corresponding to Eq. (3.102) was formulated. The successive solutions were joined together by the conditions that the penetration velocity and consequently the penetration are continuous functions of time. These two conditions correspond to Eqs. (3.103) and (3.104).

The work W performed on the rock was determined from the maximum penetration as the area bounded by the loading curve, the unloading curve and the x-axis, and the stress wave energy W_i was determined from Eq. (4.32). The efficiency η was determined as the ratio of W and W_i according to Eq. (3.6).

A modified Runge-Kutta method was used in solving the differential equations. It was coded in FORTRAN and run on an IBM 1130 computer.

The program was tested for various combinations of parameters and in all cases where a direct comparison with analytical results was possible, the error in the computed efficiency was less than a few tenths of a per cent.

The numerical analysis and the development of the computer programs were performed as a student's project at the Royal Institute of Technology in Stockholm by THURESSON (1971a, b) with the author as a supervisor.

Next, in a particular example, an application of this work will be briefly presented.

4.4.2.2. Example of results. - Assume for the sake of simplicity, that the force-penetration characteristic can be represented by the saw-tooth curve illustrated in Fig. 4.12.

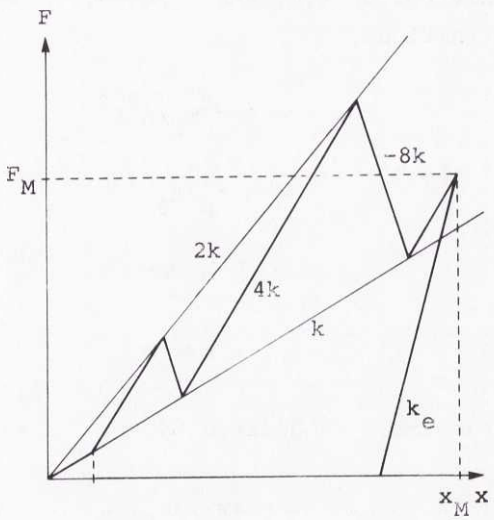

Fig. 4.12. An example of a force-penetration relation with a piece-wise linear loading section.

x_M denotes the maximum penetration and F_M denotes the corresponding force (i.e. not necessarily the maximum force). As long as the penetration velocity dx/dt is positive, the force-penetration curve is a saw-tooth curve which consists of linear segments that start and end on the straight lines $F = kx$ and $F = 2kx$. The first segment is the straight line $F = kx$ in the interval $0 \leq x < x_1$ and the rest of the segments have the slopes $4k$, $-8k$, $4k$, $-8k$, ... When the penetration velocity dx/dt becomes negative the force F is given by Eq. (2.36) where k_e denotes the slope of the unloading segment of the force-penetration curve.

The incident stress wave is again assumed to be a rectangular pulse with amplitude σ_0 and width t_p according to Eq. (4.70).

The efficiency is obtained as a function $\eta(\alpha,\beta,\gamma,\delta)$ of the parameters α, β, γ and δ where, in agreement with earlier definitions,

$$\alpha = 4kc^2M_B/A^2E^2 \tag{3.21}$$

$$\beta = t_p/t_0 \tag{3.26}$$

$$t_0 = AE/kc \tag{3.17}$$

$$\gamma = k/k_e \tag{2.38}$$

The parameter δ is defined by

$$\delta = kx_1/A\sigma_0 \tag{4.82}$$

Since kx_1 is the value of the force F at the end of the first segment of the force-penetration curve, and $A\sigma_0$ is the force in a cross section of the drill rod which results from the incident stress wave, δ is closely connected with the number

of segments of the force-penetration curve that are run through. In particular, it is apparent from Section 3.4 that, independent of the values of α and β, the first segment is not completely run through if $\delta>4$.

Numerical results for η are plotted in Figs. 4.13 and 4.14. The results are compared with the corresponding results for η when the force-penetration relationship is linear during loading, i.e.

$$F = hkx \tag{4.83}$$

where h is a non-dimensional parameter and $1\leq h\leq 2$. These latter results are obtained from Section 3.4.

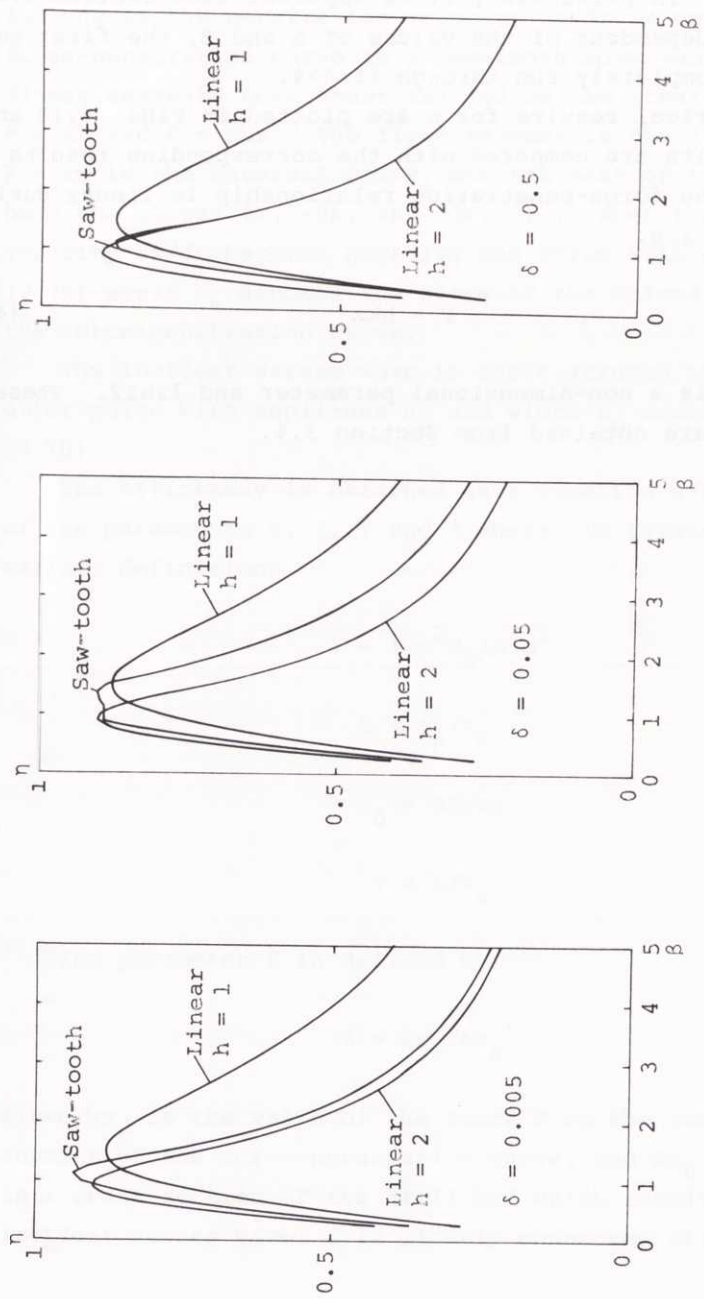

Fig. 4.13. η versus β for the linear force-penetration relationship F = hkx (h = 1 and 2) compared with η versus β for the saw-tooth force-penetration relationship illustrated in Fig. 4.12. $\alpha = 1$, $\gamma = 0.001$.

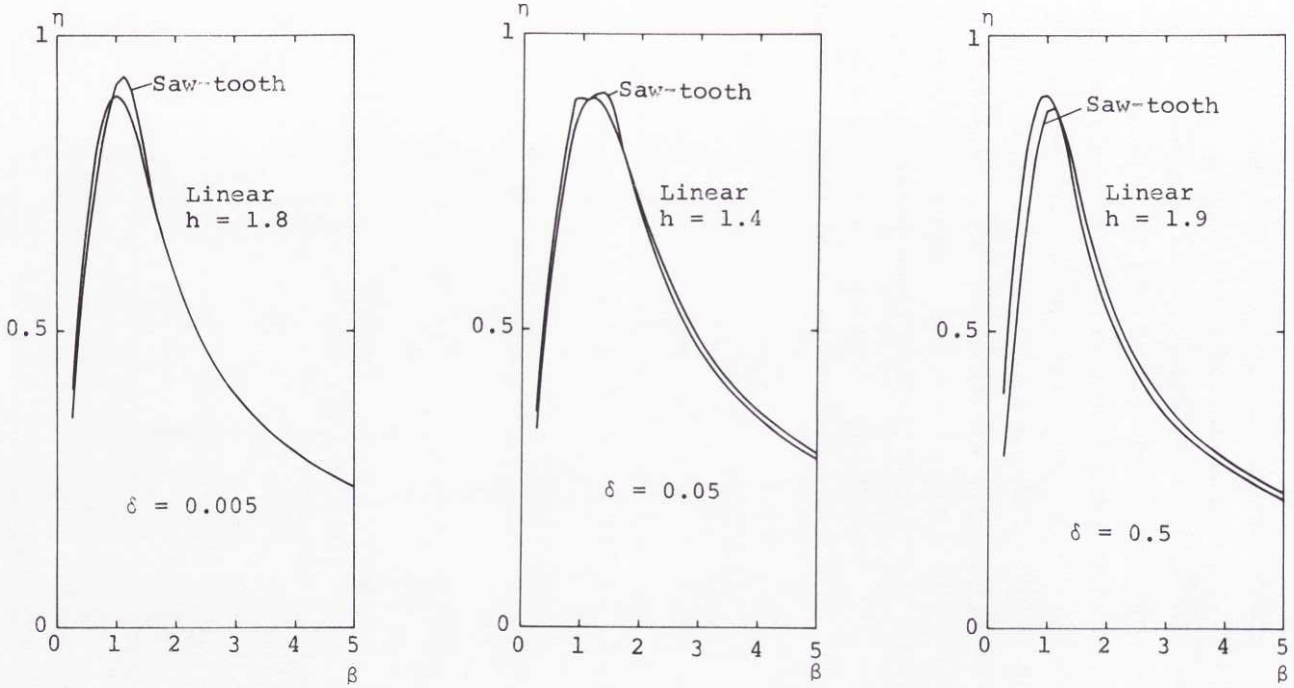

Fig. 4.14. η versus β for the linear force-penetration relationship $F = hkx$ (selected values of h, $1<h<2$) compared with η versus β for the saw-tooth force-penetration relationship illustrated in Fig. 4.12. $\alpha = 1$, $\gamma = 0.001$.

4.4.2.3. Discussion. - The relationship between η and β when the force-penetration curve has a saw-tooth shape has the same general features as the corresponding relationship when the force-penetration characteristic is linear. However, as in the case of a parabolic force-penetration relationship, a basic difference is that the efficiency depends on the stress wave amplitude in the non-linear case but not in the linear case. In spite of this amplitude dependence, it is seen from Figs. 4.13 and 4.14 that a linear approximation ($1 \leq h \leq 2$) of the saw-tooth curve gives results for the efficiency which for many purposes may be satisfactory approximations of the real efficiency. In the light of this result one may sometimes be justified in considering the linear loading force-penetration characteristic earlier employed in Chapters 3 and 4 as a linear approximation of a much more complex real force-penetration characteristic.

5. STRESS WAVE TRANSMISSION THROUGH JOINTS

5.1. Introduction

As was stated in Section 1.2, several rods are sometimes joined together in hammer drilling. At each joint the incident stress wave σ_i gives rise to one reflected stress wave σ_r and one transmitted stress wave σ_t. Even if after a number of reflections back and forth in the rods, stress wave energy originating from reflected stress waves σ_r arrives at the bit, it seems reasonable to assume that the energy associated with each reflected stress wave σ_r is insignificant in connection with rock destruction. The reason is that the stress waves originating from reflected stress waves σ_r at the joints arrive at the bit too late and at too low amplitude levels compared with the main stress wave that is transmitted straight through the joints (Cf. the results obtained for a triangular stress wave with $\Theta = 0$ in Section 4.3.2). Therefore, there are reasons to consider only the energy associated with the stress wave that is transmitted straight through the joints as useful energy.

As was shown by TAKAOKA, HAYAMIZU & MISAWA (1958 in Japanese; see FAIRHURST, 1961a), stress wave reflections at the joints are not the only source of energy losses in connection with stress wave transmission through joints between rods. Frictional losses in the joints may also be considerable However, these losses depend to a large extent on the detailed design of the joints (threads etc.) and may be difficult to take into consideration in a general manner.

FISCHER (1960) treated the joint simply as a cylindrical swell on the rod and thereby the influence of friction was neglected. A similar treatment will be given here. An attempt to consider in a more complete way the state of stress in the different parts of the joint was made by means of photoelastic techniques by BABENKOV, IVANOV & HESIN (1965). However, their rod and joint models were flat, which of course does not either give a true description.

As is illustrated in Fig. 5.1, it is assumed that the drill rods and joints are cylindrical, homogeneous and of the same material. The geometry is characterized by the rod cross section area $A_R = A$, the joint cross sectional area A_J and the joint length L_J, while the material is characterized by the Young's modulus $E_R = E_J = E$, the density $\rho_R = \rho_J = \rho$ and the sonic velocity $c_R = c_J = c$ according to Eq. (3.1).

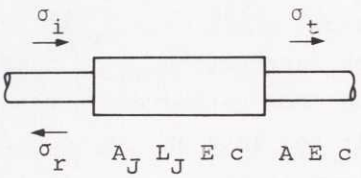

Fig. 5.1. Joint between two equal rods.

Even if the rod and joint materials are assumed to be the same, the joints will sometimes be considered as rigid bodies ($E_J \to \infty$, $c_J \to \infty$) in contrast with the rods. The geometric conditions under which this is a good approximation will be obtained from the analyses.

The motion of the rods is further assumed to be governed by the one-dimensional wave equation (Appendix B) while the motion of the joints is assumed to be governed by either the one-dimensional wave equation or, when the joints are considered to be rigid, rigid body mechanics.

The effects of gravity are neglected and before the arrival of the incident stress wave σ_i at a joint at time $t = 0$, the joint and the joined rods are at rest and are free from stresses.

In the following sections several problems in connection with stress wave transmission through joints between equal rods will be considered. First, the efficiency of energy transfer, defined as the ratio of transmitted stress wave energy and incident stress wave energy, i.e. (Appendix B)

$$\eta = \int \sigma_t^2 dt / \int \sigma_i^2 dt \qquad (5.1)$$

will be determined for a single joint treated as an elastic swell on the rod. Then the efficiency will be determined when the joint is treated as a rigid body and the results of the elastic swell and the rigid body treatments will be compared. Since it will become apparent that the results are often not very different, the rigid body treatment will be employed in determining which stress wave of a given duration gives maximum energy transfer through a single joint. The rigid body treatment is also preferred in the study of stress wave energy transfer through an arbitrary number of joints. In this case, the efficiency is again defined according to Eq. (5.1), where σ_i is now the stress wave incident towards the first joint and σ_t is the stress wave which is transmitted straight through all the joints. Finally, a comparison will be made between theory and a simple experiment.

5.2. Single Elastic Joint

5.2.1. Stress wave transmission

Assume first that the incident stress wave at the first rod-joint interface is a step function, i.e.

$$\sigma_i = -\sigma_0 \quad , \quad t \geq 0 \qquad (5.2)$$

Then, according to the elementary stress wave theory (Appendix B), it is easily found that at the second rod-joint interface the transmitted stress wave is determined by

$$\sigma_t = -\sigma_n \qquad (n = 1, 2, \ldots)$$
$$(n-1/2)t_J \leq t < (n+1/2)t_J \tag{5.3}$$

where

$$\sigma_n = (1-p^{2n})\sigma_0 \tag{5.4}$$

$$p = (r-1)/(r+1) \tag{5.5}$$

$$r = A_J/A \tag{5.6}$$

and

$$t_J = 2L_J/c \tag{5.7}$$

From Eqs. (5.2) and (5.3) the transmitted stress wave σ_t can also be obtained for any incident stress wave σ_i that can be represented as a superposition of step functions. If in particular, σ_i is the rectangular pulse

$$\sigma_i = \begin{cases} -\sigma_0 , & 0 \leq t < t_p \\ 0 , & t_p \leq t \end{cases} \tag{4.70}$$

where the duration of the pulse t_p is a multiple of t_J, i.e.

$$t_p = mt_J \qquad (m = 1, 2, \ldots) \tag{5.8}$$

then the transmitted stress wave is determined by

$$\sigma_t = \begin{cases} -\sigma_n & (n = 1, 2, \ldots, m) \\ -\sigma_n + \sigma_{n-m} & (n = m+1, m+2, \ldots) \end{cases}$$
$$(n-1/2)t_J \leq t < (n+1/2)t_J \tag{5.9}$$

This result is illustrated in Fig. 5.2.

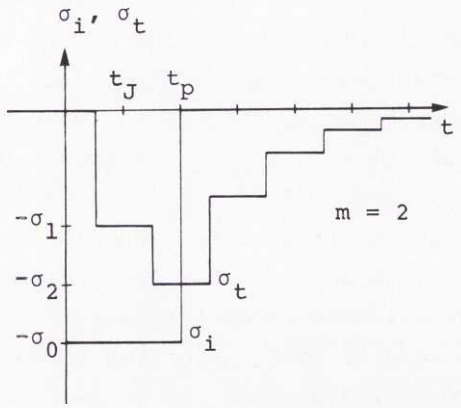

Fig. 5.2. Transmitted stress wave σ_t through one elastic joint when the incident stress wave σ_i is a rectangular pulse.

5.2.2. Efficiency

When the incident stress wave is the rectangular pulse given by Eqs. (4.70) and (5.8), the efficiency can be obtained from Eqs. (5.1), (4.70), (5.8) and (5.9) as

$$\eta = (1/m)\{\sum_{n=1}^{m}(\sigma_n/\sigma_0)^2+\sum_{n=m+1}^{\infty}(-\sigma_n/\sigma_0+\sigma_{n-m}/\sigma_0)^2\} \quad (5.10)$$

If Eq. (5.4) is substituted into Eq. (5.10) this result can be simplified to

$$\eta = 1-2p^2(1-p^{2m})/(1-p^4)m \quad (5.11)$$

In particular, Eqs. (5.5) and (5.11) show that $\eta \to 1$ when $m \to \infty$ or $r \to 1$.

In the derivation of Eq. (5.11) it has been assumed that $m = 1, 2, \ldots$. However, it is realized that when $0<m<1$, the transmitted stress wave consists of separate pulses with amplitude levels equal to those of the single pulse obtained when $m = 1$. In the case $0<m<1$ the length of each single pulse is

equal to the length of the incident stress wave, while in the case m = 1, the length of a portion of the transmitted stress wave with constant amplitude is also equal to the length of the incident stress wave. Therefore, when $0<m\leq 1$, the efficiency η is independent of m and is obtained from Eq. (5.11) with m = 1.

It is a straight-forward procedure to extend the analysis to arbitrary values of $m>0$. For the purposes here, however, this extension will not be of interest.

Numerical results for η according to Eqs. (5.11) and (5.5) are plotted in Fig. 5.3.

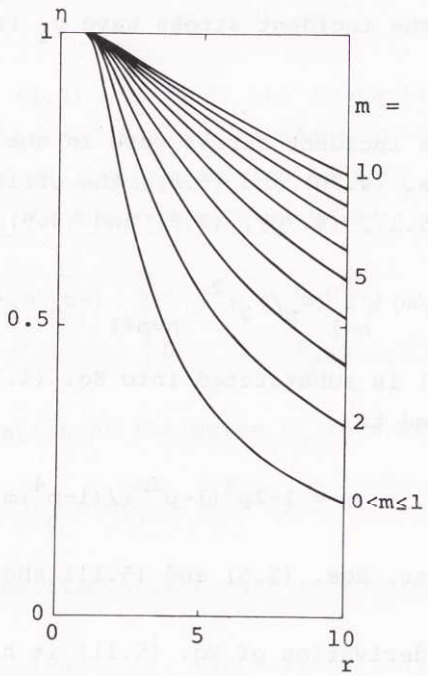

Fig. 5.3. Efficiency η versus r for different values of m. $r = A_J/A$, $m = t_p/t_J$ (sometimes $= L_H/L_J$). Elastic joint.

5.2.3. Discussion

When the joint is treated as an elastic swell on the rod, the transmitted stress wave, as is illustrated in Fig. 5.2, becomes a piece-wise constant function of time. As can be seen from Eq. (5.4), the amplitude of the transmitted stress wave is lower than the amplitude of the incident stress wave.

As is illustrated in Fig. 5.3, the efficiency η is independent of the parameter m when $0<m\leq 1$, but is an increasing function of m when $m\geq 1$ ($m = 1, 2, \ldots$). This means that a stress wave which is long compared with the joint is favourable with respect to efficiency. In Fig. 5.3, it is also illustrated that the efficiency η is a decreasing function of the parameter r (≥ 1). Thus, it is favourable with respect to efficiency if the joint has as far as possible the same cross sectional area as the rods.

5.3. Single Rigid Joint

5.3.1. Stress wave transmission

The equation of motion of the rigid joint is (Appendix B)

$$M_J du/dt = -A(\sigma_r+\sigma_i)+A\sigma_t \tag{5.12}$$

where

$$M_J = \rho A_J L_J \tag{5.13}$$

is the mass of the joint, u is the velocity of the joint in the propagation direction of the incident stress wave σ_i and σ_i, σ_r and σ_t denote the stress waves at the rod-joint interfaces.

The velocity u can be expressed in terms of σ_t as (Appendix B)

$$u = -(c/E)\sigma_t \tag{5.14}$$

and the condition that the velocities of the two rod-joint interfaces are the same takes the form (Appendix B)

$$-\sigma_t = \sigma_r - \sigma_i \tag{5.15}$$

If u and σ_r are eliminated, Eqs. (5.12) (5.14) and (5.15) result in the differential equation

$$(M_J c/2EA)\, d\sigma_t/dt + \sigma_t = \sigma_i \tag{5.16}$$

Since it is assumed that u(0) = 0, Eq. (5.14) gives the initial condition

$$\sigma_t(0) = 0 \tag{5.17}$$

In Eqs. (5.16) and (5.17) it is convenient to introduce the non-dimensional time

$$\tau = t/t_0 \tag{5.18}$$

and the non-dimensional stresses

$$s_i = \sigma_i/\sigma_0 \tag{5.19}$$

and

$$s_t = \sigma_t/\sigma_0 \tag{5.20}$$

where

$$t_0 = M_J c/2EA \tag{5.21}$$

and σ_0 is a normalizing stress. Eqs. (5.16) and (5.17) are then transformed into

$$ds_t/d\tau+s_t = s_i \tag{5.22}$$

and

$$s_t(0) = 0 \tag{5.23}$$

respectively.

By introduction of the Laplace transforms $\tilde{s}_i(s)$ and $\tilde{s}_t(s)$ of $s_i(\tau)$ and $s_r(\tau)$ respectively, Eqs. (5.22) and (5.23) yield

$$\tilde{s}_t(s) = H_J(s)\tilde{s}_i(s) \tag{5.24}$$

where

$$H_J(s) = 1/(s+1) \tag{5.25}$$

Thus, the solution $s_t(\tau)$ can be obtained as the inverse Laplace transform of $H_J(s)\tilde{s}_i(s)$, i.e.

$$s_t(\tau) = L^{-1}\{H_J(s)\tilde{s}_i(s)\} \tag{5.26}$$

If, in particular, $\sigma_i(t)$ is again the rectangular pulse given by Eq. (4.70), i.e.

$$s_i(\tau) = \begin{cases} -1 & , \quad 0\leq\tau<\lambda \\ 0 & , \quad \lambda\leq\tau \end{cases} \tag{5.27}$$

where

$$\lambda = t_p/t_0 \tag{5.28}$$

or, according to Eqs. (5.21), (5.28), (5.13) and (3.1),

$$\lambda = 2(A/A_J)(ct_p/L_J) \tag{5.29}$$

then the transmitted stress wave becomes

$$s_t = -g_1(\tau)+g_1(\tau-\lambda) \tag{5.30}$$

where $g_1(\tau) = 0$ when $\tau<0$ and

$$g_1(\tau) = 1-e^{-\tau} \tag{5.31}$$

when $\tau\geq 0$. This result is illustrated in Fig. 5.4.

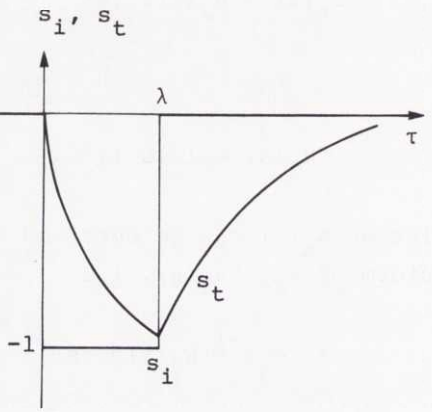

Fig. 5.4. Transmitted stress wave s_t through one rigid joint when the incident stress wave s_i is a rectangular pulse.

5.3.2. Efficiency

In terms of non-dimensional variables, the efficiency defined by Eq. (5.1) can be expressed as

$$\eta = \int s_t^2 d\tau / \int s_i^2 d\tau \tag{5.32}$$

When, in particular, the incident stress wave is a rectangular pulse, Eqs. (5.27), (5.30), (5.31) and (5.32) yield

$$\eta = 1-(1-e^{-\lambda})/\lambda \tag{5.33}$$

Numerical results for η, according to Eq. (5.33), are plotted in Fig. 5.5.

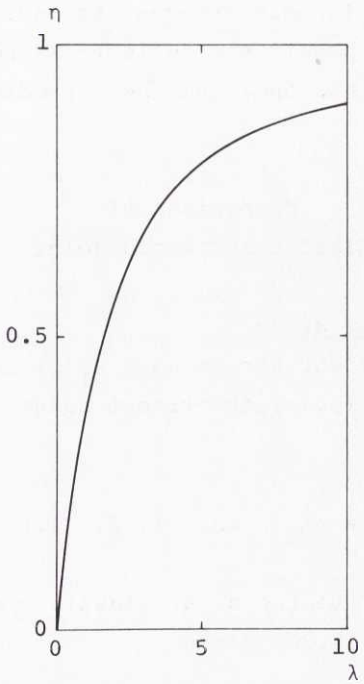

Fig. 5.5. Efficiency η versus λ. $\lambda = t_p/t_0$ where $t_0 = M_J c/2EA$. Rigid joint.

5.3.3. Discussion

When the joint is treated as a rigid body, the transmitted stress wave, as illustrated in Fig. 5.4, becomes a continuous function of time. As can be seen from Eqs. (5.30) and (5.31), the amplitude of the transmitted stress wave is lower than the amplitude of the incident stress wave.

In this case the efficiency η can be expressed as a function of the single parameter λ, which is directly proportional to m but inversely proportional to r. As is illustrated in

Fig. 5.5, η is an increasing function of λ. Therefore, the result obtained for the rigid joint is qualitatively the same as that obtained for an elastic joint. However, it is clear that results obtained for the rigid joint must be erroneous when r is near or equal to one. For, in the latter case, the theory predicts a reflected stress wave and an efficiency less than one, and these predictions are obviously not correct.

5.4. Comparison of Elastic and Rigid Joint

5.4.1. Stress wave transmission

When the incident stress wave $\sigma_i(t)$ is a step function, according to Eq. (5.2), the time t assumes one of the discrete values

$$t = nt_J \quad (n = 1, 2, \ldots) \tag{5.34}$$

and the joint is treated as an elastic swell, Eqs. (5.3), (5.4), (5.5) and (5.20) yield

$$s_t = -1+\{(r-1)/(r+1)\}^{2t/t_J} \tag{5.35}$$

By introduction of the non-dimensional time τ, according to Eq. (5.18), Eqs. (5.34) and (5.35) are transformed into

$$\tau = 4n/r \quad (n = 1, 2, \ldots) \tag{5.36}$$

and

$$s_t = -1+\{(r+1)/(r-1)\}^{-(r/2)\tau} \tag{5.37}$$

respectively.

When $r \to \infty$ Eq. (5.37) yields

$$\lim_{r\to\infty} s_t = -1+e^{-\tau} \tag{5.38}$$

Therefore, it is realized that when $r \to \infty$ and the incident stress wave is the rectangular pulse given by Eq. (5.27), the transmitted stress wave is given by Eqs. (5.30) and (5.31) for the elastic as well as for the rigid joint. However, it must also be remembered, of course, that when the mass of the joint M_J is constant and the ratio $r = A_J/A$ becomes very large, the joint assumes the shape of a disc and the theory of one-dimensional stress waves is no longer applicable.

5.4.2. Efficiency

According to Eqs. (5.6), (5.7), (5.8) and (5.29), λ is related to m and r as

$$\lambda = 4m/r \qquad (m = 1, 2, \ldots) \tag{5.39}$$

If m and p, according to Eqs. (5.39) and (5.5) respectively, are substituted into Eq. (5.11), the efficiency when the joint is treated as an elastic swell can be expressed as

$$\eta = 1-\{(r^2-1)^2/r^2(r^2+1)\}\left[1-\{(r+1)/(r-1)\}^{-(r/2)\lambda}\right]/\lambda \tag{5.40}$$

When $r \to \infty$ Eq. (5.40) yields

$$\lim_{r\to\infty} \eta = 1-(1-e^{-\lambda})/\lambda \tag{5.41}$$

Therefore, when $r \to \infty$, the efficiency is given by Eq. (5.33) for the elastic as well as for the rigid joint.

Numerical results for η according to Eqs. (5.39), (5.40) and (5.41), have been computed for m = 1, 2, ... For $0<m<1$ the value computed for m = 1 is valid. These results are plotted in Fig. 5.6, where the determined points for m = 1, 2, ... are connected with straight lines.

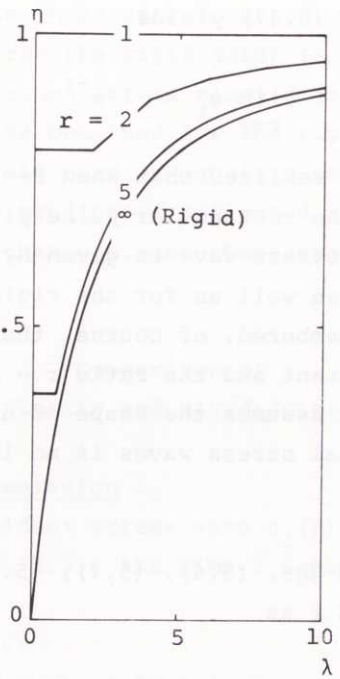

Fig. 5.6. Efficiency η versus λ for different values of r. λ = 4m/r. Points representing m = 1, 2, ... are connected with straight lines. Elastic and rigid joint.

5.4.3. Discussion

It can be seen that the elastic swell and the rigid body treatments of the joint give the same results when, for a constant value of λ, m and r→∞ (i.e. when the joint becomes short and thick). It should also be observed that the rigid joint treatment results in efficiencies which are lower than those obtained from the elastic joint treatment. When m≥1 and (say) r≥4, however, the difference between the results is small.

Consider as a particular example the situation when $m = 5$ and $r = 4$. Then, according to the treatment of the joint as an elastic swell, the efficiency becomes $\eta = 0.836$. In this case $\lambda = 5$ and, according to the treatment of the joint as a rigid body, the efficiency becomes $\eta = 0.801$, i.e. only 0.035 lower.

In the remaining part of this chapter it will be convenient to treat the joints as rigid bodies.

5.5. Maximum Efficiency for an Incident Wave of a Given Length

5.5.1. Introduction

In Sections 5.2 - 5.4, efficiency of stress wave energy transfer through a single joint between two equal rods was studied for the case that the incident stress wave had a predetermined shape as a rectangular pulse. In particular, it was found that the efficiency approaches 1 when the pulse becomes very long. In practical situations, however, the length of the stress wave is mainly related to the length of the hammer by which it has normally been generated, and therefore it is not possible to increase its length above certain limits. Because of this limitation, it is natural to consider next stress waves of a predetermined length but of various shapes, and ask what stress wave shape results in the highest efficiency. Also, it is of interest to see if it is possible to generate such a stress wave in practice and if the corresponding efficiency is considerably higher than that obtained for a rectangular stress wave of the same length.

In the present section, answers will be given to the above-mentioned questions. As in Sections 5.2 - 5.4, a single joint between two equal rods will be considered and, therefore, the efficiency of energy transfer can be expressed in terms of the incident stress wave $s_i(\tau)$ and the transmitted stress wave $s_t(\tau)$ as

$$\eta = \int_{-\infty}^{\infty}\{s_t(\tau)\}^2 d\tau \Big/ \int_{-\infty}^{\infty}\{s_i(\tau)\}^2 d\tau \qquad (5.32)$$

For the sake of simplicity, it is assumed that the joint behaves like a rigid body. This means that the transmitted stress wave $s_t(\tau)$ is related to the incident stress wave $s_i(\tau)$ by the differential equation

$$ds_t/d\tau + s_t = s_i \qquad (5.22)$$

and the initial condition

$$s_t(0) = 0 \qquad (5.23)$$

Also, it is assumed that $s_t(\tau) \equiv 0$ when $\tau<0$ and that the duration of the incident stress wave is λ, i.e. $s_i(\tau) \equiv 0$ when $\tau<0$ and $\tau>\lambda$.

Eqs. (5.22) and (5.23) can alternatively be replaced by the equation

$$s_t(\tau) = e^{-\tau}\int_0^{\tau} e^{s} s_i(s)\,ds \qquad (5.42)$$

It is now easy to see that Eqs. (5.32), (5.22) and (5.23) or, alternatively, Eqs. (5.32) and (5.42), express how η depends on the function $s_i(\tau)$ in the given interval $0\leq\tau\leq\lambda$.

The function $s_i(\tau)$, $0\leq\tau\leq\lambda$, will now be determined in such a way that, for a given value of λ, the efficiency η assumes its maximum value. Also, the corresponding maximum efficiency η will be determined as a function of λ.

5.5.2. Analysis and results

In order to restate the problem in a more convenient way, Eq. (5.22) is Fourier transformed into

$$i\omega\hat{s}_t(\omega) + \hat{s}_t(\omega) = \hat{s}_i(\omega) \qquad (5.43)$$

where $\hat{s}_t(\omega)$ and $\hat{s}_i(\omega)$ are the Fourier transforms of $s_t(\tau)$ and $s_i(\tau)$ respectively ($\hat{s}_t(\omega) = \int_{-\infty}^{\infty} e^{-i\omega\tau} s_t(\tau)d\tau$ etc.).

By using Parseval's relation and Eq. (5.43), Eq. (5.32) can be transformed into

$$\eta = \int_{-\infty}^{\infty} \hat{K}(\omega)\hat{s}_i(\omega)\bar{\hat{s}}_i(\omega)d\omega / \int_{-\infty}^{\infty} |\hat{s}_i(\omega)|^2 d\omega \tag{5.44}$$

where $\bar{\hat{s}}_i$ denotes the complex conjugate of $\hat{s}_i$ and

$$\hat{K}(\omega) = 1/(1+\omega^2) \tag{5.45}$$

By using the convolution theorem and again Parseval's relation, Eq. (5.44) can be transformed into

$$\eta = \int_0^{\lambda} (K*s_i)(\tau)\bar{s}_i(\tau)d\tau / \int_0^{\lambda} |s_i(\tau)|^2 d\tau \tag{5.46}$$

where

$$K(\tau) = (1/2)e^{-|\tau|} \tag{5.47}$$

$$K*s_i = \int_0^{\lambda} K(\tau-s)s_i(s)ds \tag{5.48}$$

and where use has been made of the condition that $s_i(\tau) \equiv 0$ for $\tau<0$ and $\tau>\lambda$.

By introducing the notation (f,g) for the inner product $\int_0^{\lambda} f(\tau)\bar{g}(\tau)d\tau$ of the functions $f(\tau)$ and $g(\tau)$, Eq. (5.46) can be written in a more compact way as

$$\eta = (K*s_i, s_i)/(s_i, s_i) \tag{5.49}$$

Since multiplication of $s_i(\tau)$ with a constant factor ($\neq 0$) obviously does not influence the efficiency η, it may, without loss of generality, be assumed that

$$(s_i, s_i) = 1 \tag{5.50}$$

and consequently, the efficiency η takes the form

$$\eta = (K^*s_i, s_i) \tag{5.51}$$

The problem initially stated is now transformed into determining $s_i(\tau)$, subject to the subsidiary condition (5.50), in such a way that η, as given by Eq. (5.51), attains its maximum value. Since the kernel $K(\tau-s)$ in the integral transform K^*s_i is symmetric, i.e.

$$K(\tau-s) = K(s-\tau) \tag{5.52}$$

the solution of the problem can be obtained from the solution of the eigenvalue problem (see e.g. COURANT & HILBERT, 1970)

$$K^*s_i^1 = \eta^1 s_i^1 \tag{5.53}$$

where η^1 is the largest eigenvalue and

$$s_i^1 = s_i \tag{5.54}$$

is the corresponding eigenfunction. According to Eqs. (5.50), (5.51), (5.53) and (5.54), the maximum efficiency η becomes equal to the largest eigenvalue η^1, i.e.

$$\eta = \eta^1 \tag{5.55}$$

Eqs. (5.53)-(5.55) yield

$$K^*s_i = \eta s_i \tag{5.56}$$

or, explicitly,

$$\int_0^\lambda K(\tau-s)s_i(s)ds = \eta s_i(\tau) \tag{5.57}$$

This homogeneous integral equation can, by repeated differentiation, be transformed into the equivalent differential equation

$$d^2s_i/d\tau^2+\Omega^2 s_i = 0 \qquad (5.58)$$

with the boundary conditions

$$ds_i/d\tau(0) = s_i(0) \qquad (5.59)$$

and

$$ds_i/d\tau(\lambda) = -s_i(\lambda) \qquad (5.60)$$

In Eq. (5.58) Ω is related to η as

$$\eta = 1/(1+\Omega^2) \qquad (5.61)$$

Eqs. (5.58)-(5.60) yield for $0\leq\tau\leq\lambda$

$$s_i = D_1\{\Omega\cos(\Omega\tau)+\sin(\Omega\tau)\} \qquad (5.62)$$

where Ω is related to λ by the equation

$$\tan(\Omega\lambda) = 2\Omega/(\Omega^2-1) \qquad (5.63)$$

Eq. (5.61) shows that the smallest positive root $\Omega(\lambda)$ of Eq. (5.63) corresponds to the maximum efficiency η (= the largest eigenvalue η^1).

The constant D_1 ($\neq 0$) in Eq. (5.62) does not affect the efficiency η and can be chosen arbitrarily, for example so that $s_i<0$ and Eq. (5.50) is satisfied.

From Eqs. (5.62) and (5.63) it can be seen that $s_i(0) = s_i(\lambda)$ and that $|s_i(\tau)|$ attains its maximum value for $\tau = \lambda/2$.

Numerical results for $s_i(\tau)$ according to Eqs. (5.62) and (5.63) are plotted in Fig. 5.7. D_1 was chosen so that $s_i(\lambda/2) = -1$. In Fig. 5.8, the efficiency $\eta(\lambda)$ according to Eqs. (5.61) and (5.63) is plotted. In the same diagram is also plotted the efficiency $\eta(\lambda)$ according to Eq. (5.33), which is obtained when $s_i(\tau)$ is a rectangular pulse with the length λ. In Fig. 5.9, the difference $\Delta\eta$ between the two above-mentioned efficiencies is plotted.

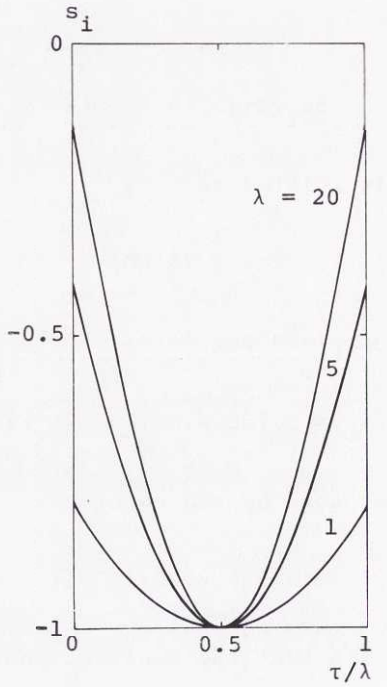

Fig. 5.7. Incident stress wave $s_i(\tau)$ of length λ giving maximum energy transfer through a single rigid joint versus τ/λ for different values of λ. $\lambda = t_p/t_0$ where $t_0 = M_J c/2EA$.

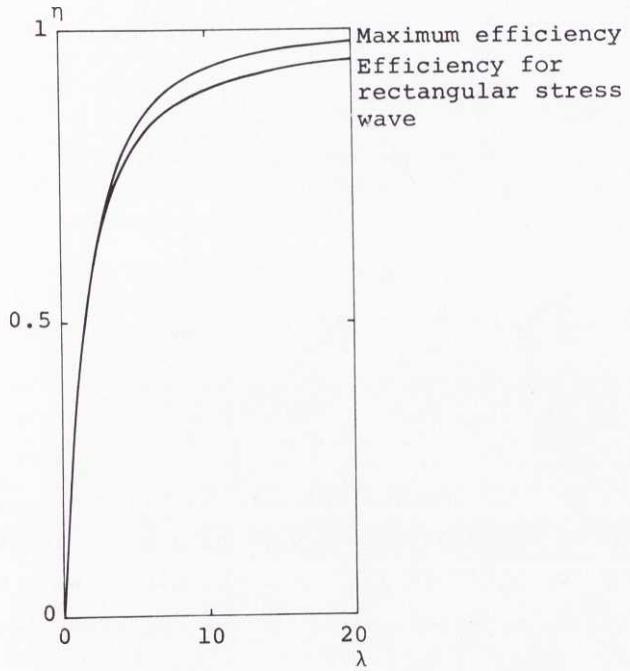

Fig. 5.8. Efficiency η versus λ for a rectangular incident stress wave and for the incident stress wave of the same length that gives the maximum possible energy transfer. One rigid joint. $\lambda = t_p/t_0$ where $t_0 = M_J c/2EA$.

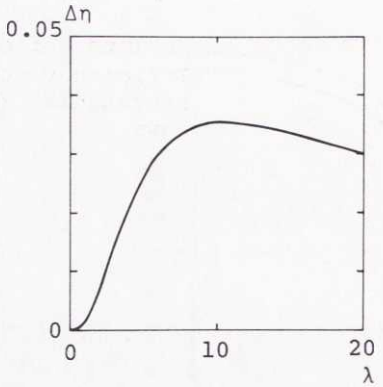

Fig. 5.9. Difference between the maximum possible efficiency for an incident stress wave of a given length and the efficiency for a rectangular incident stress wave of the same length versus λ. Rigid joint. $\lambda = t_p/t_0$ where $t_0 = M_J c/2EA$.

5.5.3. Discussion

From Eqs. (5.62) and (5.63) and Fig. 5.7, it can be seen that the incident stress wave that yields the maximum possible efficiency η for a given length λ of the stress wave is generally constituted by a symmetric portion of a half sine period. This portion is an increasing function of λ. Thus, for very small values of λ ($\lambda \to 0$), the incident stress wave degenerates into a rectangular pulse, whereas for very large values of λ ($\lambda \to \infty$), the stress wave degenerates into a pulse shaped as a half sine period.

In Fig. 5.8, it can be seen that the efficiency η depends on the stress wave length parameter λ in a similar way as it does when the incident stress wave is a rectangular pulse. Thus, $\eta \to 0$ when $\lambda \to 0$ and $\eta \to 1$ when $\lambda \to \infty$. It can also be seen from Figs. 5.8 and 5.9 that, if the incident stress wave is a rectangular pulse of a given length, the efficiency η can never be increased as much as 0.04 by only changing the shape

of this stress wave. Consider as a particular example again the situation when $\lambda = 5$. Then, for a rectangular incident stress wave the efficiency $\eta = 0.801$ cannot be increased by more than approximately 0.026. This means in other words that the loss can be decreased from 19.9 per cent to 17.3 per cent but not less than that. However, it should be noticed that the stress wave shape which leads to maximum efficiency is not easily generated by impact. For larger values of λ the reduction of loss becomes more important. When, for example, $\lambda = 20$ (which would be exceptional in percussive drilling), the losses can theoretically be reduced by more than 50 per cent. In such a case, however, the efficiency is anyhow very near 100 per cent.

5.6. Several Rigid Joints

5.6.1. Stress wave transmission

When transmission of a stress wave through one rigid joint is considered, the relation between the Laplace transforms $\tilde{s}_t(s)$ and $\tilde{s}_i(s)$ of the transmitted and incident stress waves, respectively, is given by Eqs. (5.24) and (5.25). If, instead, stress wave transmission through N equal joints between $N+1$ equal rods is considered, and if repeated reflections between the joints are not taken into account, then obviously

$$\tilde{s}_t(s) = \{H_J(s)\}^N \tilde{s}_i(s) \tag{5.64}$$

where

$$H_J(s) = 1/(s+1) \tag{5.25}$$

$\tilde{s}_t(s)$ denotes the Laplace transform of the stress wave $s_t(\tau)$ which is transmitted through the Nth joint, and $\tilde{s}_i(s)$ denotes the Laplace transform of the stress wave $s_i(\tau)$ which is incident towards the first joint.

Thus, the solution $s_t(\tau)$ can be obtained as the inverse Laplace transform of $\{H_J(s)\}^N \tilde{s}_i(s)$, i.e.

$$s_t(\tau) = L^{-1}\{[H_J(s)]^N \tilde{s}_i(s)\} \tag{5.65}$$

If, in particular, $s_i(\tau)$ is again the rectangular pulse with length λ given by Eq. (5.27), then Eqs. (5.64) and (5.25) yield

$$\tilde{s}_t(s) = (-1+e^{-\lambda s})/s(s+1)^N \tag{5.66}$$

This expression for $\tilde{s}_t(s)$ can be transformed into

$$\tilde{s}_t(s) = (-1+e^{-\lambda s})\{1/s - \sum_{n=1}^{N} 1/(s+1)^n\} \tag{5.67}$$

Hence, after inverse Laplace transformation, the transmitted stress wave is obtained as

$$s_t = -g_N(\tau)+g_N(\tau-\lambda) \tag{5.68}$$

where $g_N(\tau) = 0$ when $\tau<0$ and

$$g_N(\tau) = 1 - \sum_{n=1}^{N} \tau^{n-1}e^{-\tau}/(n-1)! \tag{5.69}$$

when $\tau \geq 0$. This result is illustrated in Fig. 5.10.

If, in particular, $N = 1$, Eq. (5.69) agrees with Eq. (5.31).

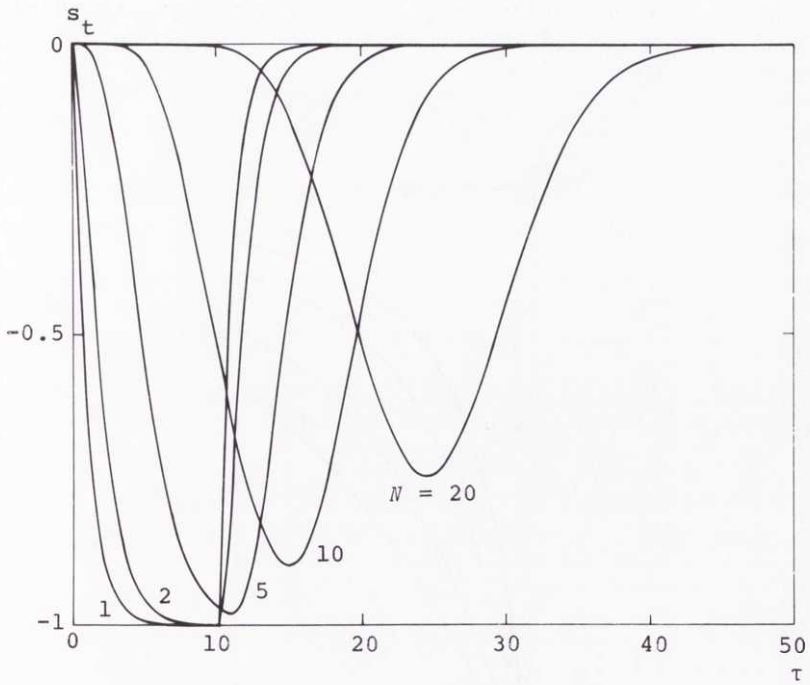

Fig. 5.10. Transmitted stress wave s_t through N rigid joints when the incident stress wave s_i is a rectangular pulse and $\lambda = 10$.

5.6.2. Efficiency

From Eqs. (5.32) and (5.27) the efficiency of stress wave energy transfer through the N joints is obtained as

$$\eta = (1/\lambda)\int_0^\infty s_t^2 d\tau \qquad (5.70)$$

where $s_t(\tau)$ is given by Eqs. (5.68) and (5.69). Consequently, η is a function of λ and N, and if, in particular, $N = 1$, Eqs. (5.68)-(5.70) yield the result already obtained in Eq. (5.33).

Numerical results for η according to Eqs. (5.68)-(5.70) are plotted in Fig. 5.11.

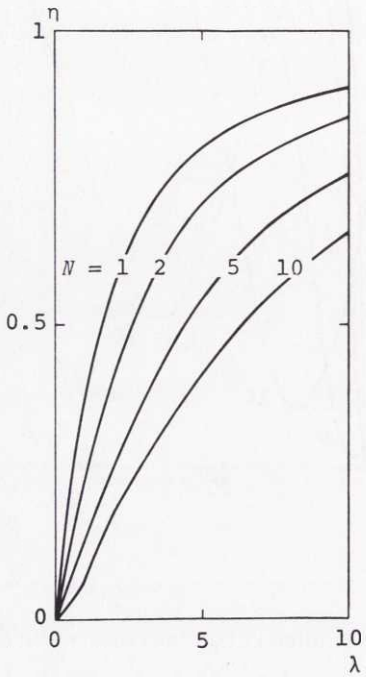

Fig. 5.11. Efficiency η versus λ for different numbers of rigid joints N. $\lambda = t_p/t_0$ where $t_0 = M_J c/2EA$.

5.6.3. Discussion

The amplitude of the transmitted stress wave is an increasing function of the parameter λ but a decreasing function of the number of joints N. From Fig. 5.11 it can be seen that the same is true for the efficiency η, i.e. η is an increasing function of λ but a decreasing function of N. It can also be shown that the relative loss of energy when a joint is added (N is in-

creased to $N+1$) becomes less with an increasing number of joints N. This implies that the stress wave, when passing the joints, is transformed in a favourable way with respect to transmission through joints.

5.7. Experiment

5.7.1. Equipment

The apparatus used in the tests is illustrated in Fig. 5.12.

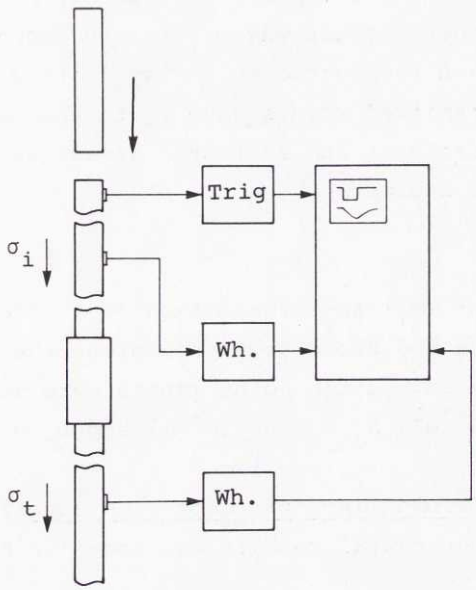

Fig. 5.12. Experimental apparatus.

A standard joint was placed between two equal standard rods in a drop-hammer with a cylindrical hammer. The cross sectional area of the hammer was approximately equal to the cross sectional area of the rods and its length was $L_H = 0.50$ m. Therefore, when striking one of the rods, the hammer produced an approximately rectangular stress wave σ_i of width $t_p = 0.2$ ms.

On the upper rod two sets of strain gauges, compensated for bending, were mounted. The upper gauges were connected via a trigger unit to the trig input of a Tektronix oscilloscope and the lower gauges were connected to the input of one of the channels of the oscilloscope via a conventional Wheatstone bridge circuit.

On the lower rod, another set of strain gauges, also compensated for bending, were mounted. These gauges were connected to another channel of the oscilloscope, again via a conventional Wheatstone bridge circuit.

The trigger unit was adjusted to give two output triggering pulses, the first pulse immediately before the arrival of the incident stress wave σ_i to the second gauge on the upper rod and the second pulse immediately before the arrival of the transmitted stress wave σ_t to the gauge on the lower rod. The incident and reflected stress waves were recorded by means of a camera.

5.7.2. Procedure

Incident (σ_i) and transmitted (σ_t) stress waves were recorded. The rod cross sectional area, the joint cross sectional area and the joint length were determined to be $A = 1.16\ 10^{-3} m^2$, $A_J = 3.05\ 10^{-3} m^2$ and $L_J = 0.220$ m respectively.

5.7.3. Results and comparison of theory and experiment

The experimental results are shown in Fig. 5.13.

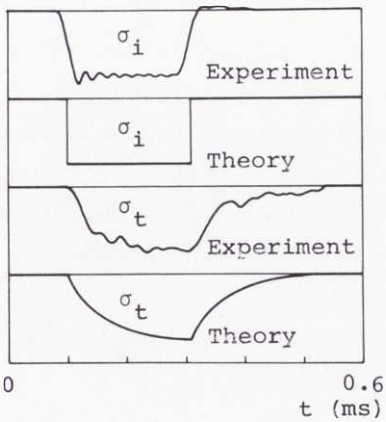

Fig. 5.13. Comparison between theoretical and experimental results.

From the incident stress wave record, the duration (half-width) of the incident stress wave can be determined as t_p = 0.21 ms. According to Eqs. (5.21), (5.13) and (3.1) and the assumption that c = 5.1 10^3 m/s, t_0 = 0.057 ms is further obtained. Hence, Eq. (5.28) yields λ = 3.68. From Eqs. (5.7) and (5.8) and from Eq. (5.6) the parameters m and r are determined as m = 2.44 and r = 2.63 respectively.

The theoretical result, also shown in Fig. 5.13, is obtained as follows:

The incident wave is approximated with a rectangular pulse with amplitude σ_0:

$$\sigma_i/\sigma_0 = \begin{cases} -1 & , \quad 0 \leq t < t_p \\ 0 & , \quad t_p \leq t \end{cases} \tag{3.147}$$

The result obtained in Section 5.3 for the rigid joint is chosen for the transmitted wave (since m is not an integer in the situation considered, the result obtained in Section 5.2 for the elastic joint is not applicable). Thus, according to Eqs. (5.19), (5.20), (5.30), (5.18) and (5.28), the transmitted wave can be expressed as

$$\sigma_t/\sigma_0 = -G_1(t)+G_1(t-t_p) \tag{5.71}$$

where

$$G_1(t) = g_1(t/t_0) \tag{5.72}$$

and where $g_1(t/t_0)$ is given by Eq. (5.31).

5.7.4. Discussion

The agreement between theory and experiment, as illustrated by Fig. 5.13, is quite satisfactory for many practical purposes. However, there are small oscillations in the measured stress waves without correspondence in the theoretical stress waves. This deviation is essentially caused by the limitations of the elementary stress wave theory (Appendix B). One part of the deviation between the transmitted stress waves may also be caused by the repeated reflections, not considered in the theory, which take place in the joint (Sections 5.2 and 5.4). Another part of the deviation may, of course, be explained by the fact that the joint is not homogeneous as was assumed in the theory.

6. SUMMARY AND CONCLUSIONS

A model describing the penetration of a conical indentor into a brittle rock material has been analysed.

A necessary condition for chip formation has been formulated in terms of indentor geometry (θ), friction between indentor and rock (ϕ_f) and rock material properties (ϕ) as

$$\theta+\phi_f+\phi<\pi/2 \tag{2.11}$$

The value of the force acting on the indentor at chip formation (F^*) has been obtained as a function of the inelastic part of the penetration (x_d), the indentor geometry, the friction between bit and rock and the rock material properties (ϕ, σ_c) as

$$F^* = k_{co}x_d^2 \tag{2.15}$$

where k_{co} is an increasing function of θ, ϕ_f, ϕ and σ_c which is illustrated in Fig. 2.10.

A lower bound (κ_{co}) has been obtained for the ratio of crater volume (V) and work (W) performed by the force acting on the indentor, i.e.

$$V/W\geq\kappa_{co} \tag{2.21}$$

where κ_{co} is a function of θ, ϕ_f, ϕ and σ_c which is illustrated in Fig. 2.13. κ_{co} is a decreasing function of θ and ϕ_f, which indicates that a sharp cone angle and a low friction is favourable.

The results obtained for a conical indentor have been compared with the corresponding results obtained for a wedge-shaped indentor by PAUL & SIKARSKIE (1965). Many results are similar. Thus, for example, the condition (2.11) is identical

to that obtained for a wedge-shaped indentor if θ denotes the half wedge-angle. A main difference, however, is that for a wedge the force-penetration envelope is linear instead of parabolic.

The theoretical results obtained for a conical indentor have also been compared with experimental results. The best agreement between theory and experiment as regards the force-penetration envelope (2.15) is obtained when too low values are assigned to the parameters ϕ_f, ϕ and σ_c. This implies that for actual values of these parameters, the theory gives an overestimation of the force at chip formation. Similar results were obtained by Paul & Sikarskie for a wedge, and in both cases, the high predicted value of the force at chip formation is believed to be principally due to the assumption that the Coulomb-Mohr failure criterion must be simultaneously satisfied over the whole final surface of failure.

For the values of ϕ_f, ϕ and σ_c which give the best agreement between theory and experiment as regards the force-penetration envelope (2.15), agreement is also obtained between theory and experiment as regards the inequalities (2.11) and (2.21).

Since in the case of a cone-shaped indentor there are no disturbing end-effects as in the case of a wedge-shaped indentor, it is believed that, with corresponding simplifying assumptions, a truer description of the penetration process is obtained for the cone. Therefore, it appears to be favourable to consider a cone-shaped indentor in further developing the model which was first introduced by Paul & Sikarskie. Such further development should comprise an improved failure criterion which need not be satisfied simultaneously over the whole final surface of failure. This implies that more importance is ascribed to the initiation of failure.

Models describing three basic methods of percussive rock destruction have been established and analysed. In general, the force-penetration relationship has been assumed to be linear during the loading as well as the unloading phase. The motions of the hammers and the drill rod (with the same material and cross sectional area as the hammers) have been described by means of one-dimensional stress wave theory, whereas the motions of the bits have been described by means of rigid body mechanics. Maximum forces (f_M) acting between bits and rock and efficiencies (η) of the transfer of kinetic impact energy to work in rock destruction have been determined as functions of parameters essentially representing bit mass ($\alpha = 4kc^2M_B/A^2E^2$), hammer length ($\beta = 2kL_H/AE$) and the degree of elastic deformation of rock ($\gamma = k/k_e$).

As regards the churn drilling method the results are illustrated in Figs. 3.3 and 3.4. When $\alpha = 0$ and $\beta > 0.3517$, they take the simple forms

$$f_M = 2(2e^{-(1/2)e^{-\beta}} - 1) \tag{3.57}$$

and

$$\eta = 2(1-\gamma)(2e^{-(1/2)e^{-\beta}} - 1)^2/\beta \tag{3.58}$$

For any value of α, f_M is an increasing function of β, whereas $\eta/(1-\gamma)$ is a decreasing function of β. Thus, f_M is near $\alpha^{1/2}$ for low values of β and approaches a constant higher value for high values of β, whereas $\eta/(1-\gamma)$ is near 1 for low values of β and approaches 0 for high values of β. This implies that from an energy conversion point of view, a short and stiff hammer with a sharp bit working in soft rock is a favourable combination. This is due to the fact that for such a combination the elastic as well as the kinetic energy contained in the hammer is very small when penetration ceases.

Theoretically $\eta = 1-\gamma$ for a rigid hammer. Therefore, it can be concluded from Eq. (3.58) when a cylindrical impact tool behaves nearly as a rigid hammer. Since $\eta > 0.90(1-\gamma)$ when $\beta < 0.50$, a criterion can be formulated e.g. as $\beta << 2$. Such a criterion is of significance in many drop-hammer investigations.

As regards the down-the-hole drilling method, the determination of f_M as well as η has been based upon a single impact between hammer and bit. This implies that f_M and η represent lower bounds of those values that would be obtained if the possibility of repeated impacts were taken into account. The results are illustrated in Figs. 3.6 and 3.7.

For any value of α, f_M is an increasing function of β, whereas $\eta/(1-\gamma)$ has a maximum for a value of β which depends on the value of α. Thus, f_M is near 0 for low values of β and approaches a constant value for high values of β, whereas $\eta/(1-\gamma)$ assumes a maximum value with respect to β which, for intermediate values of α, may be higher than 0.90. Further $\eta/(1-\gamma)$ approaches 0 for high values of β.

The fact that $\eta/(1-\gamma)$ is larger than 0.90 for certain combinations of α and β, indicates that, in the neighbourhood of such combinations of α and β, the consideration of repeated impacts would not seriously influence the results. When $\alpha/2\beta << 1$ and $\beta << 1$, however, repeated impacts would influence the results to a large extent (Cf. churn drilling when $\alpha = 0$).

As regards the hammer drilling method, the determination of f_M as well as η has been based upon only the first stress wave reflection at the bit. This implies that f_M and η represent lower bounds of those values that would be obtained if the repeated reflections occurring in the drill rod were taken into account. The results are illustrated in Figs. 3.10 and 3.11. When $\alpha = 0$, they take the simple forms

$$f_M = 2(1-e^{-\beta}) \qquad (3.139)$$

and

$$\eta = 2(1-\gamma)(1-e^{-\beta})^2/\beta \qquad (3.140)$$

The dependence of f_M and $\eta/(1-\gamma)$ on α and β is qualitatively similar to the dependence obtained in the case of the down-the-hole drilling method. Also in this case, $\eta/(1-\gamma)$ exceeds 0.90 for certain intermediate values of α and β.

The fact that $\eta/(1-\gamma)$ is larger than 0.90 for certain combinations of α and β indicates that, in the neighbourhood of such combinations of α and β, the consideration of repeated stress waves would not seriously influence the results.

If, in hammer drilling, $\alpha = 0$ (which may correspond to an integral drill steel), then the maximum value of $\eta/(1-\gamma)$ is 0.815 for $\beta = 1.26$. The maximum value of $\eta/(1-\gamma)$ for any values of α and β, however, is 0.902 for $\alpha = 2.329$ and $\beta = 1.970$. Therefore, the effect of adding a proper bit mass in this case is to increase the efficiency.

The two necessary conditions $\alpha = 2.329$ and $\beta = 1.970$ for maximum efficiency, $\eta/(1-\gamma) = 0.902$, yield two equations relating the six quantities bit mass (M_B), force-penetration constant (k), cross sectional area of hammer and rod (A), hammer length (L_H), sonic velocity (c) and Young's modulus (E). If c and E are given by the values valid for steel and if maximum efficiency is desired, this implies that only two of the four quantities M_B, k, A and L_H can be chosen arbitrarily . This is illustrated in Fig. 3.12, and it is seen that combinations of M_B, k, A and L_H that correspond to maximum efficiency often correspond as well to normal percussive rock drill designs.

If the quantities M_B, k, A and L_H are chosen in such a way that the efficiency assumes its maximum value, $\eta/(1-\gamma) = 0.902$, the sensitivity in the efficiency to changes in these quantities is quite low. Thus, if M_B is changed up or down by a factor of two, the relative decrease in η is not

greater than approximately 9 per cent. Similarly, if L_H is changed up or down by a factor of two, the relative change of η is not greater than approximately 36 per cent. Changes in k or A cause intermediate changes of η. One implication that immediately follows is that from only an efficiency point of view, the design parameters of a percussive rock drill are not very critical. This explains why penetration velocity for different rock drills are sometimes observed to be, within certain limits, essentially proportional to the power (same rock and hole diameter). Another implication is that, even if there are large variations of the conditions at the bottom of the drill hole from one hammer stroke to another and even if there are large variations in the different layers of rock, it should still be possible to keep the average efficiency high.

Similar conclusions about high efficiencies which are relatively insensitive to changes in the parameters M_B, k, A and L_H can be obtained also for the churn and down-the-hole drilling methods. Also, for these methods, the high efficiencies should be possible to obtain for reasonable values of M_B, k, A and L_H.

The high possible efficiency of energy transfer to the rock (more than 90 per cent) and the insensitivity of the efficiency to different parameter changes do in fact, together with the relatively low specific energy for the rock destruction process employed (of the order of the compressive strength of the rock material), to a large extent explain the successful use of the conventional methods of percussive rock destruction. This also partly explains why there has as yet been no real breakthrough for "exotic" methods of rock destruction.

The results obtained for the churn drilling method, the down-the-hole drilling method and the hammer drilling method are compared in Figs. 3.13 and 3.14. Generally, it is found that, for a constant impact velocity, the hammer drilling method results in the lowest forces acting between bit and

rock while the churn drilling method results in the highest forces acting between bit and rock. Further, the hammer drilling method generally gives an efficiency which is less than or equal to (when $\alpha>1$ and $\beta>\pi\alpha/2\Gamma$) that of the down-the-hole drilling method, while the efficiency of the churn drilling method may be higher or lower than the efficiencies of the other methods. For sufficiently low values of β, however, the churn drilling method gives the highest efficiency.

Two conditions, which both ought to be satisfied in order to justify the rigid body description of the bit, have been formulated. They are given by Eqs. (3.2) and (3.3) or by Eqs. (3.66) and (3.67). In eight situations where these conditions are well satisfied, theoretical and experimental results for reflected stress waves have been compared for an experimental set up corresponding to the hammer drilling method. Some minor deviations between theory and experiment can be explained by the limitations of the one-dimensional stress wave theory, the description of the incident stress wave as a perfect rectangular pulse and the treatment of the bit as a rigid mass. The observed deviations are not essential in connection with the determination of maximum bit force or efficiency. However, they are certainly essential with respect to e.g. fatigue of drill rods. It is believed that similar results would be obtained regarding the churn drilling method and the down-the-hole drilling method. This remains, however, to be proved by experimental investigations.

In the particular case when the bit is massless ($\alpha = 0$), it has been investigated under which circumstances there is no energy transferred to the rock during the second stress wave reflection at the bit in hammer drilling. The result is that no energy is transferred if (and only if)

$$\beta \geq \beta_0(\gamma) \tag{4.30}$$

where β_0 is a decreasing function of γ which is illustrated in Fig. 4.2. Thus, if $\gamma = 0$ (completely inelastic deformation of the rock) there is always some transfer of energy by the second incident stress wave. If, on the other hand, $\gamma = 1$ (completely elastic deformation of the rock) there is, of course, never any transfer of energy by the second incident stress wave. For $0<\gamma<1$ there is no second energy transfer provided that the value of β is sufficiently high. This implies that the rock is sufficiently hard and/or the hammer is sufficiently long.

The importance of stress wave shape in hammer drilling has been studied for two different types of waves when the bit is massless ($\alpha = 0$). The first wave was chosen as a triangular pulse and the second wave as a piece-wise constant pulse of the type which is generated by a hammer with dynamic stiffness greater than or equal to the dynamic stiffness of the rod. The efficiencies (η) of the transfer of stress wave energy to work in rock destruction have been determined as functions of parameters essentially representing the stress wave length (β), the stress wave shape (θ and R respectively) and the degree of elastic deformation of rock (γ). The results are shown for the triangular pulse in Fig. 4.5 and for the piece-wise constant pulse in Fig. 4.8.

For a triangular pulse with its maximum amplitude in the beginning ($\theta = 0$) the maximum efficiency is $0.61(1-\gamma)$. If instead, the maximum amplitude is in the end of the pulse ($\theta = 1$) the maximum efficiency becomes much higher, viz $0.97(1-\gamma)$. This illustrates quantitatively the well-known fact that from an energy transfer point of view a stress wave with a low amplitude in the beginning and a high amplitude in the end is favourable. The fact that triangular stress pulses normally cannot be generated by the impact of a hammer does not essentially reduce the value of this result.

In the case of a stress wave generated by a cylindrical hammer, the maximum possible efficiency is obtained in a situation corresponding to a rectangular stress pulse (R = 1). In agreement with previous results in this work, this maximum efficiency is $0.815(1-\gamma)$. It should be noticed that for a sufficiently high constant value of β, an increase in the dynamic stiffness ratio R (hammer/rod) is always accompanied by a decrease in efficiency. This implies that for a relatively long hammer, made of the same material as the rod, the highest efficiency is always obtained if the cross sectional area of the hammer is the same as that of the rod. For lower values of β, on the other hand, an increase in the dynamic stiffness ratio R may be be accompanied by an increase in efficiency. This implies that for a shorter hammer, made of the same material as the rod, the highest efficiency may be obtained if the cross sectional area is greater than that of the rod.

The loading phase of the force-penetration characteristic is certainly more or less non-linear for any real combination of bit and rock. The importance of this non-linearity in hammer drilling has been studied for two different idealized force-penetration relations.

First, it was assumed that the force is proportional to the square of the penetration and, for the sake of simplicity, that the bit is massless and that the deformation of the rock is completely inelastic. For a rectangular incident stress wave, then, the efficiency takes the simple form

$$\eta = 4\tanh^3(\beta)/3\beta \qquad (4.81)$$

where the parameter $\beta = t_p/t_0$ ($t_0^2 = AE^2/2Kc^2\sigma_0$) represents the length of the incident stress wave. The result is illustrated in Fig. 4.11 where it can be seen that the maximum efficiency is 0.66, i.e. lower than in the linear case (0.815). The basic difference from the linear case is, however, that here

β depends on stress wave amplitude (σ_0) as well as on stress wave length (t_p). Thus, for example, if the stress wave length is increased, the stress wave amplitude must be properly decreased in order not to change the prevailing efficiency.

Secondly, it was assumed that the force-penetration relation has a general saw-tooth shape, that the mass of the bit is arbitrary, that the deformation of rock may be partly inelastic and that the incident stress wave is a piece-wise linear function of time. In a particular example that has been presented here, it was assumed that the saw-tooth curve is confined between two straight enevelopes with slopes k and 2k as is illustrated in Fig. 4.12. Further, a certain bit mass ($\alpha = 1$) and a certain degree of elastic deformation ($\gamma = 0.001$) were assumed to be given. The incident stress wave was assumed to be a rectangular pulse and the efficiency of energy transfer to the rock (η) was then determined as a function of parameters essentially describing the length of the incident stress wave ($\beta = t_p/t_0$ where $t_0 = AE/kc$) and relating the amplitude of the incident stress wave to the first point of discontinuity of the slope of the force-penetration curve ($\delta = kx_1/A\sigma_0$). The efficiencies were compared with those obtained when the loading portion of the force-penetration curve is linear with a slope hk ($1 \leq h \leq 2$). As a main result it is found that for certain values of h the efficiencies agree remarkably well, Figs. 4.13 and 4.14. Therefore it should often be possible to approximate a real force-penetration curve (which may be far away from a straight line) by a straight line. This justifies, to a large extent, the usually made assumption in this work that the loading portion of the force-penetration relation is linear. As in the case of a parabolic force-penetration relationship, it is also seen that the efficiency here depends on stress wave amplitude as well as stress wave length.

Generally, in this work, it has been assumed that there is only a rod with constant cross sectional area between the hammer and bit in hammer drilling. This is often a good approximation of real situations. When this is not the case, the results still often apply if only a part of the drill rod immediately above the bit is considered. In such a case the energy of the incident stress wave is considered instead of the impact energy etc.

In certain applications such as deep hole drilling, however, the losses of stress wave energy due to the influence of joints between rods are most essential. Therefore, the phenomenon of stress wave energy transfer through joints between rods has been studied.

Two different models describing the joint behaviour have been analysed. In the first case, it was assumed that the joint behaves as an elastic swell on the rod. In the second case, it was assumed that the joint behaves as a rigid body. Therefore, in both cases, only losses due to stress wave reflection were taken into account even though the frictional losses may be important.

For the transfer of stress wave energy through a single elastic joint by a rectangular stress wave, the efficiency (η) becomes a function of two parameters representing the length of the stress wave relative to (twice) the length of the joint (m) and the ratio of joint cross sectional area to rod cross sectional area (r). The result is shown in Fig. 5.3. The efficiency is an increasing function of $m>0$ (notice that the efficiency is unaffected by m when $0<m\leq 1$) and a decreasing function of $r\geq 1$, and it approaches 1 when $r\to 1$ or $m\to\infty$. Thus, long stress waves and joints with as much as possible the same cross sectional area as the rod are favourable.

When the joint is assumed to be rigid, the efficiency becomes

$$\eta = 1-(1-e^{-\lambda})/\lambda \qquad (5.33)$$

where the parameter λ is related to m and r as $\lambda = 4m/r$. This result is illustrated in Fig. 5.5.

The results obtained for the single elastic and rigid joint are compared in Fig. 5.6. When, for a constant value of λ, $r \to \infty$ the two treatments yield the same result. When (say) $m \geq 1$ and $r \geq 4$, the efficiency obtained for the rigid joint is only slightly lower than the efficiency obtained for the elastic joint.

From the analyses of a single elastic as well as a rigid joint it follows that the efficiency increases with the length of a stress wave which has a predetermined shape as a rectangular pulse. Another problem that has been studied is the following: Suppose that the length of the incident stress wave is given together with the parameters describing joint and rod geometry and material properties (for a rigid joint all these parameters can be represented by the single parameter λ defined previously). How then shall the shape of the stress wave be chosen in order to maximize the efficiency? The answer that has been found, for a rigid joint, is that the shape shall be that of a half period sine pulse which is symmetrically cut off in both ends. This is illustrated in Fig. 5.7. For small values of λ ($\lambda \to 0$) the pulse degenerates into a rectangular pulse, whereas for large values of λ ($\lambda \to \infty$) the stress wave degenerates into a half period sine pulse. The maximum possible efficiency is compared with the efficiency when the stress wave is a rectangular pulse in Figs. 5.8 and 5.9. The (absolute) difference between the efficiencies never exceeds 4 per cent. Therefore, a rectangular stress wave yields an efficiency which is not very far below the maximum possible efficiency for the same length of the stress wave. When, for example, $\lambda = 5$ the rectangular incident stress wave leads to an efficiency which is $\eta = 0.801$, while the maximum possible efficiency for the same stress wave length is only approximately 0.026 higher.

The problem of finding the most favourable shape of a stress wave with a given length as regards transmission through N joints can possibly be solved by means of similar methods as have been employed here when $N = 1$. This problem is, however, left for subsequent investigations.

When a stress wave passes through a number of joints, the shape of the transmitted stress wave is changed by the influence of each joint. Therefore, there is not, of course, a constant relative energy loss for each joint. In order to study the efficiency of energy transfer through several joints, N equal joints between $N+1$ equal rods have been considered when the incident stress wave towards the first joint is a rectangular pulse. The efficiency of energy transfer η, based upon only the stress wave transmitted straight through the joints, is illustrated in Fig. 5.11 as a function of N and λ. η is, of course, a decreasing function of N and, again, an increasing function of λ.

The theoretical result for a stress wave transmitted through a single rigid joint has been compared with that measured in a single experiment. The agreement indicates that the theory yields reasonable results. Minor deviations between theory and experiment can be explained by the limitations of the one-dimensional stress wave theory, the fact that repeated reflections in the joint were not considered and, possibly, by the fact that the joint was treated as homogeneous. Since there was just a single experiment performed, however, more comprehensive investigations are needed in order to facilitate a conclusive judgement of the accuracy of the theory. Establishment of simple models which take into account the fact that the joint is heterogeneous and also the influence of friction appears to be an area of interest for further investigations.

In this work efficiencies for a number of processes connected with percussive destruction of rock have been determined and it has also been shown under what circumstances

certain efficiencies become as high as possible. In this connection it must be pointed out, however, that in the design of percussive rock drills overall costs and overall efficiencies must be considered. Consequently, it is seldom possible or even desirable to make every considered efficiency a maximum. Instead, some lower values of the efficiencies must be chosen. This problem of percussive rock drill design, however, is far beyond the scope of the present work.

Even if percussive destruction of rock has been primarily considered in this work, it is felt that several of the results obtained might be applicable in other connections. Thus, in Chapter 2, where penetration of an indentor into rock material has been considered, the material need not necessarily be rock. The results obtained in Chapters 3 and 4 might be applicable not only to the destruction of rock, but also to other related material destruction, compacting or forming processes. Further, the models representing bit - rock and rods - joints could as well represent other linear or non-linear and elastic or inelastic structures in general which are impulsively loaded.

REFERENCES

ABRAMSON, H.N., PLASS, H.J. & RIPPERGER, E.A., 1958, Stress wave propagation in rods and beams. *Advances in Appl. Mech., 5*, 111-194, Academic Press, Inc., New York.

ARNDT, F.-K., 1958, Theoretische Erkenntnisse ueber die Vorschubkraft beim schlagenden Bohren und Ihre Bestaetigung mit Hilfe einer neuartigen Versuchseinrichtung. *Glueckauf, 94*, Heft 35/36, 1178-1186.

ARNDT, F.-K., 1959, Untersuchung ueber die Energieuebertragung beim Schlagvorgang im Blickfeld des schlagenden Bohrens. *Foerd. Forschg. Geb. Bohr-u. Schießtechn., 7*, 1-132.

ARNDT, F.-K., 1960, Der Schlagablauf in Kolben und Stange beim schlagenden Bohren. *Glueckauf, 96*, Heft 24, 1516-1524.

BABENKOV, I.S., IVANOV, K.I. & HESIN, G.L., 1965, *Transmission of stress pulses along drill tool* (translation by I. Shelkovnikov). Hallfasfhetslaera, Fysikum, Uppsala.

BAILEY, J.J., 1967, On the performance of percussive drills. *Ninth symposium on rock mechanics*, Colorado School of Mines.

BENJUMEA, R. & SIKARSKIE, D.L., 1969, A note on the penetration of a rigid wedge into a nonisotropic brittle material. *Int. J. Rock Mech. Min. Sci., 6*, 343-352.

BERRY, C.W., 1959, *Effect of varying bit shape on force-penetration characteristics in rock for impulsive loading.* M. S. thesis, University of Minnesota.

BERTHOLF, L.D., 1966, *Longitudinal elastic wave propagation in finite cylindrical bars.* Ph. D. thesis, Washington State University.

CHARLES, R.J. & DE BRUYN, P.L., 1956, Energy transfer by impact. *Min. Engng, 8*, 47-53.

CHEATHAM, J.B., JR., 1958, An analytical study of rock penetration by a single bit tooth. *Eighth drilling and blasting symposium*, University of Minnesota.

CHEATHAM, J.B., JR., 1964, Indentation analysis for rock having a parabolic yield envelope. *Int. J. Rock Mech. Min. Sci., 1*, 431-440.

CHREE, C., 1889, The equations of an isotropic elastic solid in polar and cylindrical coordinates, their solution and application. *Trans. Camb. Phil. Soc., 14*.

COOK, N.G.W. & HUSTRULID, W.A., 1970, The efficiency of a pneumatic-powered percussive rockdrilling system. *The South African Mechanical Engineer*, September, 312-316.

COULOMB, C.A., 1776, Sur une application des règles de maximis et minimis à quelques problèmes de statique, relatifs à l'architecture. *Mémoires de Mathématique et de Physique*, Académie Royale des Sciences, par divers savans, Année 1773, Paris.

COURANT, R. & HILBERT, D., 1970, *Methods of mathematical physics*, vol. 2, pp. 122-125. Interscience Publishers, Inc., New York.

DAHL, H.O., 1932, Hammare och borr. *Jernkontorets Annaler*, Haeft. 5, 205-219 (in Swedish).

DAVIES, R.M., 1948, A critical study of the Hopkinson pressure bar. *Phil. Trans. Royal Soc. of London*, series A, *220*, 375-457.

DE JUHASZ, K.J., 1942, Graphical analysis of impact of elastic bars. *J. appl. Mech., 9*, A-122 - A-128.

DE JUHASZ, K.J., 1949, Graphical analysis of impact of bars stressed above the elastic range. *J. Franklin Inst., 247*, 15-48, 113-142.

DE SAINT-VENANT, B., 1867, *Journal de Mathématiques*, 2e série, *12*, 237-376.

DE SAINT-VENANT, B., 1868, *Comptes Rendus, 66*, 650-653.

DONNELL, L.H., 1930, *Trans. Amer. Soc. Mech. Engrs, 52*, 153.

DUTTA, P.K., 1968, The determination of stress waveforms produced by percussive drill pistons of various geometrical designs. *Int. J. Rock Mech. Min. Sci., 5*, 501-518.

FAIRHURST, C., 1961a, Wave mechanics of percussive drilling. *Mine Quarry Engng, 27*, 122-130.

FAIRHURST, C., 1961b, Wave mechanics of percussive drilling. *Mine Quarry Engng, 27,* 169-178.

FAIRHURST, C., 1961c, Wave mechanics of percussive drilling. *Mine Quarry Engng, 27,* 327-328.

FAIRHURST, C. & KIM, D.K., 1958, Energy transfer in percussive drilling. *Eighth drilling and blasting symposium,* University of Minnesota.

FINKEL, M., KALLDIN, B., LUNDBERG, B., LUNDQVIST, B. & MEYER, O., 1969, *Kompendium i bergborrning.* Atlas Copco AB, Stockholm (in Swedish).

FISCHER, H.C., 1960, *On longitudinal impact I-VI.* The Hague Martinus Nijhoff.

FRANKLAND, J.M., 1948, Effects of impact on simple elastic structures. *Proceedings of the Society of Experimental Stress Analysis, 6,* 7-25.

FU, C.C., 1970, A method for the numerical integration of the equations of motion arising from a finite-element analysis. *J. appl. Mech., 37,* 599-605.

FU, C.C. & PAUL, B., 1968, Stability of motion of impact tools. *Int. J. Solids Structures, 4,* 897-905.

FU, C.C. & PAUL, B., 1970, Energy transfer through chains of impacting rods. *Int. J. num. Meth. Engng, 2,* 363-385.

FURBY, J., 1964, Strain wave behaviour in the percussive drilling process. *Trans. Instn Min. Metall., 73,* 393-413.

GNIRK, P.F., 1962, *An experimental investigation of the indexing phenomenon for static single-tooth penetrations in Indiana limestone at atmospheric conditions.* American Petroleum Institute progress project 67-A, August.

HAIMSON, B.C., 1965, *High velocity, low velocity and static penetration characteristics in Tennessee marble.* M. S. thesis, University of Minnesota.

HAIMSON, B.C. & FAIRHURST, C., 1971, Some bit-penetration characteristics in Pink Tennessee Marble. *Twelfth symposium on rock mechanics,* University of Missouri.

HARTMAN, H.L., 1959, Basic studies of percussion drilling. *Min. Engng. 11*, 68-75.

HARTMAN, H.L., 1962, Crater geometry relations in percussive drilling. *Mine Quarry Engng, 28*, 530-536.

HARTMAN, H.L., 1966, The effectiveness of indexing in percussion and rotary drilling. *Int. J. Rock Mech. Min. Sci., 3*, 265-278.

HOLDO, J.K., 1962, From Mont Cenis to Mont Blanc. *Atlas Copco Publication No. 5088.*

HUSTRULID, W.A., 1968, *Theoretical and experimental study of percussive drilling of rock.* Ph. D. thesis, University of Minnesota.

HUSTRULID, W.A. & FAIRHURST, C., 1967, Written contribution to the paper by J.J. Bailey. *Ninth symposium on rock mechanics*, Colorado School of Mines.

HUSTRULID, W.A. & FAIRHURST, C., 1971, A theoretical and experimental study of the percussive drilling of rock. *Int. J. Rock Mech. Min. Sci., 8*, 311-333, 335-356.

KOLSKY, H., 1963, *Stress waves in solids.* Dover Publications, Inc., New York.

LONG, V.F., 1966, An investigation aimed at improving the efficiency of percussive rock drilling. *Jl S. Afr. Inst. Min. Metall., 66*, 276-296.

LOVE, A.E.H., 1927, *The mathematical theory of elasticity.* Cambridge.

LUNDBERG, B., 1967, Spraeckning i berg - en elementaer modell. *Tryckluft*, No. 2, 46-50.

LUNDBERG, B., 1967-1971, Research published in *Atlas Copco internal reports.*

LUNDBERG, B., 1968, *Models in connection with percussive drilling - analysis and experiment.* Tekn. lic. thesis, Chalmers University of Technology.

LUNDBERG, B., LUNDQVIST, B. & MEYER, O., 1968, Statisk och dynamisk intraengning av ett skaer i berg - beraekningsmetoder, brottkriterier och experiment. *IVA- rapport 4*, pp. 7-45.

LUNDQVIST, R.G., 1968, *Rock drilling characteristics of hemispherical insert bits.* M. S. thesis, University of Minnesota.

MAURER, W.C., 1968, *Novel drilling techniques.* Pergamon Press.

MCGREGOR, K., 1967, *The drilling of rock.* CR books Ltd, London.

MIKLOWITZ, J., 1960, Recent developments in elastic wave propagation. *Applied Mechanics Reviews, 13,* 865-878.

MILLER, M.H., 1966, The effect of stress wave duration on brittle fracture. *J. Rock Mech. Min. Sci., 3,* 191-203.

MILLER, M.H. & SIKARSKIE, D.L., 1968, On the penetration of rock by three-dimensional indentors. *Int. J. Rock Mech. Min. Sci., 5,* 375-398.

MINDLIN, R.D. & HERRMAN, G., 1951, A one-dimensional theory of compressional waves in an elastic rod. *Proc. 1st U.S. Nat. Congress Appl. Mech.,* Chicago, pp. 187-191.

MOHR, O., 1900, Welche Umstande bedingen die Elastizitaetsgrenze und den Bruch eines Materiales ? *Zeitschrift des Vereines Deutscher Ingenieure,* Band 44, pp. 1524 and 1572.

NAGEL, B., 1966, *Partiella differentialekvationer.* Institutionen foer teoretisk fysik, KTH, Stockholm.

PAONE, J. & TANDANAND, S., 1966, Inelastic deformation of rock under a hemispherical drill bit. *Trans. AIME, 235,* 113-122.

PARISEAU, W.G., 1971, Wedge indentation of anisotropic geologic media. *Twelfth symposium on rock mechanics,* University of Missouri.

PARISEAU, W.G. & FAIRHURST, C., 1967, The force-penetration characteristic for wedge penetration into rock. *Int. J. Rock Mech. Min. Sci., 4,* 165-180.

PAUL, B., 1961, A modification of the Coulomb-Mohr theory of fracture. *J. appl. Mech., 28,* 259-268.

PAUL, B. & GANGAL, M.D., 1969, Why compressive loads on drill bits produce tensile splitting in rock. *Society of Petroleum Engineers of AIME.* Paper No. SPE 2392.

PAUL, B. & SIKARSKIE, D.L., 1965, A preliminary theory of static penetration by a rigid wedge into a brittle material. *Trans. Soc. Min. Engrs, 232,* 372-383.

PENNINGTON, J.V., 1954, Rock failure in percussion. *Petr. Engr., 26,* May, B-76 - B-88.

PFLEIDER, E.P. & LACABANNE, W.D., 1961, Higher air pressures for down-the-hole percussive drills. *Mine Quarry Engng, 27,* 463-468, 496-501.

POCHHAMMER, L., 1876, Ueber Fortplanzungsgeschwindigkeiten kleiner Schwingungen in einem unbegrenzten isotropen Kreiszylinder. *J. f. reine u. angew. Math.* (Crelle),*81.*

QVARNSTROM, H. & SUNDQVIST, T., 1968, Nagra datamaskinprogram foer beraekning av foerlopp vid spraeckning i berg. *Atlas Copco internal report* (in Swedish).

ROBERTS, A., HAWKES, I. & FURBY, J., 1962, Transmission of energy in percussive drilling. *Mine Quarry Engng, 28,* 447-458.

RYD, E., 1938, Moderna bergborrmaskiner. *Jernkontorets Annaler,* Haeft. 8, 467-492 (in Swedish).

RYD, E. & HOLDO, J., 1956, Percussive rock drills - their construction and method of operation. In *Manual on Rock Blasting,* pp. 12:01-1 - 12:01-35.

SCHMAUCK, M., 1969, Moeglichkeiten zur Verbesserung der Bohrarbeit mit Versenkbohrhaemmern. *Glueckauf - Forsch. - H., 30,* 219-230.

SHIMIZU, H. & TAKATA, M., 1960, Dynamic stresses in the drilling rod. *Memoirs of the faculty of engineering, Kyushu Universitu,* pp. 115-152.

SIMON, R., 1963a, Digital machine computations of the stress waves produced by striker impacts in percussive drilling machines. *Rock mechanics* (C. Fairhurst, Ed.). Pergamon Press, Oxford.

SIMON, R., 1963b, Energy balance in rock drilling. *First conference on drilling and rock mechanics,* University of Texas.

SIMON, R., 1964, Transfer of the stress wave energy in the drill steel of a percussive drill to the rock. *Int. J. Rock Mech. Min. Sci., 1,* 397-411.

SINGH, M.M. & HARTMAN, H.L., 1961, Hypothesis for the mechanism of rock failure under impact. *Fourth symposium on rock mechanics,* Pensylvania State University.

STEPHENSON, B.R., 1963, *Measurement of dynamic force-penetration characteristics in Indiana limestone.* M. S. thesis, University of Minnesota.

TAKAOKA, S. & HAYAMIZU, H., 1956, Studies on the percussive deep hole drilling of rocks. *Journal of Mining and Metallurgical Institute of Japan, 72,* 497-502 (in Japanese).

TAKAOKA, S., HAYAMIZU, H. & MISAWA, S., 1958, On the reflection of elastic waves at a rod joint. *Journal of Mining and Metallurgical Institute of Japan, 74,* 7-12 (in Japanese).

TANDANAND, S. & HARTMAN, H.L., 1961, Stress distribution beneath a wedge-shaped drill-bit loaded statically. *International symposium on mining research,* University of Missoury.

TEALE, R., 1965, The concept of specific energy in rock drilling. *Int. J. Rock Mech. Min. Sci., 2,* 57-73.

THURESSON, G., 1971a, Digital simulering av stoetvagsreflexion i ett slagborrningssystem. *Atlas Copco internal report* (in Swedish).

THURESSON, G., 1971b, Linjarisering av kraft-intraengningskarakteristik vid slaende borrning. *Atlas Copco internal report* (in Swedish).

A. FORCE-PENETRATION RECORDS

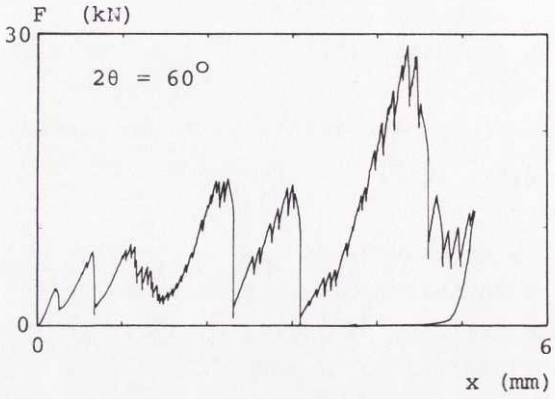

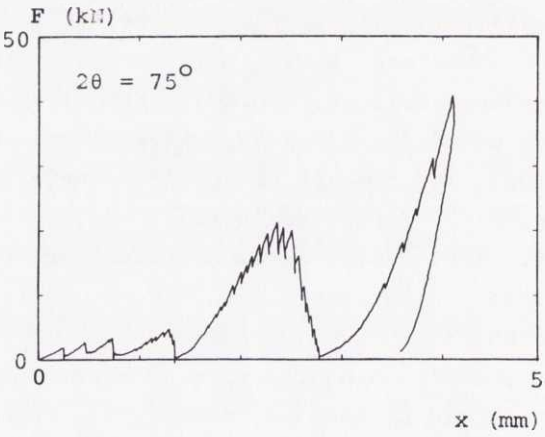

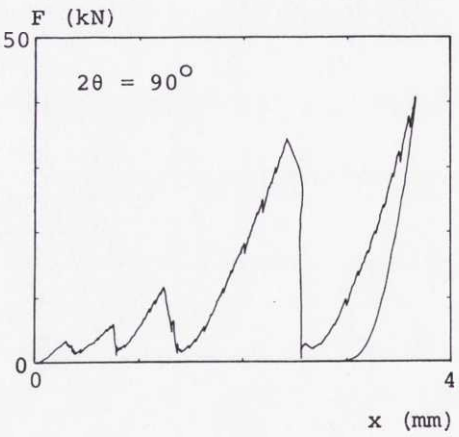

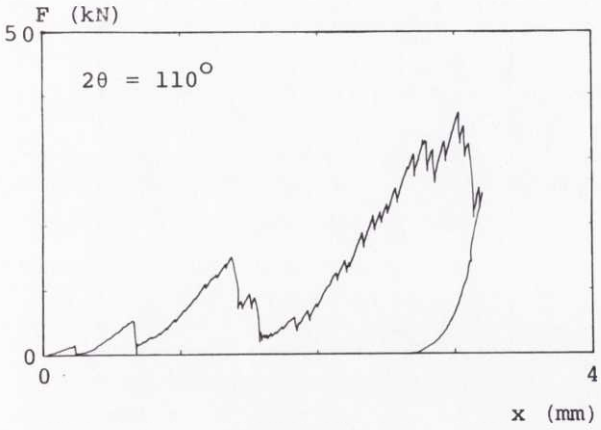
F (kN)
50
2θ = 110°
0
0
4
x (mm)

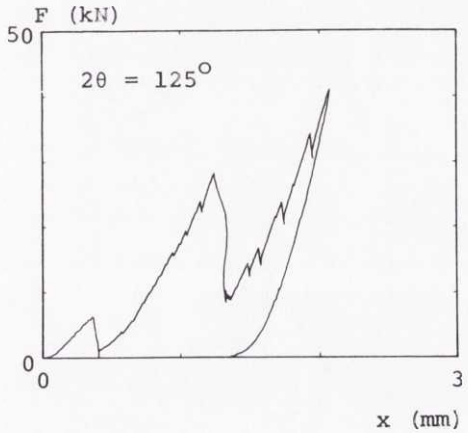
F (kN)
50
2θ = 125°
0
0
3
x (mm)

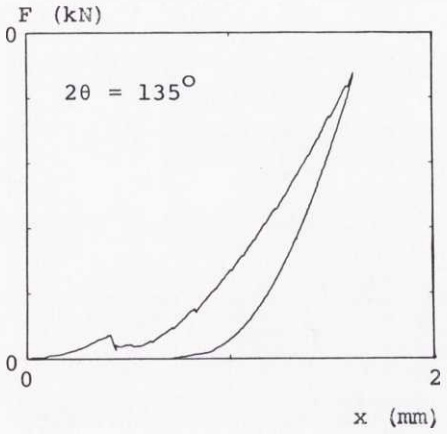
F (kN)
0
2θ = 135°
0
0
2
x (mm)

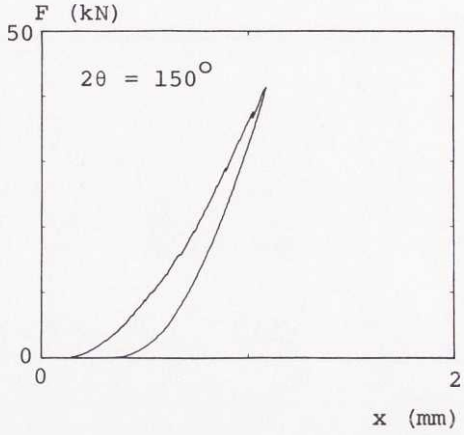
F (kN)
50
2θ = 150°
0
0
2
x (mm)

B. ELEMENTARY STRESS WAVE THEORY

B.1. Wave Equation

Consider a cylindrical rod with cross sectional area A, Young's modulus E and density ρ. Take the axis of the rod as z-axis. Assume that plane cross sections remain plane after deformation and let w(z,t) denote the longitudinal displacement of a cross section in the positive z-direction. Then, the one-dimensional wave equation

$$\partial^2 w/\partial t^2 = c^2 \partial^2 w/\partial z^2 \tag{B.1}$$

where

$$c^2 = E/\rho \tag{B.2}$$

is obtained from the equation of motion of a mass element $\rho A dz$ of the rod.

The general solution of Eq. (B.1), d'Alembert's solution, is

$$w(z,t) = w_1(z-ct)+w_2(z+ct) \tag{B.3}$$

where w_1 and w_2 are arbitrary functions that can be determined from given initial conditions (see e.g. NAGEL, 1966). The functions w_1 and w_2 can without loss of generality be expressed as

$$w_1 = w_p(z-ct)+a_1(z-ct)+b_1 \tag{B.4}$$

and

$$w_2 = w_n(z+ct)+a_2(z+ct)+b_2 \tag{B.5}$$

respectively. a_1, a_2, b_1 and b_2 are arbitrary constants and w_p and w_n are arbitrary functions which do not contain terms of the types $a_1(z-ct)+b_1$ and $a_2(z+ct)+b_2$ respectively. Therefore, the general solution w can alternatively be expressed as

$$w = w_p(z-ct)+w_n(z+ct)+\varepsilon_0 z+u_0 t+w_0 \qquad (B.6)$$

where $\varepsilon_0 = a_1+a_2$, $u_0 = c(a_2-a_1)$ and $w_0 = b_1+b_2$ are arbitrary constants.

w_p and w_n can be interpreted as particle displacement waves which propagate with the sonic velocity c in the positive and negative z-directions respectively. For steel, $E = 2.0\ 10^{11}$ N/m^2 and $\rho = 7.8\ 10^3$ kg/m^3 and therefore, according to Eq. (B.2), $c = 5.1\ 10^3$ m/s.

It should be observed that the waves w_p and w_n are not distorted during their propagation. This implies that the wave propagation is non-dispersive. According to more accurate approximate theories of elastic wave propagation, however, the propagation velocity for a harmonic wave is a function of the wave length, which means that the wave propagation is dispersive and that a propagating wave, which is not harmonic, is distorted (e.g. LOVE , 1927; MINDLIN & HERRMANN, 1951). This result is also obtained if the fundamental equations of linear elasticity are solved (POCHHAMMER, 1876; CHREE, 1889). Also, there exist not only one but infinitely many modes of wave propagation. For the lowest mode (which corresponds to the lowest wave propagation velocity for a given wave length), however, the wave propagation velocity for a harmonic wave is very near c as given by Eq. (B.2) provided that the wave length is much larger than the lateral dimensions of the bar (say more than 10 times). This result was obtained for a circular cylinder by DAVIES (1948). For waves of finite lengths, the implication is that the elementary theory presented here gives more accurate results the longer

the waves (or the significant details of the waves) are in comparison with the lateral dimensions of the rod. In situations corresponding to percussive rock destruction the elementary theory is often found to give a satisfactory accuracy (see e.g. FISCHER, 1960).

The physical interpretation of the constant w_0 is a constant displacement of the rod.

B.2. Particle Velocity and Stress

The particle velocity in the positive z-direction is

$$u = \partial w/\partial t \tag{B.7}$$

i.e. according to Eqs. (B.6) and (B.7),

$$u = u_p(z-ct)+u_n(z+ct)+u_0 \tag{B.8}$$

where (with $w_p'(z) = dw(z)/dz$)

$$u_p = -cw_p'(z-ct) \tag{B.9}$$

and

$$u_n = cw_n'(z+ct) \tag{B.10}$$

u_p and u_n can be interpreted as particle velocity waves which propagate with the sonic velocity c in the positive and negative z-directions respectively.

The physical interpretation of the constant u_0 is a constant velocity of the rod.

The strain in the rod is

$$\varepsilon = \partial w/\partial z \tag{B.11}$$

and, according to Hooke's law, the stress is

$$\sigma = E\varepsilon \tag{B.12}$$

Therefore, according to Eqs. (B.6), (B.11) and (B.12), the stress can be expressed as

$$\sigma = \sigma_p(z-ct)+\sigma_n(z+ct)+\sigma_0 \tag{B.13}$$

where

$$\sigma_p = Ew_p'(z-ct) \tag{B.14}$$

$$\sigma_n = Ew_n'(z+ct) \tag{B.15}$$

and

$$\sigma_0 = E\varepsilon_0 \tag{B.16}$$

σ_p and σ_n can be interpreted as stress waves which propagate with the sonic velocity c in the positive and negative z-directions respectively.

The physical interpretation of the constant ε_0 is a constant strain in the rod, while that of σ_0 is a constant stress in the rod.

According to Eqs. (B.9), (B.10), (B.14) and (B.15),

$$u_p = -(c/E)\sigma_p \tag{B.17}$$

$$u_n = (c/E)\sigma_n \tag{B.18}$$

For steel again, $c = 5.1\ 10^3$ m/s and $E = 2.0\ 10^{11}$ N/m^2. Normally, in percussive drilling $|\sigma_p|$ and $|\sigma_n| < 300$ MN/m^2. This implies that $|u_p|$ and $|u_n| < 7.65$ m/s, i.e. $|u_p|$ and $|u_n| << c$.

B.3. Energy

The kinetic energy due to the particle velocity u is

$$W_K = (\rho A/2)\int u^2 dz \tag{B.19}$$

while the elastic energy due to the stress σ is

$$W_E = (A/2E)\int \sigma^2 dz \tag{B.20}$$

The total energy is

$$W_T = W_K + W_E \tag{B.21}$$

If it is assumed that $u_0 = 0$ and $\varepsilon_0 = 0$, then Eqs. (B.19)-(B.21) can be expressed as

$$W_K = (A/2E)\int (\sigma_p^2+\sigma_n^2-2\sigma_p\sigma_n)\,dz \tag{B.22}$$

$$W_E = (A/2E)\int (\sigma_p^2+\sigma_n^2+2\sigma_p\sigma_n)\,dz \tag{B.23}$$

and

$$W_T = (A/E)\int (\sigma_p^2+\sigma_n^2)\,dz \tag{B.24}$$

respectively.

When, in particular, the stress waves σ_p and σ_n are not overlapping, i.e. $\sigma_p\sigma_n \equiv 0$, then

$$W_K = W_E \tag{B.25}$$

Thus, when the stress waves σ_p and σ_n are not overlapping, then the total energy W_T is composed of equal parts of kinetic energy and elastic energy.

If the stress waves σ_p and σ_n are considered for a constant value z_0 of z, then the total energy can be expressed as

$$W_T = (Ac/E)\int(\sigma_p^2+\sigma_n^2)dt \qquad (B.26)$$

The first term gives the stress wave energy associated with σ_p and the second term gives the stress wave energy associated with σ_n.

B.4. Reflection and Transmission

If at a certain position $z = z_0$, there is a change in rod configuration, then the phenomena of stress wave reflection and transmission may occur. In general, the reflected and transmitted stress waves can be determined from the conditions that (particle) velocity and force are continuous at $z = z_0$.

Consider as an example the situation when $A = A_1$, $E = E_1$ and $c = c_1$ for $z \leq z_0$, and when $A = A_2$, $E = E_2$ and $c = c_2$ for $z \geq z_0$. Assume that an incident stress wave $\sigma_{p1}(z-ct)$ arrives at $z = z_0$. Then a reflected stress wave $\sigma_{n1}(z+ct)$ and a transmitted stress wave $\sigma_{p2}(z-ct)$ are generated at $z = z_0$. Introduce for convenience $\sigma_i(t) = \sigma_{p1}(z_0-ct)$, $\sigma_r(t) = \sigma_{n1}(z_0+ct)$ and $\sigma_t(t) = \sigma_{p2}(z_0-ct)$. Then, according to Eqs. (B.8), (B.17) and (B.18), continuity of particle velocity requires

$$-(c_1/E_1)\sigma_i+(c_1/E_1)\sigma_r = -(c_2/E_2)\sigma_t \qquad (B.27)$$

Further, according to Eq. (B.13), continuity of force requires

$$A_1(\sigma_i+\sigma_r) = A_2\sigma_t \qquad (B.28)$$

By introduction of the impedance or dynamic stiffness $Z = AE/c$, one obtains

$$\sigma_r = -\{(Z_1-Z_2)/(Z_1+Z_2)\}\sigma_i \qquad (B.29)$$

$$\sigma_t = (A_1/A_2)\{2Z_2/(Z_1+Z_2)\}\sigma_i \qquad (B.30)$$

where

$$Z_1 = A_1 E_1 / c_1 \tag{B.31}$$

$$Z_2 = A_2 E_2 / c_2 \tag{B.32}$$

In particular, it is seen that when $Z_2/Z_1 \to 0$, i.e. when the end $z = z_0$ is free, then $\sigma_r = -\sigma_i$, i.e. a tensile wave is reflected as a compressive wave and vice versa. When, on the other hand, $Z_2/Z_1 \to \infty$, i.e. when the end $z = z_0$ is fixed, then $\sigma_r = \sigma_i$, i.e. a tensile wave is reflected as a tensile wave etc. When $Z_1 = Z_2$, finally, then $\sigma_r = 0$, i.e. no reflected stress wave is generated.

B.5. Impact

The problem of determining the motions and states of stress of two impacting bodies is similar to the problem of determining reflected and transmitted stress waves discussed above. The particle velocities and states of stress are obtained from Eqs. (B.8), (B.13), (B.17), (B.18) and conditions of continuity of particle velocity and force at sections that are fixed together. At the impact surfaces particle velocity and force are continuous as long as there is contact between the bodies (the state of stress is compressive on both sides). Before impact and after separation of the bodies, stress wave reflection at the two separate free ends must be considered.

Consider as a simple example the longitudinal impact between two equal semi-infinite and cylindrical rods. Assume that the velocity of the rod which at time $t = 0$ occupies $-\infty < z \leq 0$ is V while the rod, which at time $t = 0$ occupies $0 \leq z < \infty$, is initially at rest. Assume also that both rods are initially free from stresses. Then for $t \geq 0$ there is a stress wave σ_n travelling in the negative z-direction generated in the impacting rod and a stress wave σ_p travelling in the

positive z-direction generated in the impacted rod. Since obviously σ_n and σ_p are compressive, force and particle velocity must be continuous at z = 0 and therefore,

$$\sigma_n = \sigma_p \tag{B.33}$$

and

$$(c/E)\sigma_n + V = -(c/E)\sigma_p \tag{B.34}$$

From Eqs. (B.33) and (B.34) one obtains

$$\sigma_n = \sigma_p = -EV/2c \tag{B.35}$$

for $t \geq 0$ and $z = 0$. Consequently,

$$\sigma_n = \begin{cases} 0 & , \quad -\infty < z < ct \\ -EV/2c & , \quad -ct \leq z \leq 0 \end{cases} \tag{B.36}$$

and

$$\sigma_p = \begin{cases} -EV/2c & , \quad 0 \leq z \leq ct \\ 0 & , \quad ct < z < \infty \end{cases} \tag{B.37}$$

A large number of general and complex impact problems have been thoroughly treated by FISCHER (1960).

B.6. Terminology

Particle displacement waves, particle velocity waves, strain waves and stress waves are closely connected. Sometimes, they are all referred to as elastic waves. Here, however, the term stress wave is normally used.

It must be observed that the stresses σ_p and σ_n associated with stress waves are not in general equal to the stress σ in

the rod. According to Eq. (B.13), however, the stresses σ_p and σ_n are equal to the stress σ in the rod when $\sigma_0 = 0$ and for such z and t that σ_p and σ_n do not overlap.

If $\sigma_p > 0$ the wave σ_p is said to be tensile and if $\sigma_p < 0$ it is said to be compressive.

If two stress waves (or pulses) travelling in the same direction can be made equal by changing only their amplitude and length scales, they are said to have the same shape. Otherwise, they are said to have different shapes.

In most cases the stress waves are considered for a constant value z_0 of z and notations like, for example, $\sigma_i(t) = \sigma_{pl}(z_0-ct)$ are introduced. In such a case, $\sigma_i(t)$ represents the stress wave $\sigma_{pl}(z-ct)$ and from a physical point of view it is convenient to refer also to $\sigma_i(t)$ as a stress wave.

C. DETERMINATION OF $\xi(\tau)$

C.1. The Case $0<\alpha<1$

C.1.1. The interval $0\leq\tau<\beta$

With the introduction of the symbol $D = d/d\tau$, Eq. (3.22) can be expressed as

$$(D-a)(D-b)\xi = 4/\alpha \tag{C.1}$$

where

$$a = 2(-1+\Delta)/\alpha \tag{C.2}$$

$$b = 2(-1-\Delta)/\alpha \tag{C.3}$$

and

$$\Delta = (1-\alpha)^{1/2} \tag{C.4}$$

With respect to the initial conditions (3.23) and (3.24) the solution is

$$\xi = 1+\{(b+1)/(a-b)\}e^{a\tau}-\{(a+1)/(a-b)\}e^{b\tau} \tag{C.5}$$

C.1.2. The interval $\beta\leq\tau<2\beta$

Eqs. (3.31) and (C.5) yield

$$(D-a)(D-b)\xi = -4/\alpha+P_1e^{a(\tau-\beta)}+P_2e^{b(\tau-\beta)} \tag{C.6}$$

where

$$P_1 = \{(b+1)/(a-b)\}(-a^2+4a/\alpha-4/\alpha) \tag{C.7}$$

and

$$P_2 = \{(a+1)/(a-b)\}(b^2-4b/\alpha+4/\alpha) \qquad (C.8)$$

According to Eqs. (3.32), (3.33) and (C.5),

$$\xi(\beta) = \xi_1 \qquad (C.9)$$

and

$$d\xi(\beta)/d\tau = \nu_1 \qquad (C.10)$$

where

$$\xi_1 = 1+\{(b+1)/(a-b)\}e^{a\beta}-\{(a+1)/(a-b)\}e^{b\beta} \qquad (C.11)$$

and

$$\nu_1 = \{a(b+1)/(a-b)\}e^{a\beta}-\{b(a+1)/(a-b)\}e^{b\beta} \qquad (C.12)$$

The general solution of Eq. (C.6) takes the form

$$\begin{aligned}\xi = &-1+\{P_1/(a-b)\}e^{a(\tau-\beta)}\{\tau-\beta-1/(a-b)\}-\\ &-\{P_2/(a-b)\}e^{b(\tau-\beta)}\{\tau-\beta+1/(a-b)\}+\\ &+B_1e^{a(\tau-\beta)}+B_2e^{b(\tau-\beta)}\end{aligned} \qquad (C.13)$$

The constants B_1 and B_2 are determined from the conditions (C.9) and (C.10) and Eq. (C.13). The result is

$$B_1 = (R_2-bR_1)/(a-b) \qquad (C.14)$$

and

$$B_2 = (aR_1-R_2)/(a-b) \qquad (C.15)$$

where

$$R_1 = \xi_1 + 1 + (P_1 + P_2)/(a-b)^2 \qquad (C.16)$$

and

$$R_2 = \nu_1 + (P_2 - P_1)/(a-b) + (P_1 a + P_2 b)/(a-b)^2 \qquad (C.17)$$

C.2. The Case $\alpha = 1$

C.2.1. The interval $0 \le \tau < \beta$

Eq. (3.22) can be expressed as

$$(D+2)^2 \xi = 4 \qquad (C.18)$$

With respect to the initial conditions (3.23) and (3.24), the solution is

$$\xi = 1 - (1+\tau)e^{-2\tau} \qquad (C.19)$$

C.2.2. The interval $\beta \le \tau < 2\beta$

Eqs. (3.31) and (C.19) yield

$$(D+2)^2 \xi = -4 + 16(\tau-\beta)e^{-2(\tau-\beta)} + 8e^{-2(\tau-\beta)} \qquad (C.20)$$

According to Eqs. (3.32), (3.33) and (C.19),

$$\xi(\beta) = \xi_1 \qquad (C.21)$$

and

$$d\xi(\beta)/d\tau = \nu_1 \qquad (C.22)$$

where

$$\xi_1 = 1 - (1+\beta)e^{-2\beta} \qquad (C.23)$$

and

$$\nu_1 = (1+2\beta)e^{-2\beta} \tag{C.24}$$

The general solution of Eq. (C.20) takes the form

$$\xi = -1+(8/3)(\tau-\beta)^3 e^{-2(\tau-\beta)}+4(\tau-\beta)^2 e^{-2(\tau-\beta)}+ \\ +\{B_1+B_2(\tau-\beta)\}e^{-2(\tau-\beta)} \tag{C.25}$$

The constants B_1 and B_2 are determined from the conditions (C.21) and (C.22) and Eq. (C.25). The result is

$$B_1 = 1+\xi_1 \tag{C.26}$$

and

$$B_2 = 2(1+\xi_1)+\nu_1 \tag{C.27}$$

C.3. The Case $\alpha>1$

C.3.1. The interval $0\leq\tau<\beta$

Eq. (3.22) can be expressed as

$$(D^2-2aD+a^2+b^2)\xi = 4/\alpha \tag{C.28}$$

where

$$a = -2/\alpha \tag{C.29}$$

$$b = 2\Gamma/\alpha \tag{C.30}$$

and

$$\Gamma = (\alpha-1)^{1/2} \tag{C.31}$$

With respect to the initial conditions (3.23) and (3.24), the solution is

$$\xi = 1+e^{a\tau}\{(1+a)\sin(b\tau)/b-\cos(b\tau)\} \qquad (C.32)$$

C.3.2. The interval $\beta\leq\tau<2\beta$

Eqs. (3.31) and (C.32) yield

$$(D^2-2aD+a^2+b^2)\xi = -4/\alpha+P_1e^{a(\tau-\beta)}\cos\{b(\tau-\beta)\}+ \\ +P_2e^{a(\tau-\beta)}\sin\{b(\tau-\beta)\} \qquad (C.33)$$

where

$$P_1 = 8/\alpha-2a-a^2-b^2 \qquad (C.34)$$

and

$$P_2 = (4/\alpha)(b+a^2/b-1/b)-b(a-1)-a^2(a+1)/b \qquad (C.35)$$

According to Eqs. (3.32), (3.33) and (C.32),

$$\xi(\beta) = \xi_1 \qquad (C.36)$$

and

$$d\xi(\beta)/d\tau = \nu_1 \qquad (C.37)$$

where

$$\xi_1 = 1+e^{a\beta}\{(1+a)\sin(b\beta)/b-\cos(b\beta)\} \qquad (C.38)$$

and

$$\nu_1 = \{a(1+a)/b+b\}e^{a\beta}\sin(b\beta)+e^{a\beta}\cos(b\beta) \qquad (C.39)$$

The general solution of Eq. (C.33) takes the form

$$\xi = -1+(P_1/2b)(\tau-\beta)e^{a(\tau-\beta)}\sin\{b(\tau-\beta)\}-$$
$$-(P_2/2b)(\tau-\beta)e^{a(\tau-\beta)}\cos\{b(\tau-\beta)\}+$$
$$+B_1e^{a(\tau-\beta)}\sin\{b(\tau-\beta)\}+$$
$$+B_2e^{a(\tau-\beta)}\cos\{b(\tau-\beta)\} \qquad (C.40)$$

The constants B_1 and B_2 are determined from the conditions (C.36) and (C.37) and Eq. (C.40). The result is

$$B_1 = \nu_1/b+P_2/2b^2-a(1+\xi_1)/b \qquad (C.41)$$

and

$$B_2 = 1+\xi_1 \qquad (C.42)$$

D. THE INTEGRALS $I(\alpha,\beta)$ AND $J(\alpha,\beta)$

D.1. The Case $0<\alpha<1$

$$I = -(1+\Delta)e^{a\beta}/2\Delta+(1-\Delta)e^{b\beta}/2\Delta+1 \tag{D.1}$$

$$J = (1/4\Delta^2)\{-(1+\Delta)e^{2a\beta}-(1-\Delta)e^{2b\beta}+2\alpha e^{-4\beta/\alpha}+2-2\alpha\} \tag{D.2}$$

$$a = 2(-1+\Delta)/\alpha \tag{D.3}$$

$$b = -2(1+\Delta)/\alpha \tag{D.4}$$

$$\Delta = (1-\alpha)^{1/2} \tag{D.5}$$

D.2 The Case $\alpha = 1$

$$I = 1-e^{-2\beta}(2\beta+1) \tag{D.6}$$

$$J = 1/2-e^{-4\beta}(4\beta^2+2\beta+1/2) \tag{D.7}$$

D.3 The Case $\alpha>1$

$$I = 1-(1/\Gamma)\{\sin(2\Gamma\beta/\alpha)+\Gamma\cos(2\Gamma\beta/\alpha)\}e^{-2\beta/\alpha} \tag{D.8}$$

$$J = (1/2)(1-e^{-4\beta/\alpha})-(1/\Gamma^2)\{\sin(2\Gamma\beta/\alpha)+$$
$$+\Gamma\cos(2\Gamma\beta/\alpha)\}e^{-4\beta/\alpha}\sin(2\Gamma\beta/\alpha) \tag{D.9}$$

$$\Gamma = (\alpha-1)^{1/2} \tag{D.10}$$

Printed in Sweden, Gotab, Surte 71.7826